Investigation of Two Potential Treatments for Frontotemporal Dementias by Mass Spectrometry

BY

KEVIN M. KROCK

B.S., University of Toledo 2007

THESIS

Submitted as partial fulfillment of the requirements for the degree of Doctor of Philosophy in Medicinal Chemistry in the Graduate College of the University of Illinois at Chicago, 2014

Chicago, Illinois

Defense Committee

Richard B. van Breemen, Chair and Advisor
Jimmy Orjala
Michael Federle
Richard Gemeinhart, Pharmaceutics and Bioengineering
Adam Negrusz, Forensic Science

ACKNOWLEDGEMENTS

The number of people instrumental in making my dissertation research possible exceeds the allotted space. Dr. van Breemen was and is a phenomenal mentor to me and the rest of his research group. Without his steady leadership, support, and belief in my abilities, my life would be far different. His impact cannot be overstated.

Dr. Dejan Nikolic provided an enormous amount of hands-on instruction and advice. Often, there were one or two tips that saved weeks of trial and error, increasing the pace of my research. He is a great resource for LC-MS research for everybody at UIC, and never expects anything in return.

Drs. Jeff Dahl, Jerry White, Carrie Crot and Yongsoo Choi were patient teachers of instrumentation and laboratory technique. My post-graduate success comes directly from the lessons learned from them.

My fellow graduate students, Drs. Jay Kalin, Isaac Schiefer, and Yang Yuan were incredibly helpful during the didactic courses, even when in competition for grades. Their friendship also made the difficult days easier to face.

The members of my preliminary examination and dissertation defense committees deserve acknowledgement for their time and effort to improve my research plan. It is rare that you get the full attention of brilliant scientists and their input and constructive criticism has made me a better researcher.

My family has been emotionally and financially supportive of my academic career. My grandmother, Olony Matthews, mother, Pam Vaughn, and brother, Andrew Krock all deserve special acknowledgement.

KMK

TABLE OF CONTENTS

TABLE OF CONTENTS (continued)

LIST OF TABLES

LIST OF FIGURES

LIST OF FIGURES (continued)

LIST OF FIGURES (continued)

LIST OF FIGURES (continued)

LIST OF ABBREVIATIONS

%RSD	percentage relative standard deviation
3R tau	3 carboxy-terminal repeats
5-HT	5-hydroxytryptamine
5-HT6	5-hydroxytryptamine receptor subtype 6
AD	Alzheimer's disease
ADMET	absorption, distribution, metabolism, excretion and toxicology
AET	active efflux transporters
APCI	atmospheric pressure chemical ionization
APP	amyloid precursor protein
AUC	area under the curve
Aβ	amyloid β
BACE	β amyloid cleaving enzyme
BBB	blood brain barrier
CAS	Chemical Abstracts Service
CID	collision induced dissociation
CTE	chronic traumatic encephelopathy
DMPK	drug metabolism and pharmacokinetics
DNMS	delayed non-match-to-sample
EC	endothelial cells
ER	endoplasmic reticulum
ESI	electrospray ionization

LIST OF ABBREVIATIONS (continued)

eV	electronvolt
FA	formic acid
FP	fraction plate
FTDP-17-tau	frontotemporal dementia with Parkinsonism-linked to chromosome 17 and tau pathology
FTIR	Fourier transform infrared spectroscopy
GSK-3	glycogen synthase kinase subtype 3
HFIP	1,1,1,3,3,3-hexafluoroisopropanol
HPLC	high performance liquid chromatography
HRMS	high resolution mass spectrometry
HTS	high-throughput screening
HUSERMET	Human Serum Metabolome in Health and Disease
IT-TOF	ion trap-time of flight hybrid mass spectrometer
kV	kilovolts
LCMS	liquid chromatography mass spectrometry
LLOD	lower limit of detection
LLOQ	lower limit of quantitation
m/z	mass to charge ratio
MAP	microtubule associated protein
MOPS	3-(N-morpholino)propanesulfonic acid
MS	mass spectrometry

LIST OF ABBREVIATIONS (continued)

MTBR	microtubule binding region
NCE	new chemical entities
NFT	neurofibrillary tangles
PD	Parkinson's disease
PHF	paired helical filaments
PI3K	phosphatidyl inositol-3-kinase
QTOF	quadrupole-time of flight hybrid mass spectrometer
R3	third carboxy-terminal repeat
sAPPa	soluble amyloid precursor protein subtype a
SD	standard deviation
SRM	selected reaction monitoring
SRS	self-recognition sequence
tau	microtubule associated protein tau
ThS	Thioflavin S
UHPLC	ultrahigh performance liquid chromatography
UPR	unfolded protein response
UV	ultraviolet
v/v	volume to volume ratio
XCMS	"X" forms of chromatography mass spectrometry

SUMMARY

Intraneuronal tangles of the microtubule associated protein tau are a hallmark of frontotemporal dementia and other tauopathies. Tau stabilizes tubulin subunits to form microtubules in neuronal projections, but must be removed to allow transport vessicles to pass. This dynamic process is controlled by the phosphorylation state of tau; increased phosphorylation removes tau from the microtubule. Unbound tau aggregates and is unable to be cleared, so a small molecule inhibitor of aggregation could stop the progression of the pathology.

The van Breemen lab has access to various natural product fractions prepared by collaborating research groups and are not widely available. The previously published tau aggregation inhibitions screening assay utilized a fluorescence detector, which can only screen single molecule samples. A mass spectrometry based screen was developed to be able to screen natural product fractions, which is described in Chapter 2. Natural product fractions obtained from marine actinomycetes were screened in Chapter 3 and hit fractions were identified.

The three fractions which inhibited aggregation were profiled using a metabolomics approach, which is described in Chapter 4. The identification and structure elucidation of a small amount of natural product is the most difficult step, so this approach moves it to the end to minimize the number of compounds that need to be identified. The actinomycetes need to be recultured, taking several months, so the profiles of the new and old fractions can be compared to confirm the same compounds are present.

The 5-HT6 receptor antagonist, PRX-07034 is a potential treatment for memory issues related to frontotemporal dementias. Chapter 5 outlines a validated UHPLC-MS-MS method to quantitate the compound in both rat serum and brain. The behavioral effects of the treatment have been studied for nearly 10 years; however the compound was never analytically determined to reach the brain.

CHAPTER 1

INTRODUCTION

1.1 Normal Structure and Function of Tau

The microtubule associated protein tau's (referred to as simply tau) normal function is to stabilize microtubules which are vital for intracellular cargo transport. Tau is coded by one gene on chromosome 17 and is the major neuronal microtubule associated protein (MAP). Two other MAPs (MAP1 and MAP2) have been identified but are of much higher molecular weight and do not participate in deleterious fibril formation [1]. Six isoforms of tau are produced by alternative splicing of its mRNA, and each contain three or four microtubule binding regions (MTBRs), each containing 31 or 32 residues [2]. These isoforms are dubbed 3R or 4R taus, depending on the number of carboxy-terminal MTBRs. It is thought that each of these MTBRs are capable of binding a tubulin subunit and acting as a lattice to hold them in the correct position for assembly [3]. Also, three isoforms containing either one, two or zero amino-terminal 29 residue repeats have been identified, accounting for the six total isoforms known as 3R/0N, 3R/1N, 3R/2N, 4R/0N, 4R/1N, or 4R/2N. The isoforms range in total length from 352 to 441 amino acids and each repeat is associated with increased microtubule binding, making 3R/0N the least tightly bound [4]. Fully functional tau has little secondary structure except for β structure in the second and third MTBR. The six isoforms are shown in Fig. 1.1.

Fig. 1.1 The six naturally occurring isoforms of tau. They are displayed in order of most likely to form paired helical filaments (PHF) at the top to the least likely at the bottom [5].

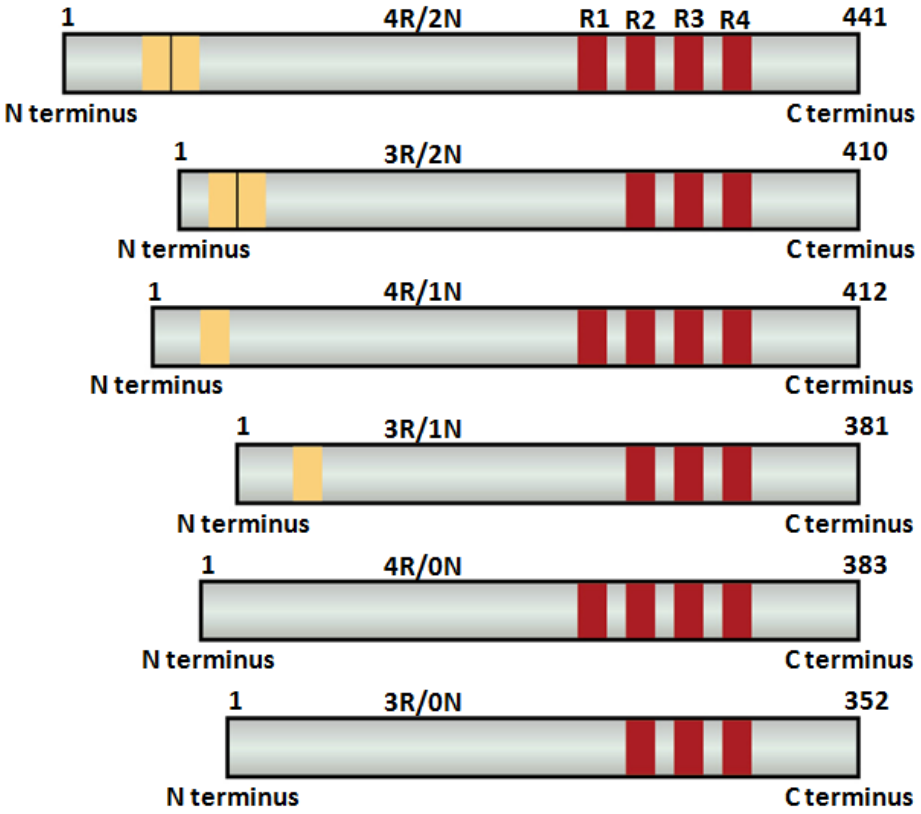

Tau's activity is regulated by the level of phosphorylation controlling tubulin polymerization into microtubules and microtubule stability, normally functioning with two or three phosphorylations per protein [6,7]. The binding of tau to the microtubule is in dynamic equilibrium. Hyperphosphorylation removes tau and allows vesicles to pass, whereas dephosphorylation allows tau to bind and promote stability of the microtubule [5].

More than 100 years after Alzheimer's disease (AD) was first identified, the molecular mechanisms behind the pathology remain ambiguous. A postmortem diagnosis still relies on the appearance of extracellular amyloid β (Aβ) plaques, and intracellular neurofibrillary tangles (NFTs) which correlate with the extent of neuronal death. Whether either or both of these are essential to pathology or simply markers of neuronal death have been much debated. Currently there are two competing broad hypotheses which will be summarized in the shortest possible way. Both have many variations on each step and too many more up and downstream effectors to list. Many other hypotheses have been proposed, implicating bacterial infections [8], aluminum [9], damage by free radicals, cholinergic dysfunction [10], and L-glutamate excitotoxicity [11].

1.2 Amyloid β, tau, and Alzheimer's Disease

The amyloid cascade hypothesis

The amyloid cascade hypothesis holds that the appearance and aggregation of Aβ is the pathology responsible for AD. The peptide sequence known as Aβ is found initially in the transmembrane domain of the amyloid precursor protein (APP). The extracellular portion can be cleaved into a longer fragment by

a-secretase, or a shorter fragment by β-secretase, also known as β amyloid cleaving enzyme (BACE). The fragments resulting from each are soluble and of no further consequence to disease progression. The specific cleavage site of a-secretase removes some of the residues that would go on to form Aβ, so this is termed the non-amyloidogenic pathway. If β-secretase acts instead, the full Aβ sequence remains and can be further processed by γ-secretase, releasing the Aβ peptide. Aβ varies in length from 39 to 43 residues, but the underlying mechanism is not clear. It is possible that there are multiple γ-secretase isoforms, or that the cleavage site is not well defined [12]. Aβ 1-40 is most commonly produced, but Aβ 1-42 is more likely to aggregate due to the two additional hydrophobic residues. The pathways of APP processing are displayed in Fig. 1.2.

In the AD brain, amyloid plaques are found in the vicinity of dead or dying neurons. Although the plaques were originally thought to be the pathological agent, Aβ oligomers are now believed to the likely neurotoxin. The addition of fibrillar Aβ to the cerebral cortex of rhesus monkeys causes neuronal loss and NFT formation up to 1.5 mm from the injection site [13]. The biochemical process of Aβ causing NFT formation is the subject of much debate. The overproduction and oligomerization of Aβ1-42 effects synaptic activity and damages neurons, causing an immune response. Abnormalities in ion transport, phosphatase and kinase activity and oxidative injury lead to decreased neurotransmitter concentrations and widespread neuronal death. AD patients exhibit increasing dementia as this process proceeds [14]. A graphical representation of this is shown in Fig. 1.3 to make a comparison to the tau tangle hypothesis.

Fig. 1.2. APP can be processed by two separate enzymes, and the resulting peptide will follow one of two distinct paths. sAPPa is not known to cause any pathology, whereas Aβ 1-40 and 1-42 are implicated in AD and other frontotemporal dementias. [15]

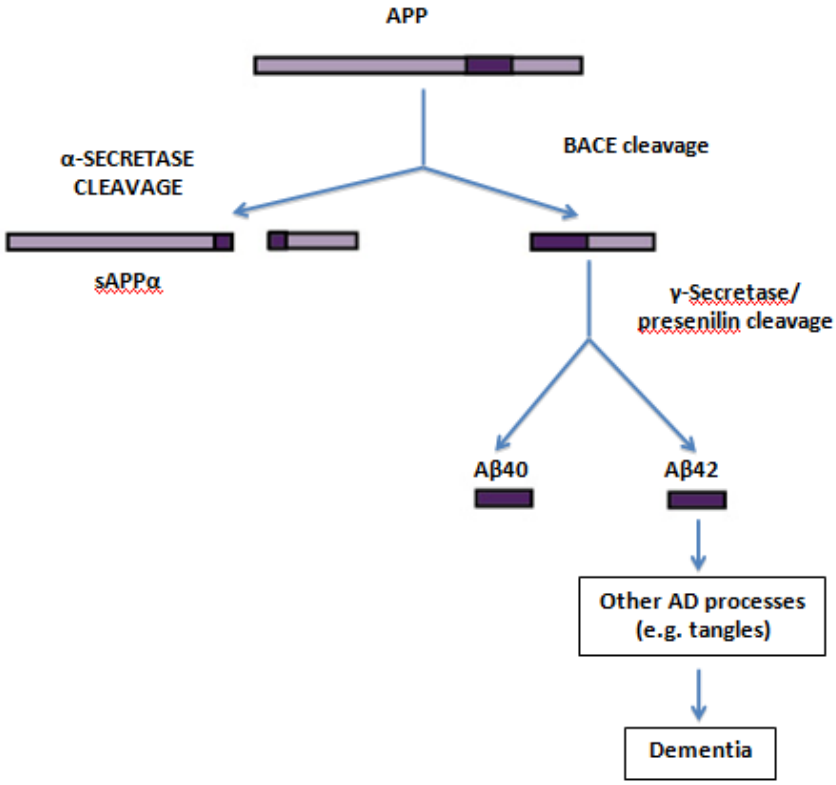

Fig. 1.3. The amyloid cascade hypothesis [14]

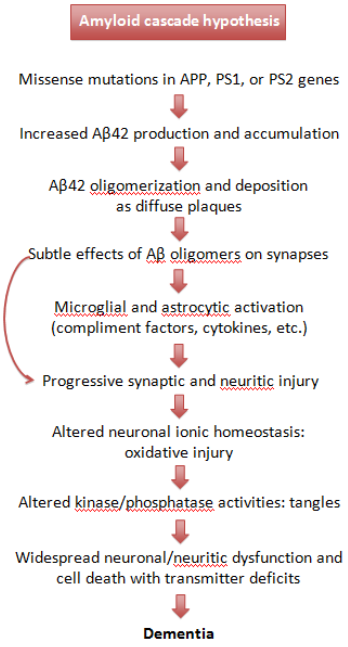

One of the most important discoveries related to AD was found using mass spectrometry; the identity of the peptide which is the main constituent of amyloid plaques. Robert Cotter and colleagues at Johns Hopkins School of Medicine identified the cleavage site of APP and the resulting secreted peptide which would be called $A\beta_{1-42}$. The group studied a Chinese hamster ovary cell culture transfected to overexpress human APP-770 and analyzed the secreted peptide product by plasma desorption mass spectrometry [16]. Once identified, the peptide was sequenced using Edman degradation [16]. The researchers were able to transfect the gene for human APP into mouse embryonic stem cells, creating the first mouse model of AD, less than two years later [17]. The overexpression of Aβ1-42 in vivo was confirmed by mass spectrometry.

The tau and tangle hypotheses

There are several problems that keep the amyloid cascade hypothesis from being fully accepted. Clinical trials investigating the use of Aβ immunotherapy, γ-secretase inhibitors and Aβ aggregation inhibitors alone and in combination have all failed to show improvement in AD patients [18]. Transgenic mouse models that express a mutation in APP leading to an increase in Aβ 1-42 and plaques do not also have neuronal deterioration [19] or tangle formation [12]. In humans, β-amyloidosis is not enough to solely cause dementia, as some individuals have as much amyloid plaque as Alzheimer's patients, but without NFTs and dystrophic neurons surrounding the plaques[20]. Also, neurofibrillary degeneration similar to AD occurs without β-amyloidosis in Guam Parkinsonism-dementia complex, chronic traumatic encephelopathy (CTE), corticobasal degeneration and Parkinson's disease [21].

The tau and tangle hypothesis posits that both aggregated tau and Aβ are

downstream effectors of an earlier pathological process, and are both involved in neuronal death, instead of NFTs being a byproduct of Aβ toxicity. See Fig. 1.4 for one proposed pathway.

A second tau and tangle hypothesis implicates a loss of function mutation in presenilin-1, which then fails to activate phoshphatidyl inositol-3-kinase (PI3K), which further downstream would allow the continued activity of a major tau kinase glycogen synthase kinase-3 (GSK-3) [22]. AD follows the same histological progression of neurodegeneration as the nonamyloid tauopathies such as Pick's disease, and the number of NFTs directly correlates with the degree of dementia. The NFTs are made up of hyperphosphorylated tau in each disease (approximately three to four times more than is normal). In frontotemporal dementia with Parkinsonism-linked to chromosome 17 and tau pathology (FTDP-17-tau), four missense mutations cause an increase in the 4R isoforms which are more susceptible than 3R isoforms of tau to hyperphosphorylation, driving self-aggregation into PHFs, then further into NFTs [23].

The aggregation and toxicity of tau

Whatever the upstream pathology, it is generally accepted that the process of tau aggregation proceeds through the steps of hyperphosphorylation, self-recognition, PHF or straight filament formation, and further assembly to NFTs. It has been reported that the same level of normal tau is present in AD brains as age matched unaffected brains. However, four to eight times as much hyperphosphorylated tau is found in AD brains [24], without an increase in tau mRNA [25]. The conclusion to be drawn from these data is that hyperphosphorylated and

Fig. 1.4 The tau and tangle hypothesis [21]

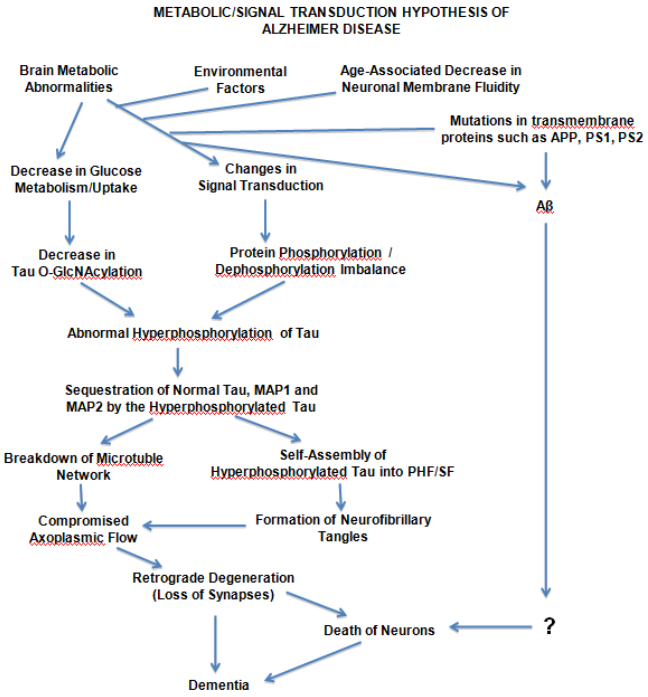

aggregated tau is less able to be cleared.

Normal tau is very hydrophilic, with long stretches of positively and negatively charged residues, and β structure in the second and third repeats (R2 and R3) of 4R tau, and in the second repeat of 3R tau. Inside these regions are the self-recognition sequences necessary for PHF formation, but are surrounded by repulsive regions. On the C-terminal side of these repeats, an acidic stretch of residues can be phosphorylated at three positions, opening up the β structure and neutralizing the repulsion between each tau protein. This new conformation allows for the self-recognition sequences to get close enough together for PHF formation. This process is shown in Fig. 1.5. It is proposed that the tyrosine residue in each peptide are responsible for initiation of PHF formation by studying the x-ray diffraction patterns of multiple PHF forming synthetic peptides[26]. The tyrosine residues stay localized in the intersheet space between proteins. The authors of the study recommend targeting this location with small molecules capable of interacting with and preventing aromatic hydrophobic interaction. Further hydrogen bonding occurs following the initial hydrophobic interaction[27], with lysine facing outward into the aqueous environment[26].

As the structure grows from filaments to fibrils to tangles, normal tau is sequestered along with the hyperphosphorylated species [28], as well as MAP1 and MAP2 [29]. It has also been reported that hyperphosphorylated tau fibrils are able to seed the formation of normal tau into fibrils in yeast models [30]. The removal of these proteins causes a failure in microtubules stability and neuronal death.

Fig. 1.5 All six isoforms of tau are capable of self-assembly in the manner displayed here. Hyperphosphorylated tau loses its β structure, allowing the self-recognition sequences to approach each other in the proper orientation for PHF then fibril formation. [21].

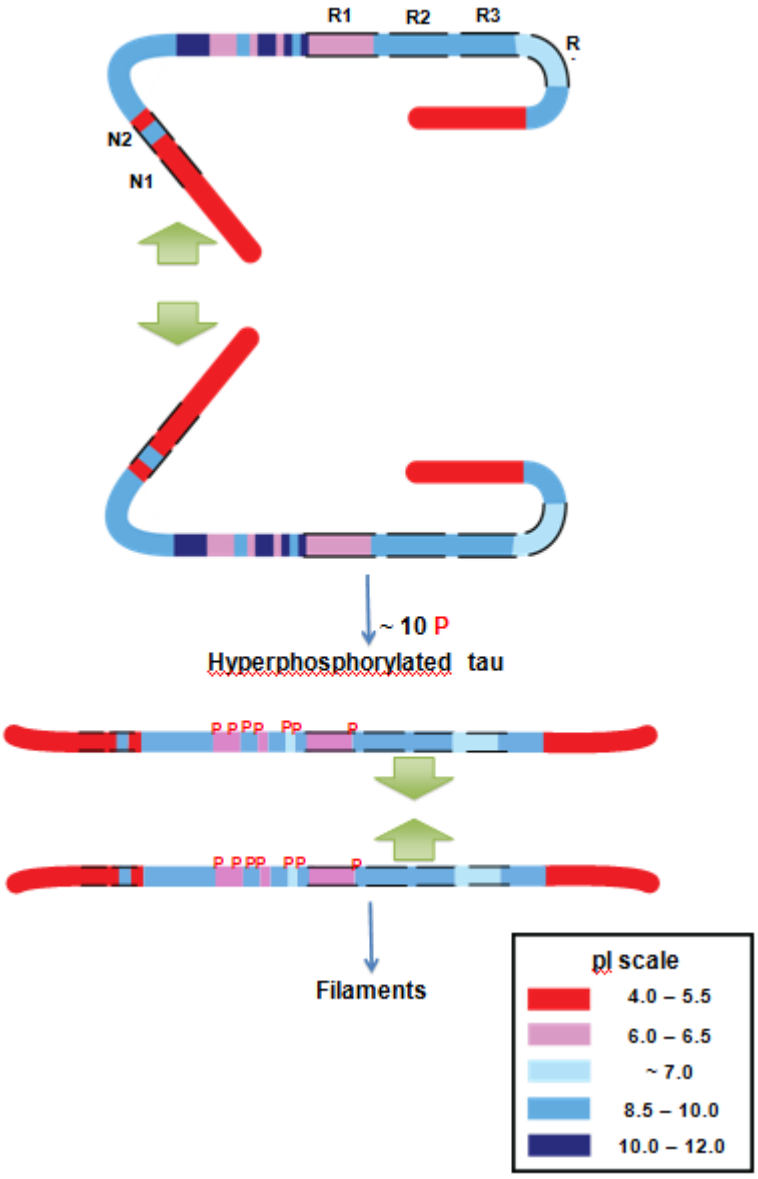

There are other explanations for the toxic event caused by aggregated tau. An increase in fibrils in the somatodendritic compartment is associated with fragmentation of the Golgi apparatus and abnormal morphology of the rough endoplasmic reticulum [7]. This has been observed in neuronal cultures and mouse models of AD. It is proposed that tau fibrils stress the ER thereby activating the unfolded protein response (UPR) and signaling for apoptosis in the affected neuron. This response has been demonstrated with a variety of misfolded proteins relating to Alzheimer's, Huntington's and Creutzfeld-Jacob diseases. Increased, but ineffective proteolytic activity in the cytoplasm leads to a secondary accumulation of proteins inside the ER, triggering the UPR [31].

There is some disagreement as to whether hyperphosphorylation drives tau aggregation into PHFs or if increased phosphorylation occurs due to aggregation. For this study, it is not necessary to distinguish between the two options. The self-recognition sequence (SRS) of tau is not affected by phosphorylation. Extensive work has been carried out to determine the residues necessary for filament formation, and changes outside of the SRS have little or no effect in both full length tau and the AcPHF6 construct. This construct's name comes from the six amino acid sequence necessary for PHF formation and it is acetylated on the amino terminus to mimic its position in the interior of tau.

The fact that mutations in tau cause NFTs but not amyloid plaques, yet mutations in APP give rise to both plaques and tangles, argue that amyloid pathology occurs upstream of tau aggregation in the AD brain. However, tau aggregation alone is enough to cause dementia. It is possible that Aβ exacerbates

a tauopathy which is progressing slowly and brings on a faster rate of decline. Regardless of upstream pathology, the aggregation of tau is neurotoxic and provides a potential druggable target that may be useful in the treatment or prevention of AD, CTE and the other tauopathies. However, the target cannot be validated until an inhibitor reaches the market.

1.3 Protein Aggregation Assay History

The experimental methods in this study built on the work on direct analysis of protein aggregation by mass spectrometry developed in the van Breemen laboratory by Dr. Xun Cheng. While different peptides are studied, the same approach is used and described here to show the tau specific changes that were made. Dr. Cheng's method was developed to measure the remaining amount of Aβ after a period of aggregation and subsequent filtration of the aggregates. Synthetic $A\beta_{1-40}$ was prepared and purified, dried and reconstituted in double distilled water to make a final concentration of 114 μM. The inhibitors were added singly to give a concentration of 200 μM, and the solution was allowed to incubate for 20 h at 37° C. The solution was centrifuged through a 10,000 molecular weight cut-off Millipore (Bedford, MA) regenerated cellulose ultrafiltration membrane to remove the aggregated protein. The filtrate was analyzed by flow injection positive ion mass spectrometry using a Micromass (Manchester, UK) Quattro II triple quadrupole mass spectrometer. The area under the curve for mass to charge ratio (*m/z)* 1083 was determined and compared with the negative control. Peaks of Aβ monomer from incubations with previously published inhibitors showed an increase

in the Aβ monomer relative to control, and therefore indicated inhibition of aggregation [32].

The method of Cheng, *et al.* [32] suffers from several limitations which are addressed in this dissertation. First, the procedure is low throughput and labor intensive, as only four compounds were tested. Also, flow injections suffer from ill-defined peak shape, which makes accurate AUC determinations difficult. Another limitation is that no reference compound was used to normalize the inherent fluctuations in instrument sensitivity. The molecular weight cutoff filters are quite expensive and limit the feasibility of utilizing them for high-throughput screening (HTS).

1.4 Short Peptide Segments to Study Assembly into Fibrils

The peptide sequence necessary for tau self-assembly into fibrils has been determined, and the unimportant regions of the protein can be omitted from assays to allow easier analysis and lower protein costs. The benefits of this simplified model are that the level of phosphorylation can be ignored, and small molecules that intervene in the self-recognition step can be identified. Recombinant tau lacking the self-recognition sequences (^{275}VQIINK^{280} in R2 and ^{306}VQIVYK^{311} in R3, known as PHF6) found in the MTBRs fail to form β sheet structures and higher order structures [33]. It was determined that acetylated short peptides based on the tau self-recognition sequences were capable of β-sheet formation and further polymerization, which could be measured using transmission electron microscopy, far-UV circular dichroism, Fourier transform infrared spectroscopy, and Thioflavin S fluorescence [34]. In order to mimic the charge distribution of the internal region of tau, the peptides

were acetylated on the amino terminus and amidated on the carboxy terminus, and the terminology "AcPHF6" is used to describe the construct.

The assay described here will not be the first to measure tau aggregation. The current method of screening utilizes UV detection of Thioflavin S, which binds tau fibrils, and works for full length tau as well as for short segments of tau. The kinetics of self-assembly were determined for a range of peptide constructs including AcPHF6 and other closely related segments. The constructs were dissolved in 20 mM MOPS buffer to make a concentration of 2.2 μM peptide, with 10 μM Thioflavin S as a fibril binding fluorophore, and the aggregation was initiated by the addition of sodium chloride at150 mM. The fluorescence of each mixture was determined every second for up to one hour. It was determined that the aggregation followed a seeded nucleation-elongation mechanism, and the first order rate constant of AcPHF6 aggregation was found to be $8.54 \times 10^3 \times s^{-1}$. Other related peptide constructs showed a lower rate, with some near zero. When analyzed by circular dichroism spectroscopy, the AcPHF6 construct showed a mean residue elipticity increase at 190 nm, characteristic of β sheet conformation, relative to the non-aggregating constructs. FTIR was used to study the structure of the fibrous peptides, and AcPHF6 showed low frequency amide I bonds between 1610 cm^{-1} and 1637 cm^{-1} and lacked a peak between 1684 cm^{-1} and 1704 cm^{-1}. These data indicate that the constructs form parallel β-sheet configuration. The transmission electron micrographs showed clear formation of filaments of ~5 nm in width and 1 to 2 μm in length, made from two parallel protofilaments [34].

1.5 Blood Brain Barrier

One reason for the general failure of small molecule treatments for AD is that most drugs are unable to penetrate the blood brain barrier (BBB), with reports as high as 95 to 98% of drugs currently on the market [35]. However, a successful tau aggregation inhibitor or CTE treatment capable of treating dementia patients must be able to do so, as direct cranial infusion in humans has proved problematic in clinical trials [36]. The BBB can be thought of as three distinct barriers; a physical endothelial barrier, an enzymatic barrier and an efflux barrier[37]. Drugs able to cross the BBB do so by lipid mediated free diffusion, usually have a molecular weight under 400 Da and typically contain fewer than 10 hydrogen bond donors or acceptors[38]. However, a chemical library used for screening should not be limited to compounds with these characteristics, as further examination may reveal a useable pharmacophore. Carrier-mediated BBB transport is also a possibility, as in the case of a metabolite of dopamine, dihydroxyphenylalanine, used in Parkinson's disease (PD) treatment [35]. Other polar substances with transporters capable of being saturated include single amino acids and glucose [39]. However, our understanding of carriers is poor, and no structure-transport relationships have been identified, as one would a structure-activity relationship. At this point, it would be lucky for a hit to be transported, but not out of the realm of possibility. Multiple laboratories are investigating the linking of small molecules to a known transported substrate.

The physical BBB is made up of specialized endothelial cells (ECs) located on the intraluminal side of the brain's capillaries. These specialized cells differ from

normal ECs by a having a high transendothelial electrical resistance and lacking fenestrations. Also, tight junctions between the specialized ECs block paracellular diffusion of small molecules from the blood to the brain parenchyma, also known as the luminal and abluminal sides, respectively [39]. Astrocytic cell end-feet push in between the specialized ECs to help stabilize the barrier[40], and nearby pericytes and neurons are believed to signal for differentiation and regulation of the BBB [41].

The enzymatic portion of the BBB presents a multitude of potentially inactivating enzymes both intracellularly and on the surface of the plasma membrane. Adenosine is an example of a circulating nucleoside which is capable of entering the brain by a transporter, but has no effect due to rapid enzymatic degradation [38].

Finally, the BBB also serves as a barrier by expelling small molecules using active efflux transporters (AETs). The best studied AET is the P-glycoprotein. If active efflux is found to be a limiting factor in BBB penetration, one strategy is to co-administer an AET inhibitor with the small molecule of interest [35].

1.6 5-Hydroxytriptamine Receptor Antagonists as Treatment for Dementias

A separate strategy from the inhibition of tau aggregation to improve the lives of frontotemporal dementia patients is to mask symptoms caused by the underlying pathology. While not changing the clinical outcome, increased cognition can improve the quality of life for patients and caretakers.

The serotonin system is comprised of neurons in the dorsal and ventral raphe nuclei which project to every region of the brain involved in cognition. At least 15

distinct receptors mediate the action of one neurotransmitter known as serotonin or 5-hydroxytryptamine, which gives the receptors the commonly used name of 5-HT receptors. There are 7 main families numbered sequentially as 5-HT1 through 5-HT7 and subfamilies of those receptors account for the other 8 distinct receptors [42]. Splice variants exist for many of the subtypes, bringing the number of distinct protein products to 30 or more, all of which recognize serotonin as a ligand [43]. This study focused on the 5-HT6 receptor, for which a small molecule antagonist was rationally designed by collaborative researchers [44].

The 5-HT6 receptor is distributed in regions of the brain responsible for memory formation, and the serotonergic system modulates many neurotransmitter pathways [45]. Cholinergic transmission is regulated by the serotonergic system and is implicated in cognitive decline [46,47]. Further evidence that 5-HT6 inhibition may be useful to reverse cognitive decline associated with dementia comes from testing rats in the water maze test. When treated with a direct injection of antisense oligonucleotides which knock down the 5-HT6 receptor specifically, rats improved spatial learning and memory in the test [48,49]. Small molecules capable of inhibiting the serotonergic receptor following oral administration would be much preferred to the repetitive direct cranial injection of oligonucleotides, which serve as a proof of principle, but is a poor clinical treatment option. Several compounds have been shown to bind the receptor in vitro, and are covered in the introduction to Chapter 5.

5-HT6 receptor antagonists have been shown to be effective in delayed non-match-to-sample (DNMS) tasks, an animal testing method which requires the animal to choose the reverse decision to the previous occasion [50]. This test has been shown

to identify age-related deficits in humans [51], primates [52], and rodents [46], making it a good way to evaluate compounds for efficacy. Lesions of one or more of the hippocampus, prefrontal cortex and subiculum occur with dementias, and also impair the performance of subjects on the DNMS task.

CHAPTER 2

DEVELOPMENT OF A NOVEL TAU AGGREGATION ASSAY

2.1 Introduction

Natural products provide a wider variety of chemical structures displaying more chiral centers and greater steric complexity than synthetic chemical libraries [53]. Among the new chemical entities (NCEs) filed between 1981 and 2002, 49% were natural products or were based on natural product leads[54]. However, pharmaceutical industry funding of natural product research began to fall in the 1990s partially due to the increased emphasis on HTS, combinatorial chemistry, and better defined molecular targets [55]. Many HTS assays require the testing of a single compound at a known concentration to determine a hit, removing the vast libraries of natural product fractions from consideration. Another contributing factor to the decline of natural product research in private industry is the relative difficulty of isolation, identification, and scale up of identified hits. It is possible to make a larger library using combinatorial chemistry at a lower cost than to fractionate extracts from natural sources. The counter-argument to this line of reasoning is that a greater structural diversity will be represented in the natural products, requiring the screening of fewer "wells" to generate a lead compound.

There are several reasons natural products make good potential inhibitors of protein-protein interactions. Natural product libraries are made up of privileged structures, evidenced by their binding to a wide variety of protein targets in many therapeutic areas [56]. Organisms have evolutionary pressure to form molecules

capable of interacting with protein targets to elicit an effect [57]. These somewhat promiscuous ligands can be rationally modified to provide more specific and tighter binding during the drug development process [57]. There are fewer unique protein architectures formed by folding than is theoretically predicted [58] and differing protein sequences can give rise to the same overall folding [59]. Molecules able to interact with one endogenous fold will be able to affect different proteins in higher organisms [60]. Proteins with very different functions have evolved from common ancestral proteins retaining similar active sites [61].

The larger size of natural products and their tendency to interact with a variety of folds at the surfaces of proteins make them more likely to be hits for the disruption of protein aggregation than synthetic molecules designed with a specific target in mind. Binding to the active site of an enzyme requires a smaller molecule with a few strong interactions, whereas blocking the self-recognition sequence of a protein calls for a larger molecule with many weak interactions. For example, a scaffold isolated from soil actinomycetes lead to the development of three phase-III drugs, tacrolimus, rapamycin and ascomycin, which all bind the FK506-binding protein and modulate the signal transduction pathway of T-cell activation and growth [62-64]. See Fig. 2.1 for the structures of several selected small molecule protein-protein interaction inhibitors. This research provides a pathway for identification of a lead compound which can be further developed into drug candidates.

The screening for inhibitors of tau construct aggregation has been previously confined to pure, single compounds due to three distinct limitations of the fluorescence assays that have been used to date. These limitations can be

Fig. 2.1. The structures of rapamycin (A), tacrolimus (FK506) (B), and ascomycin (C), all of which bind the FK506-binding protein immunophilin proteins, but modulate the protein-protein interactions involved in signal transduction differently.

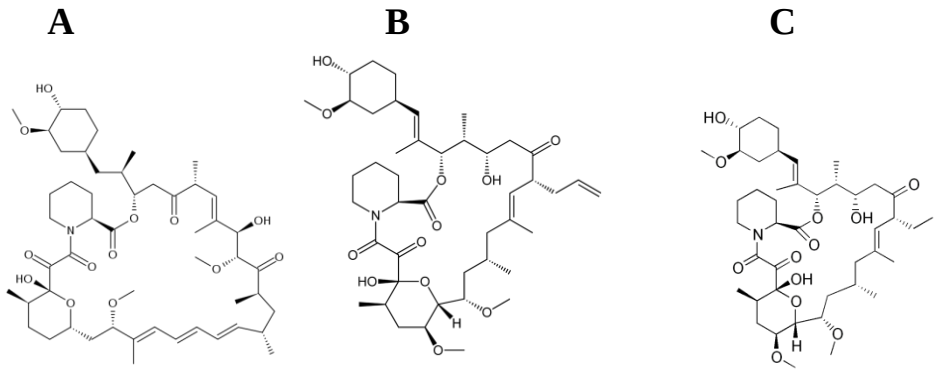

described as a relatively high protein and analyte consumption, a high rate of false positives or negatives caused by the absorption of excitation or emission wavelengths, and quenching of fluorescence by iron or copper ions commonly found in natural product extracts and fractions. When screening using a longer construct or full length tau, these costs would become much more important to consider, and may limit the amount of compounds that can be screened.

A mass spectrometry-based assay would probably be more sensitive than its fluorescence counterpart, allowing for the reduced consumption of both peptide and compound tested, for the following reasons. A published 96-well plate fluorescence assay used 20 µg of construct per well [65]. The testing of one plate would consume nearly 2 mg of AcPHF6 construct. Natural products are commonly stored and distributed at 5 mg/mL, and testing would require at least 10 µL per well. This amount is not practical for natural products from microbial incubations, for example, since ~5 µL (of 5 mg/mL solution) per fraction is typically obtained from a 2 L microbial incubation, which can take several months to obtain (Prof. Brian Murphy, UIC, personal communication). This is especially important for natural product isolations which can yield just several micrograms per fraction collected.

Natural product fractions are often turbid, colored, able to absorb UV light, or fluoresce, any of which can cause dramatic increases in background noise of light-based screening assays [66]. When screening a mixture of compounds, one minor interfering constituent can render the assay useless for all of the other compounds being tested. One method for getting around this problem is the use of europium during competitive binding assays. However, radioisotopes increase assay costs in

terms of materials and disposal of wastes as well as increasing risks to lab personnel [66].

Copper, commonly found in fractions of natural product extracts, has been shown to quench fluorescence in screening assays. The phenomenon is reversible by addition of copper chelators [67], but this not practical for large-scale screening. The fluorescence quenching of fluorophores by iron has been used to spectromerically determine the concentration of the metal in solution. The interference in a fluorescence assay by these commonly occurring metals precludes the testing of natural products in fluorescence based assays. Therefore, another assay method is needed to screen for natural products that prevent aggregation of tau or other proteins.

2.2 Materials and Methods

2.2.1 Reagents

LCMS-grade acetonitrile and ammonium acetate were purchased from Thermo Fisher (Fair Lawn, NJ). Formic acid (FA), DMSO, pyrimethamine, sodium chloride, and 1,1,1,3,3,3-hexafluoroisopropanol (HFIP) were purchased from Sigma-Aldrich (St. Louis, MO).

2.2.2 Construct Synthesis and Purification

The peptide AcPHF6 (Fig. 2.2), which was used as a surrogate for tau in the MS-based aggregation assay, was synthesized by the Protein Research Lab (UIC, Chicago, IL) using Fmoc protected amino acids and acetylated on the aminoterminus by reaction with acetic anhydride in the presence of pyridine. After

synthesis, the construct was dissolved in a 1:1 mixture of HFIP and 87% FA, purified by HPLC and lyophilized. The dry peptide construct was stored in a desiccator until use in the aggregation assay.

2.2.3 Sample Preparation

The incubation solution contained 20 mM ammonium acetate buffered to pH 7.4 using aqueous ammonia, 4.5 μM pyrimethamine (internal standard, structure in Fig. 2.2), and 15 mM sodium chloride to promote aggregation. The aggregation kinetics of tau have been found to be highly dependent on buffer conditions, and previously described methods note that an increasing concentration of NaCl increases the aggregation rate [68]. A 98 μL aliquot of incubation solution was pipeted into an autosampler vial (Fisherbrand, Fisher Scientific), to which 1 μL of natural product extract dissolved in DMSO was added. At the time of LC-MS-MS analysis, 1 μL of 2 mM AcPHF6 in HFIP was added to the autosampler vial and vortex mixed.

2.2.4 Assay Development

The use of selected reaction monitoring (SRM) mass spectrometry allows for great selectivity of the analyte while minimizing background noise and noise from contaminants. SRM is the "acquisition of data in tandem mass spectrometry data in which a precursor ion of a particular fragmentation product from that precursor is selected in the second stage[69]." The precursor ion of AcPHF6 was selected by obtaining a positive ion electrospray mass spectrum in scan mode using a Shimadzu (Kyoto, Japan) LCMS-8030 triple quadrupole mass spectrometer. The expected $[M+H]^+$ was observed at *m/z* 790.

Fig. 2.2. The structures of the AcPHF6 construct (A) and, pyrimethamine (B).

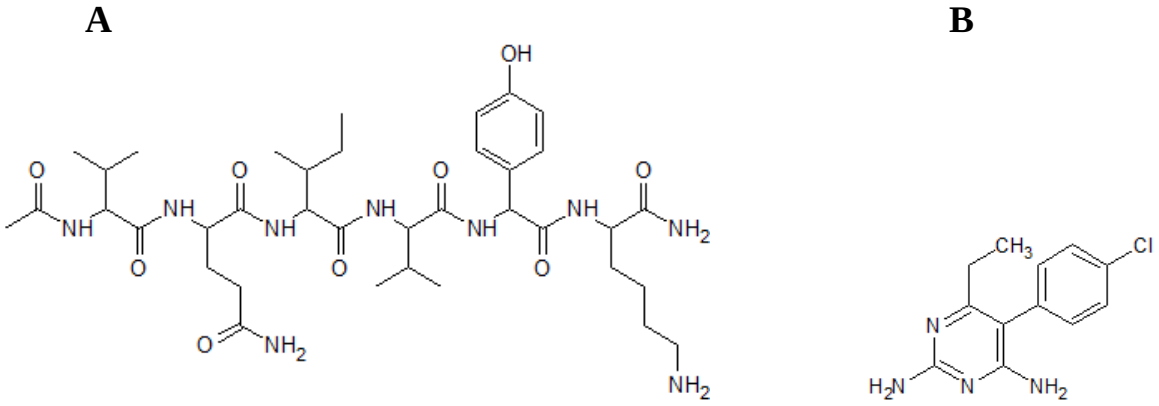

The product ions resulting from collision-induced dissociation (CID) of *m/z* 790 were measured using a product ion scan function with Shimadzu LabSolutions software. By changing the CID collision energy, different abundances of product ions were produced. Repeated flow injections of the AcPHF6 and pyrimethamine were made to determine the collision energy at which the highest abundances of structurally significant fragment ions could be produced. Figs. 2.3 and 2.4 show the effect of changing the collision energy on both AcPHF6 and pyrimethamine on product ion abundance. By increasing the intensity of product ion instrument response, a greater sensitivity is achieved. This increased sensitivity allows for the quantitation of lower concentrations of AcPHF6 than would be otherwise possible. The use of 50 eV resulted in the highest abundance of counts, whereas the possible lower settings of 45 and 40 eV decreased the counts. The combination of precursor ion *m/z*, optimized collision energy, and product ion *m/z* values define the parameters of an SRM experiment. Two transitions of each analyte were monitored for quality control, since changes in their ratio would indicate interference by co-eluting compounds or impurities in the mobile phase. A reference ion ratio was set at 40%, with a 20% variance in area allowed.

Fig. 2.3. Positive ion electrospray CID product ion mass spectra of AcPHF6 using CID energy settings of -50 eV (A), -45 eV (B), and -40 eV (C). The maximum instrument value of -50 eV was chosen to fragment the precursor ion of *m*/z 790 to the product ions of *m*/z 270 and *m*/z 129 because it resulted in the highest count abundance.

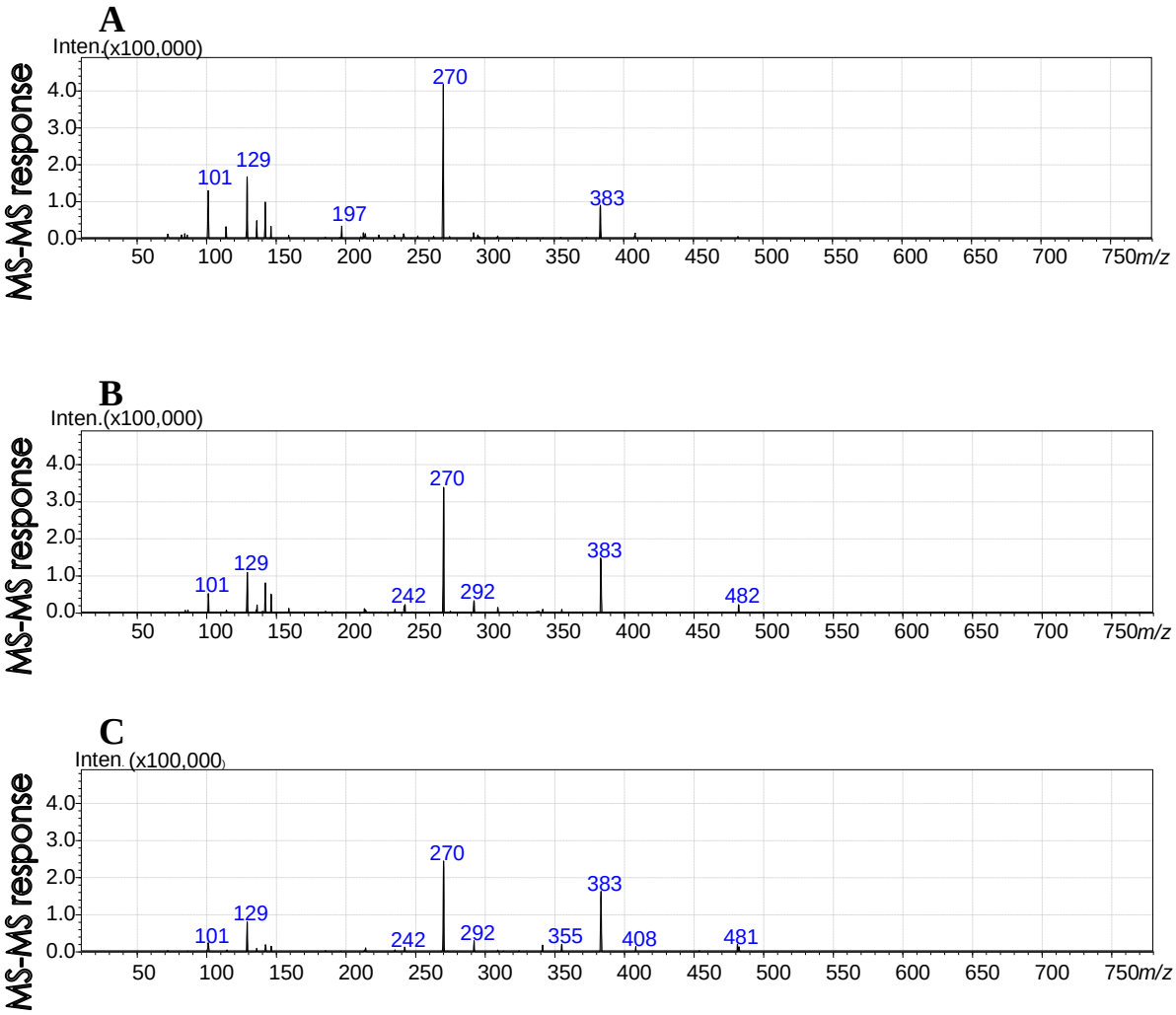

Fig. 2.4. Positive ion electrospray CID product ion mass spectra of pyrimethamine (internal standard) using CID energies of -40 eV (A), -35 eV (B), and -30 eV (C). A collision energy of 35 eV was chosen for the SRM of *m*/z 249 to *m*/z 177 and a collision energy of 30 eV was chosen for the SRM of *m*/z 249 to the product ion of *m*/z 233.

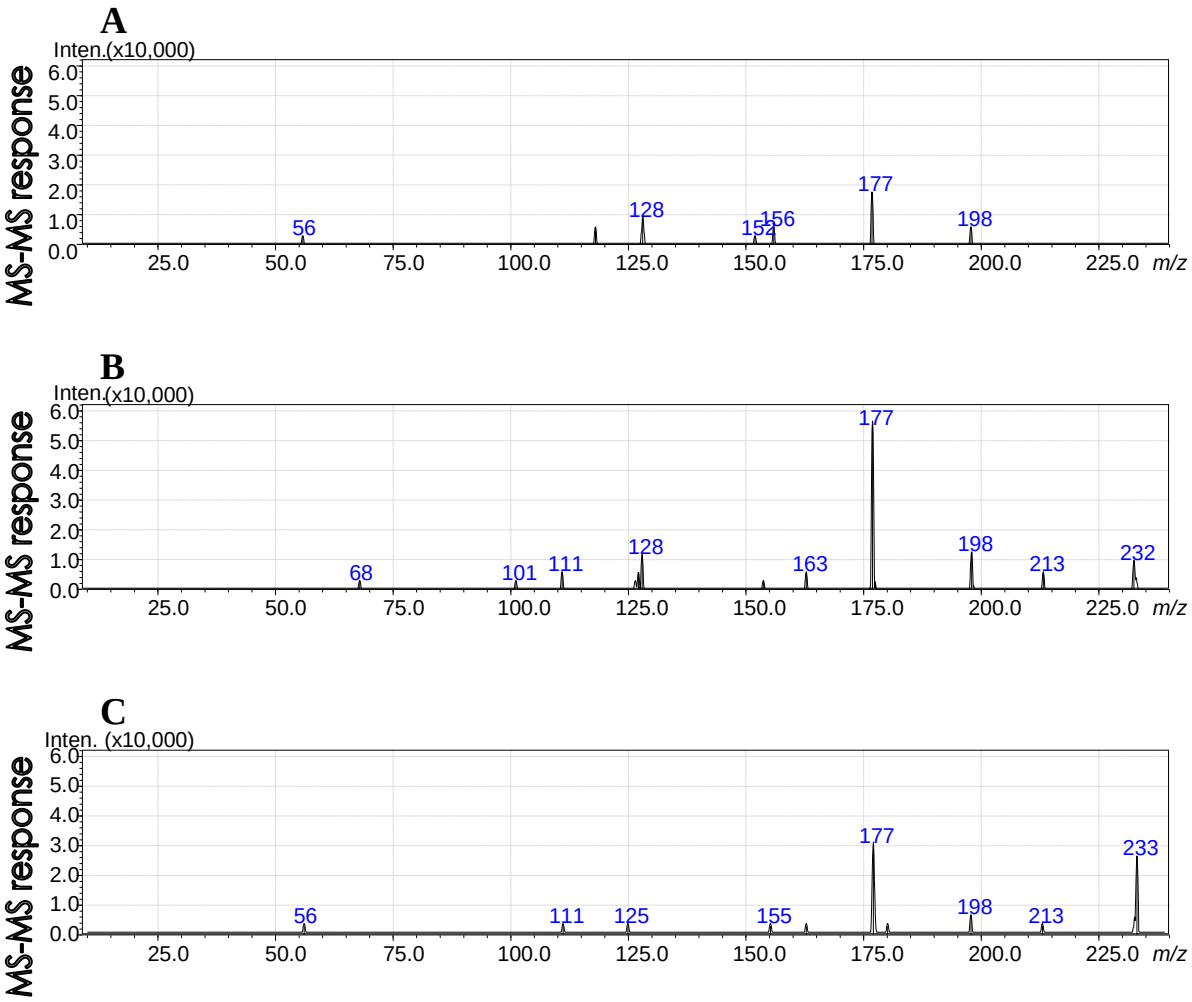

A Shimadzu Nexera LC-30AD UHPLC system interfaced to a Shimadzu LCMS-8030 mass spectrometer was used equipped with a solvent degasser, refrigerated autosampler (4°C), and column oven (40°C). The UHPLC mobile phase consisted of isocratic acetonitrile/0.2 % FA in deionized water (18:82; v/v) at a flow rate of 0.4 mL/min. Separations were obtained using a Shimadzu Shimpack XR-ODS III (2.0 x 50 mm, with 1.6 µm packing) UHPLC column, and the sample injection volume was 0.1 µL. The 8030 triple quadrupole mass spectrometer was operated in positive mode using an electrospray source and SRM. The SRM transitions of *m*/z 790 to 270 and *m*/z 790 to 129 were monitored for AcPHF6, and the SRM transitions of *m*/z 249 to 177 and *m*/z 249 to 233 were recorded for the internal standard pyrimethamine. The following instrument parameters were used: an interface voltage of 4.5 kV, a heat block temperature of 400°C, a desolvation temperature of 250 °C, and a dwell time of 25 msec per SRM transition. The area of each peak in the SRM chromatograms was determined, and the ratio of the quantifier transitions for AcPHF6 and pyrimethamine were computed and graphed every 2 min for 39 min.

2.2.5 Choice of Internal Standard

The selection of an appropriate internal standard for this mass spectrometry-based aggregation assay provided some unique challenges. The gold standard of an internal standard in mass spectrometry is a stable isotope labeled version of the analyte to be measured. However, in an aggregation assay, the labeled construct would simply aggregate along with the analyte, so that their peak area ratios would be expected to remain unchanged.

To achieve the shortest possible chromatographic separation, the internal standard needed to have a retention time similar to the AcPHF6 construct. While the internal standard and analyte should have similar retention times, coelution would not be ideal because of the possibility of interference caused by ion suppression of one by the other. It was found that caffeine and pyrimethamine, two readily available standards, eluted most closely to the analyte. The internal standard needed to be stable for at least 24 h in solution. A mixture of AcPHF6, caffeine and pyrimethamine was made in 20 mM ammonium acetate (pH 7.4) and incubated without NaCl in 3 different autosampler vials. The raw peak areas (AUCs) were plotted over time (Fig. 2.5) and pyrimethamine was determined to be the most appropriate internal standard for this analysis based on stability. The decreasing concentrations of pyrimethamine and caffeine are likely due to adsorption of the compounds onto the interior surface of the autosampler vial. The incubation solution was made fresh every day and was only stored in the vial for 12 hours maximum; highlighted by the green box in Fig. 2.5.

2.2.6 Choice of AcPHF6 Stock Solvent

Aggregation assays using AcPHF6 have previously dissolved this monomer in water for immediate use [68,70]. Once dissolved in water, aggregation of ACPHF6 will slowly occur, potentially altering inter assay results. Therefore, improved assay procedures were needed to increase reproducibility. Enhanced throughput was also needed. HFIP treatment has been reported to keep AcPHF6 in its monomeric form in solution [26], but it had to be determined whether using this solvent would

Fig. 2.5. The raw peak areas (AUCs) plotted over time to determine whether the potential internal standards pyrimethamine and caffeine were unstable in solution. While the experiment was carried out over 80 hours, only the 16 hour time point was necessary once the assay was developed (green box).

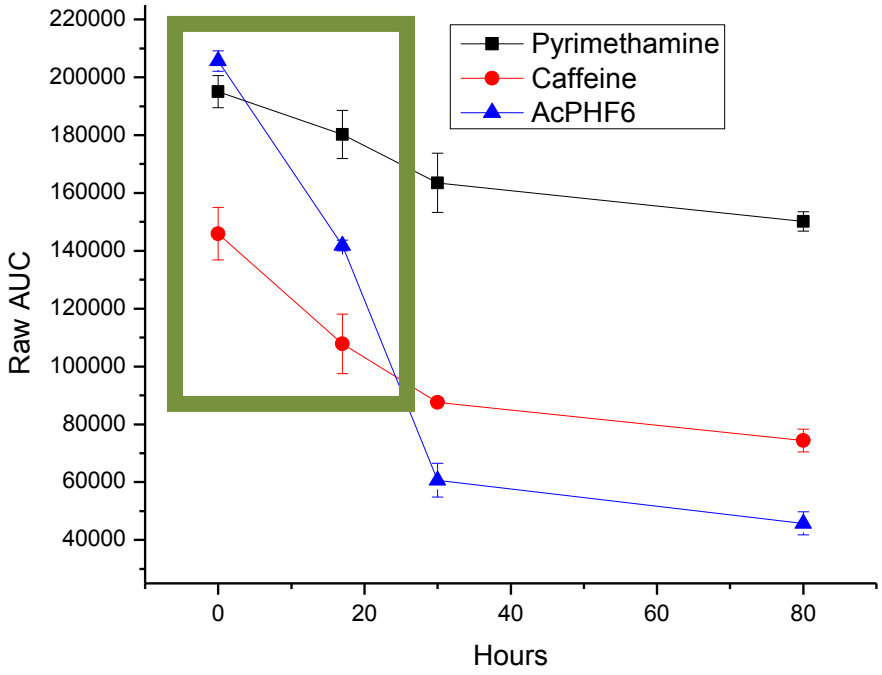

affect the aggregation assay. AcPHF6 was either dissolved directly into water or into HFIP to a concentration of 2 mM and 1 µL added to 99 µL of incubation buffer as described above. The same LC-MS-MS method and data analysis were followed as described above.

2.2.7 Considerations When Using Salts an a Mass Spectrometry Based Assay

Another hurdle in the development of this assay was the incompatibility of LC-MS with sodium chloride, which was used to speed aggregation and increase throughput. Nonvolatile salts are known to deposit crystals on the electrospray source as the surrounding mobile phase evaporates. Even small amounts of salt can build up over time, decreasing ionization efficiency of the source, and making it necessary to interrupt analysis for instrument maintenance. The experiment to determine the time necessary to wash NaCl through the analytical column following sample injection used caffeine as a surrogate, because it can be detected by the mass spectrometer. A 1 µL injection of 2 µM caffeine in water was made under conditions that would not retain this analyte, and the SRM transition of *m*/z 195 to 138 corresponding to caffeine was analyzed over time. The UHPLC system was set to 50% acetonitrile and 50% 0.1% FA in deionized water at a flow rate of 0.4 mL/min, which is the same flow rate used in the AcPHF6 aggregation assay. The same UHPLC column, PEEK tubing, and LC flow diversion valve was used as well.

2.2.8 Disaggregation Study

This experiment was carried out as was the AcPHF6 aggregation assay described above, except that 30 min after initiation, an equal volume of HFIP was added directly to the autosampler vial. Then, UHPLC-MS-MS analysis was carried out

as before to determine if AcPHF6 was reversed by HFIP. A ratio of the AcPHF6 AUC to the internal standard AUC was graphed to determine if HFIP could disaggregate AcPHF6. By using an internal standard, dilution of sample resulted in the same area ratio.

2.3 Results and Discussion

The UHPLC-MS-MS AcPHF6 aggregation assay was used as a proof of principle test to determine the feasibility of screening a library of natural products. This MS-based assay would overcome the problems associated with fluorescence assays. The assay was tested for precision, reliability, reproducibility, and freedom from carryover.

In order to determine whether a stock solution of AcPHF6 could be prepared in HFIP or would require water, stock solutions in each solvent were prepared at 2 mM and analyzed as described in section 2.3.3. The advantage of using HFIP as the stock solvent is that it inhibits fibril formation, allowing the same stock solution to be spiked into an aqueous buffer where aggregation can occur. Previous studies have required the construct to be brought up in water and used immediately. The AUC ratio of each the conditions were plotted in Fig. 2.6. The result is that the aggregation rate was not changed significantly by the HFIP solvent. A 100 fold dilution is enough to initiate aggregation.

Fig. 2.6. The aggregation of AcPHF6 using either HFIP (black squares, n=3) or water (red circles, n=1) was plotted over time to determine whether HFIP could be used to prepare the stock solvent. The stock solution of HFIP prevented aggregation from occurring prior to analysis and did not interfere with aggregation once diluted 100-fold into incubation buffer.

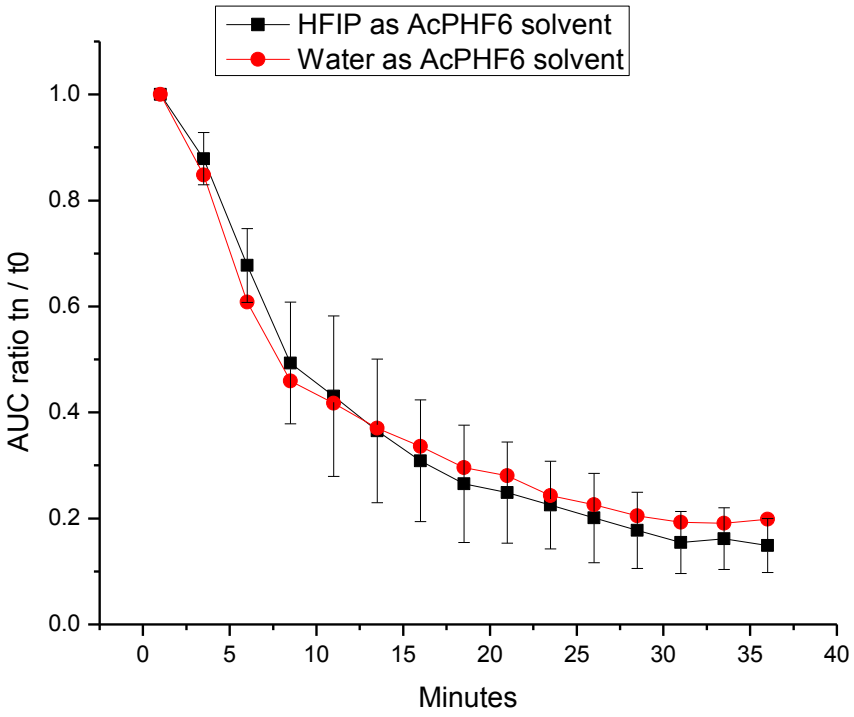

The elution of the unretained caffeine is displayed in Fig. 2.7 and models the rate at which NaCl would be pumped through the HPLC system. This information was necessary to determine the point at which the UHPLC flow diversion valve should be switched from sending the mobile phase to waste to sending it to the mass spectrometer for analysis. This step enhances throughput by preventing signal suppression, decreased ionization efficiency, and electrospray needle clogging. Based on the data in Fig. 2.7, the divert valve should be switched from waste to the mass spectrometer after 0.5 min. Since caffeine is more hydrophobic than sodium and chloride ions, this provides a upper limit as to the time that the ions could be retained by a reverse phase column.

2.3.1 Analytical Method Validation

It is important to validate the analytical method used to prove the method is precise, reproducible and rugged in the range of analytical conditions. Furthermore, the reliability of the assay should be tested so that method development will not be required on each new day of screening. The UHPLC system, mass spectrometer and software all need to be validated as a system.

A system suitability standards mixture was utilized to evaluate inter-assay system performance. The sample used was a screening vial which was allowed to aggregate to its endpoint. There was still enough monomer in solution to make a measurement at the lowest concentration of AcPHF6 that could be expected to occur during the screening assay. The internal standard had previously been determined to be stable long-term (Fig. 2.5).

Fig. 2.7. The positive ion electrospray UHPLC-MS/MS SRM chromatogram of caffeine using mobile phase conditions that eluted this analyte without retention. This experiment was used to determine the void volume of the system used to analyze AcPHF6 aggregation. Based on these data, NaCl in the incubation solution would elute before 0.5 min.

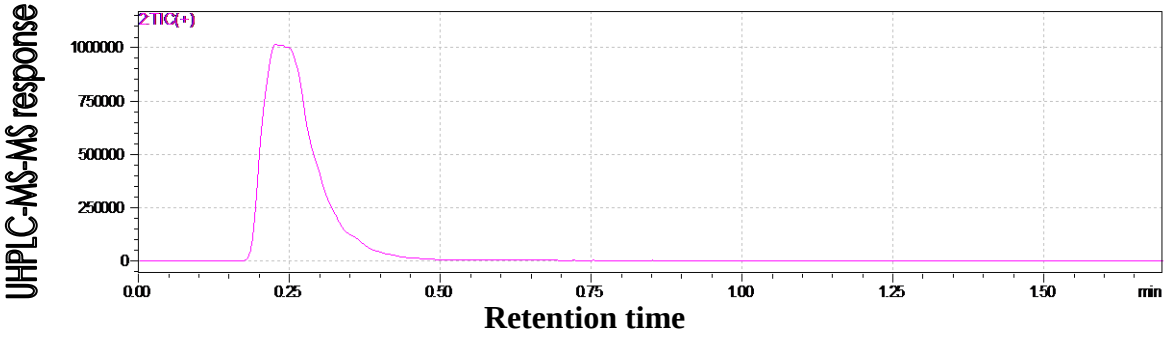

The retention time of the analyte and internal standards must be reproducible over many analyses. While no formal guidelines are in place for this type of study, a relative standard deviation of 5 % (%RSD) or less demonstrated that the UHPLC-MS system was operating in a reproducible manner. Five consecutive analyses used the same vial of 20 µM AcPHF6 and 4.5 µM pyrimethamine, and the chromatograms are shown in Fig. 2.8. The retention times were determined automatically by LabSolutions software and the mean, SD, and %RSD were calculated and summarized in Table I. The %RSD was determined to be 0.606% and 0.641% for AcPHF6 and pyrimethamine respectively. These values far exceed commonly used guidelines and are indicative of a stable, reproducible LC-MS system.

To determine the fluctuation in instrument performance and inherent error, the AUC was calculated for quantifier and qualifier SRM transitions of AcPHF6. The ratio of these areas was calculated and the mean, standard deviation (SD) and %RSD of the ratio is shown in Table II. The same calculation was performed for the internal standard. The %RSD for each was less than 1%, which is considerably better than the UHPLC system specification of less than or equal to 2%.

The area ratios of the quantifier SRM transitions for AcPHF6 and pyrimethamine were determined (Table III). Although the raw area values varied significantly from injection to injection, the ratios remained relatively constant, with a %RSD of about 3.7%. The raw areas likely varied due to the volume actually injected by the autosampler.

Fig. 2.8. Retention time reproducibility of the UHPLC-MS system was tested by making 5 repeat injections of AcPHF6 containing the internal standard pyrimethamine onto the system as previously described. The retention times were determined at maximum peak height.

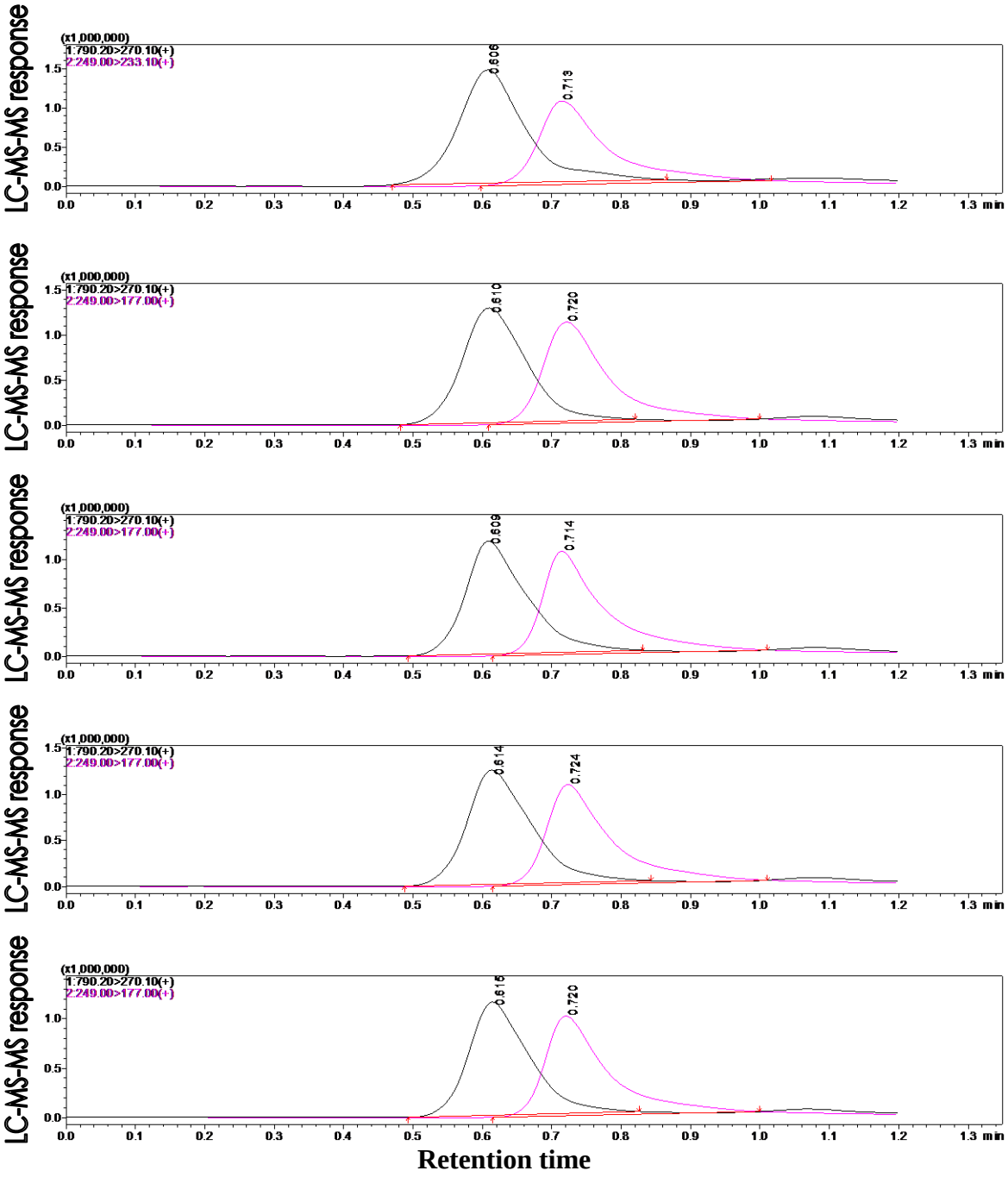

TABLE I. THE RETENTION TIMES OF 5 REPEAT INJECTIONS WERE DETERMINED BY USING A SOFTWARE ALGORITHM, AND THE MEAN, SD, AND %RSD WERE CALCULATED TO DETERMINE THE SYSTEM VARIABILITY. THE UHPLC SYSTEM SPECIFICATION WAS ≤2%RSD

	Rep 1	Rep 2	Rep 3	Rep 4	Rep 5	Mean	Std. Dev.	%RSD
AcPHF6	0.606	0.610	0.609	0.614	0.615	0.611	0.00370	0.606
Internal standard	0.713	0.720	0.714	0.724	0.720	0.718	0.00460	0.641

TABLE II. THE RAW AUCS OF THE UHPLC-MS/MS SRM QUANTIFIER AND QUALIFIER FOR ACPHF6 AND INTERNAL STANDARD PYRIMETHAMINE. THE AREA RATIOS WERE USED TO CHECK FOR INSTRUMENT FLUCTUATION.

	AcPHF6 Quant	**AcPHF6 Qual**	**AcPHF6 AUC Ratio**	**Int Std Quant**	**Int Std Qual**	**Int Std AUC Ratio**
Replicate 1	9,863,385	3,074,932	3.208	8,347,405	7,542,286	1.107
Replicate 2	8,240,900	2,549,323	3.233	7,486,963	6,677,605	1.121
Replicate 3	7,262,229	2,275,838	3.191	6,764,475	5,988,370	1.130
Replicate 4	8,072,913	2,508,173	3.219	7,169,396	6,377,478	1.124
Replicate 5	7,005,150	2,181,504	3.211	6,412,410	5,738,212	1.117
Mean	8,088,915	2,517,954	3.212	7,236,130	6,464,790	1.120
Std. Dev.			0.0152			0.0086
%RSD			0.4740			0.7641

TABLE III. UHPLC-MS/MS SRM AREA RATIOS OF ACPHF6 TO INTERNAL STANDARD REMAINED NEARLY CONSTANT FROM INJECTION TO INJECTION, SHOWING THAT ERROR INTRODUCED BY THE AUTOSAMPLER INJECTING SLIGHTLY DIFFERENT VOLUMES IS CANCELED OUT BY THE USE OF AN INTERNAL STANDARD. IT ALSO PROVES THAT PYRIMETHAMINE IS A SUITABLE INTERNAL STANDARD, BECAUSE AS THE RAW AREA OF ACPHF6 INCREASES, SO DOES THE IS.

	AcPHF6 Quant	IS Quant	Quant AUC Ratio
Replicate 1	9,863,385	8,347,405	1.182
Replicate 2	8,240,900	7,486,963	1.101
Replicate 3	7,262,229	6,764,475	1.074
Replicate 4	8,072,913	7,169,396	1.126
Replicate 5	7,005,150	6,412,410	1.092
Mean	8,088,915	7,236,130	1.115
Std. Dev.			0.0418
%RSD			3.7489

Mass spectrometry-based assays can be prone to carryover, which is the reintroduction of analytes not sufficiently washed out of the previous injection. Often introduced by the autosampler needle or precolumn tubing, carryover must be assessed to determine the robustness of the assay. Carryover can be tested for by injecting a solvent blank sample after injecting a non-zero sample or standard. After analyzing the 5 replicates described previously, a 0.1 µL injection of deionized water was made using the same method, but with one modification. The switching valve was not used so that the entire chromatogram could be monitored for a carryover peak. This was done so that a carryover peak would not be missed as the void volume was sent to waste. The chromatograms for all four transitions monitored are displayed in Fig. 2.9. No significant carryover was observed in the 53rd analysis of the day during the screening of natural products.

AcPHF6 allowed to aggregate could be disaggregated by the addition of HFIP as shown in Fig. 2.10. The assay follows the same general pattern as previous research by the Goux and Nowick research groups [68,70,71]. HFIP unfolds proteins and breaks aggregation of many proteins, including tau [34,72,73]. The six electronegative fluorine atoms likely serve as hydrogen bond acceptors and displace the hydrogen bonding between amino acids responsible for the aggregation . Fig. 2.11 shows the aggregation occurring over time, indicated by the decrease in monomer as the construct forms higher order structures. The interruption of this process would be considered a positive hit of a tested fraction, since the aggregation of AcPHF6 models the pathologic aggregation of tau; a hallmark of frontotemporal dementias.

Fig. 2.9. The injection of blanks throughout the screening process is useful to monitor for carryover. These UHPLC-MS/MS SRM chromatograms show no carryover even though this was the 53rd injection in a series of natural products screening.

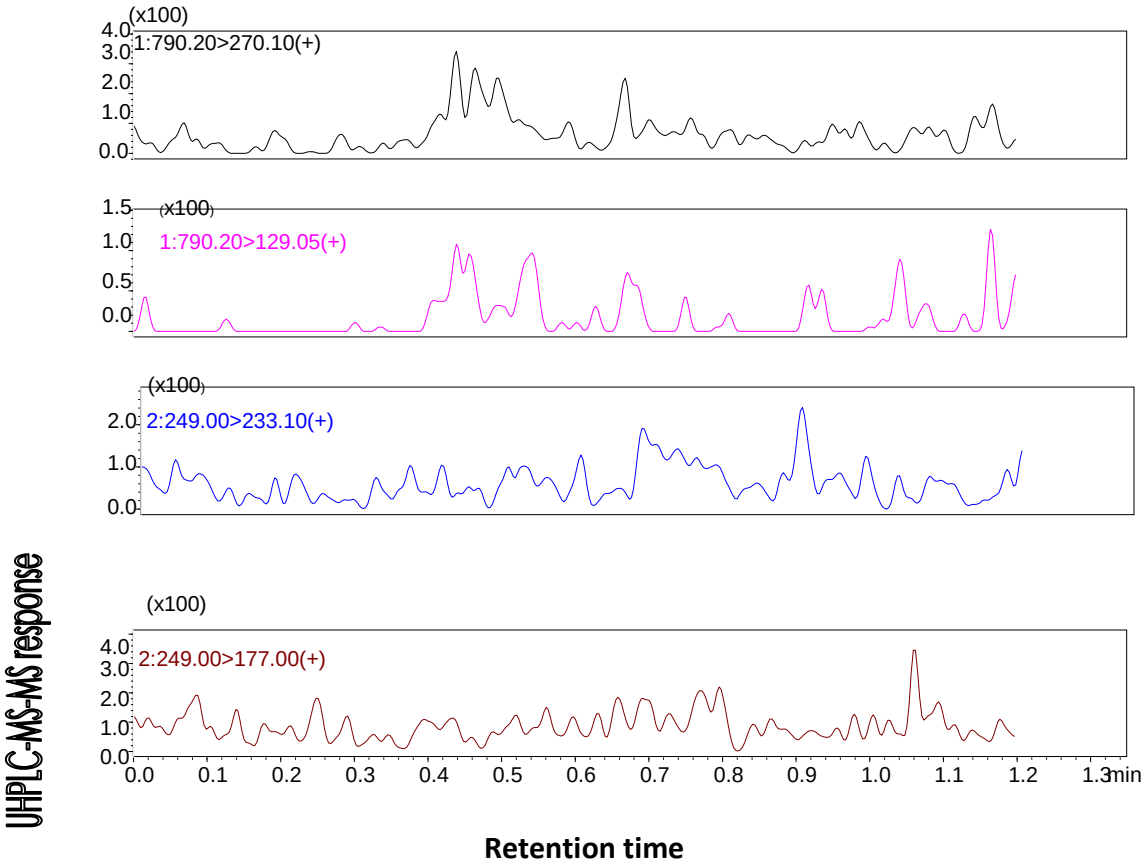

Fig. 2.10. After previously described mass spectromeric analysis and data processing, the area ratio of AcPHF6 to internal standard was graphed over time to demonstrate the ability to disaggregate the incubation solution in real time. The time point after which HFIP was spiked in is denoted by the arrow.

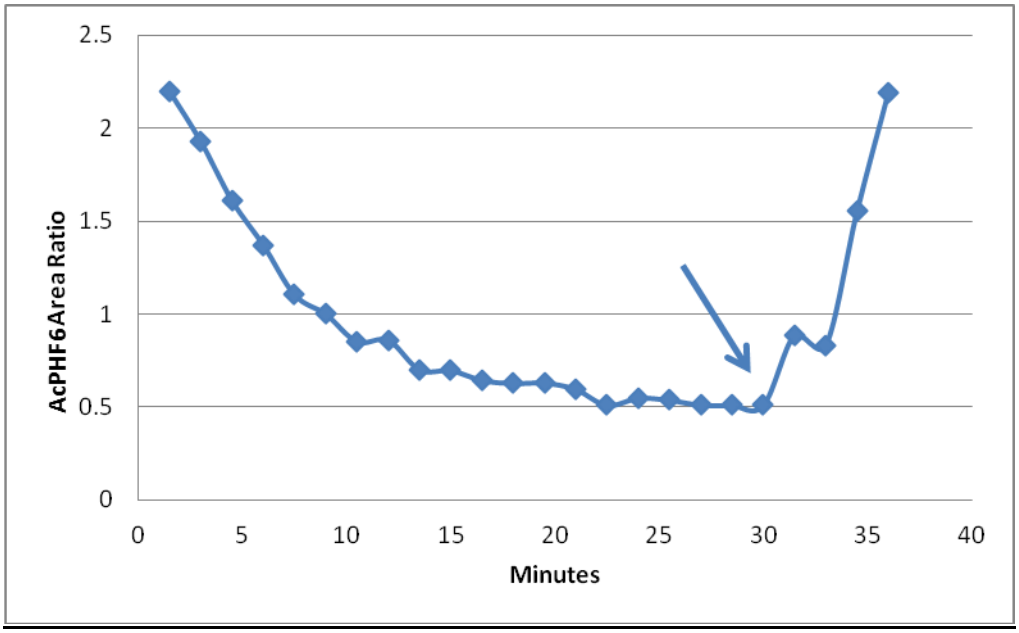

Fig. 2.11. The area ratio of AcPHF6 to the internal standard was determined every 2.5 min to monitor the aggregation over time for 4 replicates.

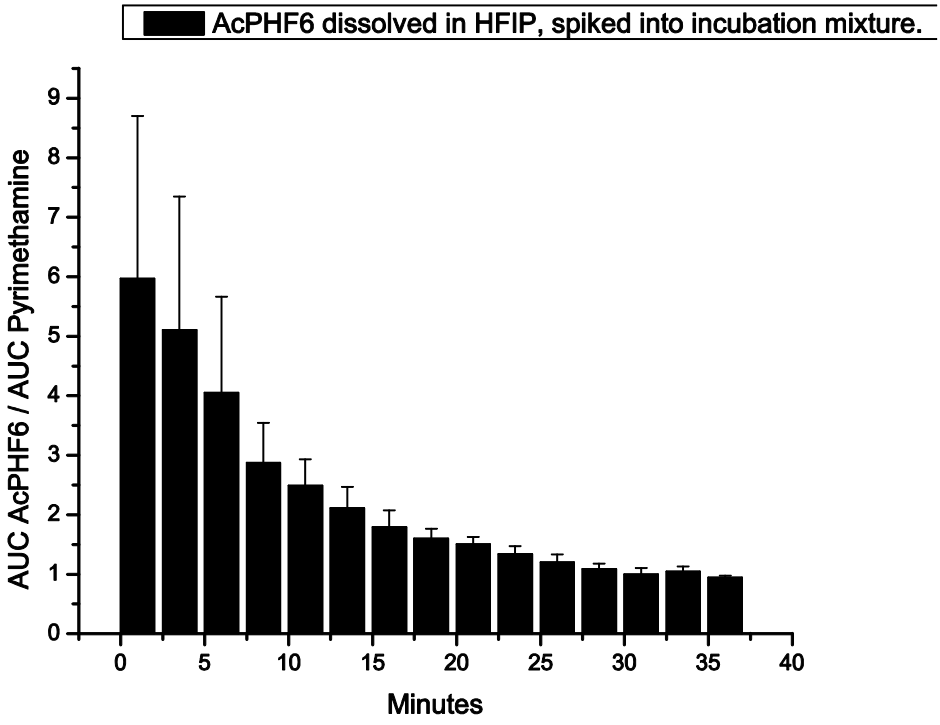

2.4 Conclusion

A novel UHPLC-MS/MS method to measure tau protein aggregation was developed. The amount of AcPHF6 monomer remaining in an incubation solution could then be used for the evaluation of natural product inhibitors of aggregation. The assay is capable of monitoring the monomer directly, instead of the previous approach of using fluorescence measurement, which does not work well with natural product screening. The assay can be adapted to a high-throughput format to test multiple natural product fractions available to the laboratory, which was the next step in this research project. As a proof of concept experiment, the addition of an equal volume of HFIP caused the breakup of aggregation, which could be observed in real time.

The optimized UHPLC-MS-MS method was determined to be specific for the analytes tested and free from carryover and excessive noise. A suitable internal standard, pyrimethamine, was found and used to normalize volume injection error by the autosampler, as well as to correct for fluctuations in instrument response. It was determined that disaggregating AcPHF6 in HFIP prior to the assay did not affect subsequent aggregation kinetics compared with water, and this was consistent with the literature. The use of a flow switching valve was investigated and found suitable to remove NaCl prior to introduction to the mass spectrometer, which improves performance when analyzing many samples per day. Finally, the analytical method was partially validated and checked for excessive retention time changes, instrument fluctuation and applicability of pyrimethamine as an internal standard to correct for instrumentation fluctuation.

CHAPTER 3

HIGH-THROUGHPUT SCREENING OF NATURAL PRODUCTS IN THE ACPHF6 AGGREGATION ASSAY

3.1 Introduction

Goux and colleagues developed the AcPHF6 construct based on the nucleation sequence in full length tau [68]. The benefits of this simplified model are that the level of phosphorylation can be ignored, and small molecules that intervene in the self-recognition step can be identified. Recombinant tau lacking the self-recognition sequences (^{275}VQIINK^{280} in R2 and ^{306}VQIVYK^{311} in R3 and known as PHF6) found in the MTBRs fail to form β-sheet structure and polymerize [33]. It was determined that acetylated short peptides based on the tau self-recognition sequences were capable of β-sheet formation and further polymerization by transmission electron microscopy, far-UV circular dichroism, Fourier transform infrared spectroscopy, and Thioflavin S fluorescence [34]. In order to mimic the charge distribution of the internal region of tau, the peptides were acetylated on the amino terminus and amidated on the carboxy terminus. The name "AcPHF6" is used to describe the construct.

A series of inhibitors of AcPHF6 aggregation were rationally designed by the Nowick research group at University of California, Irvine. They exploited the feature for AcPHF6 to self-assemble by synthesizing a macrocycle with the VQIVYK motif as well as an interfering strand to halt growth of the β-sheets in solution (Fig. 3.1) [70]. The lower strand uses two amino acid residues and the molecular template Hao, which

Fig. 3.1. (A) The β-sheet forming AcPHF6 highlighting the leading edge hydrogen bonding with the next construct in the growing aggregate.(B) Tau aggregation inhibitor 1a. Note that the top strand of inhibitor 1a contains the same VQIVYK motif found in AcPHF6 which hydrogen binds to the fibril. The covalently bound bottom strand blocks further hydrogen bond formation and continuation of the β-sheet.

A

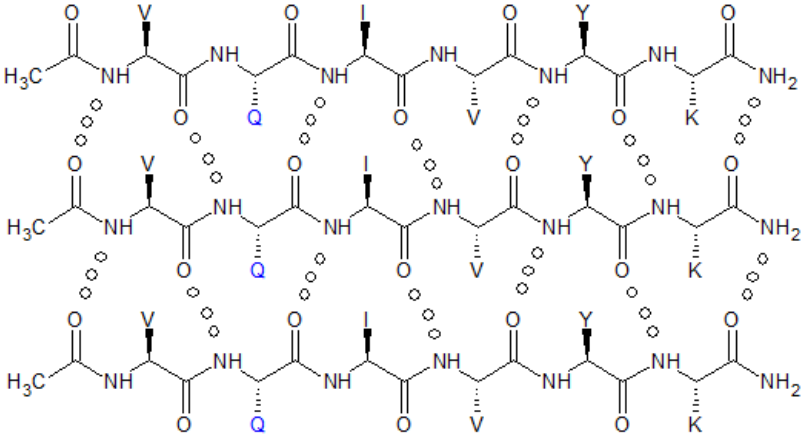

B

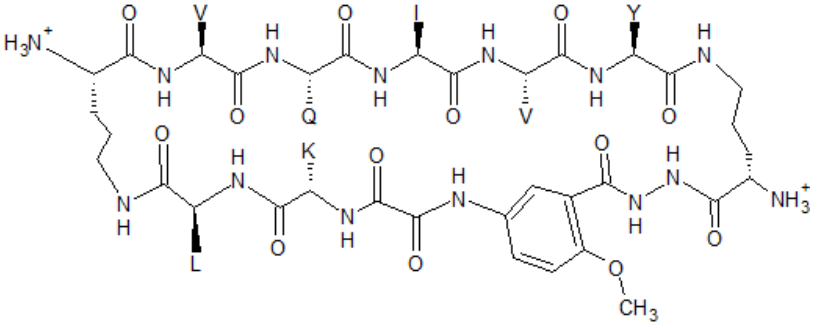

is a tripeptide β-strand surrogate lacking hydrogen bond forming heteroatoms [74]. The template is so-named because it is comprised of hydrazine, 5-amino-2-methoxybenzoic acid and oxalic acid groups [71]. Fmoc and Bmoc protected Hao can be incorporated into synthetic peptides, as it behaves just like natural amino acids. Solid phase and solution phase synthesis can both be used to incorporate Hao into the strand. The upper and lower strands are linked by two δ--linked ornithines to model β-turns. Overall, a top strand exposes a H-bonding edge and H-bond blocking is performed by the bottom strand. R6 and R7 can contain any amino acid to optimize for folding, solubility and side chain hydrophobicity. For inhibitor 1a (Fig. 3.1), the hydrophobic residue leucine was used at R7 to match the similarly hydrophobic valine at R1. Lysine was incorporated at R6 to match the hydrophilic glutamine at R2 [71].

Nowick's research groups' inhibitors were tested for the ability to prevent, delay or minimize AcPHF6 aggregation using the Goux-developed fluorescence based assay and the following conditions: 100 μM AcPHF6 in 16 mM MOPS buffer is incubated with Thioflavin S (ThS), which binds aggregates and is read by an increase in fluorescence over 120 min. The analysis used an excitation wavelength of 440 nm and followed the resulting emission at 480 nm, with 5 nm slit widths for both. ThS without AcPHF6 showed a static baseline level of fluorescence, but did not increase over time. A range of concentrations of inhibitor 1a were added to 100 μM AcPHF6, including 0, 25, 50 and 100 μM. It was found that the 25 μM inhibitor 1a had negligible effect, 50 μM delayed aggregation by about 30 min, and 100 μM prevented aggregation completely[70].

3.2 Materials and Methods

3.2.1 Reagents

Macrocycle 1a was synthesized, purified, lyophilized, and provided by Mandy Zhang of the James Nowick lab group at University of California, Irvine. Stored at room temperature until needed, 1a was solubilized in deionized water for use. Aqueous aliquots of 1a were kept at -20 ºC for a maximum of 2 weeks. Five 96-well plates containing approximately 5 µL of 5 mg/mL natural product extracts derived from marine actinomycetes were provided by the Brian Murphy lab at UIC and were stored at -20 °C. HPLC-grade acetonitrile and ammonium acetate were purchased from Fisher Scientific (Fair Lawn, NJ). Formic acid (FA), pyrimethamine, sodium chloride, and 1,1,1,3,3,3-hexafluoroisopropanol (HFIP) were purchased from Sigma-Aldrich (St. Louis, MO). AcPHF6 was synthesized by the Protein Research Lab (UIC) using Fmoc protected amino acids and acetylated on the amino terminus by reaction with acetic anhydride in the presence of pyridine. The construct was dissolved in a 1:1 (v/v) mixture of HFIP and 87% formic acid, purified by using HPLC, and lyophilized. Finally, the construct was dissolved in HFIP to make a 2 mM solution.

3.2.2 Procedure for High Throughput Screening

Incubation solution was prepared as described in Chapter 2, and 98 µL containing internal standard (pyrimethamine) was pipeted to each of 13 autosampler vials per batch. Natural product extract (1 µL of a 5 mg/mL) for screening was added to the first 12 vials, and 1 µL of DMSO was added to the 13th as a negative control (blank). Once the UHPLC-MS system was ready for analysis, 1 µL of 2 mM AcPHF6 dissolved in HFIP was added to the first vial, vortexed and the

analysis was started. Once the first vial was injected onto the column, AcPHF6 was added to the second vial, vortexed and placed in the autosampler for analysis. This process was repeated for the remaining vials in the batch. Great care was taken to ensure that 1 min elapsed from the addition of AcPHF6 until the sample was injected onto the column. After initial time points for each of the 13 vials was taken, Shimadzu LabSolutions software was programmed to repeat the analyses in order, resulting in a 1 min post-addition "initial" reading and a 27th min "final" reading.

3.2.3 Instrument Conditions for the Proof of Principle Assay and Screening

An isocratic flow of 82% of 0.2% FA in deionized water and 18% acetonitrile was pumped at a flow rate of 0.4 mL/min by a Shimadzu Nexera LC-30AD UHPLC system equipped with a solvent degasser, refrigerated autosampler (4°C), and column oven (40°C). A Shimadzu Shimpack XR-ODS III (2.0 x 50 mm, with 1.6 µm packing) column capable of withstanding a backpressure of 10,000 psi was used to separate the mixture. A 0.1 µL aliquot was injected for each analysis. The Shimadzu 8030 triple quadrupole mass spectrometer was operated in positive ion mode using an electrospray source. Instrument parameters were optimized for the SRM analysis of the AcPHF6 transitions of *m*/z 790 to 270 and *m*/z 790 to 129. The internal standard (pyrimethamine) transitions of *m*/z 249 to 177 and *m*/z 249 to 233 were also recorded for all singly protonated molecules. The following instrument parameters were used: an interface voltage of 4.5 kV, a heat block temperature of 400°C, a desolvation temperature of 250 °C, and dwell time of 25 msec per transition. A column cleaning method of 0 to 95% B over 5 min then holding at 95% B for 3 min was used between batches.

3.2.4 Use of Autosampler to Automate Sample Preparation

The use of robotics can greatly increase sample throughput by extending the workday from 8 to 24 h. The AcPHF6 aggregation assay was designed to take advantage of automated sample preparation, simply requiring the mixing of two solutions and making two UHPLC-MS/MS analyses separated by a 30 min incubation. The Shimadzu CTO-30 autosampler was programmed to perform these functions by using command line functions in the LabSolutions software [75].

Conical autosampler vials containing 100, 200 or 500 µL incubation solutions were placed into the 105 vial autosampler rack. One autosampler vial was filled with 50 µL of 2 mM AcPHF6 dissolved in HFIP and placed in the standards autosampler rack. The UHPLC-MS/MS conditions were used as previously described for the aggregation assay. Commands were written so that 1 µL of AcPHF6 solution was transferred to one incubation autosampler vial. Then the vial was mixed by drawing and expelling 25 µL of the mixture into the autosampler needle and sample loop 10 times at a draw speed of 35 µL/sec. This is the maximum speed and volume allowed by the system.

3.3 Results and Discussion

3.3.1 Use of Autosampler to Automate Sample Preparation Results

Three diluent volumes were used to check for complete mixing by the autosampler. If mixing was complete, then there should be a linear relationship between increasing final concentration of the analyte and increasing AUC of the transition monitored. One µL of 2 mM AcPHF6 dissolved in HFIP was added to 100, 200 and 500 µL of incubation solution, and the results graphed in Fig. 3.2. The AUC of

Fig. 3.2. UHPLC-MS/MS SRM chromatograms of 1 µL of 2 mM AcPHF6 in HFIP apported and mixed with 100 µL (A), 200 µL (B) and 500 µL (C) of incubation solution. The AUCs are 6,521,000, 6,561,000 and 6,473,000 respectively. (D) The AUCs were graphed against expected concentration. If the solutions were adequately mixed, a linear increase in AUC values with increasing concentration would be expected.

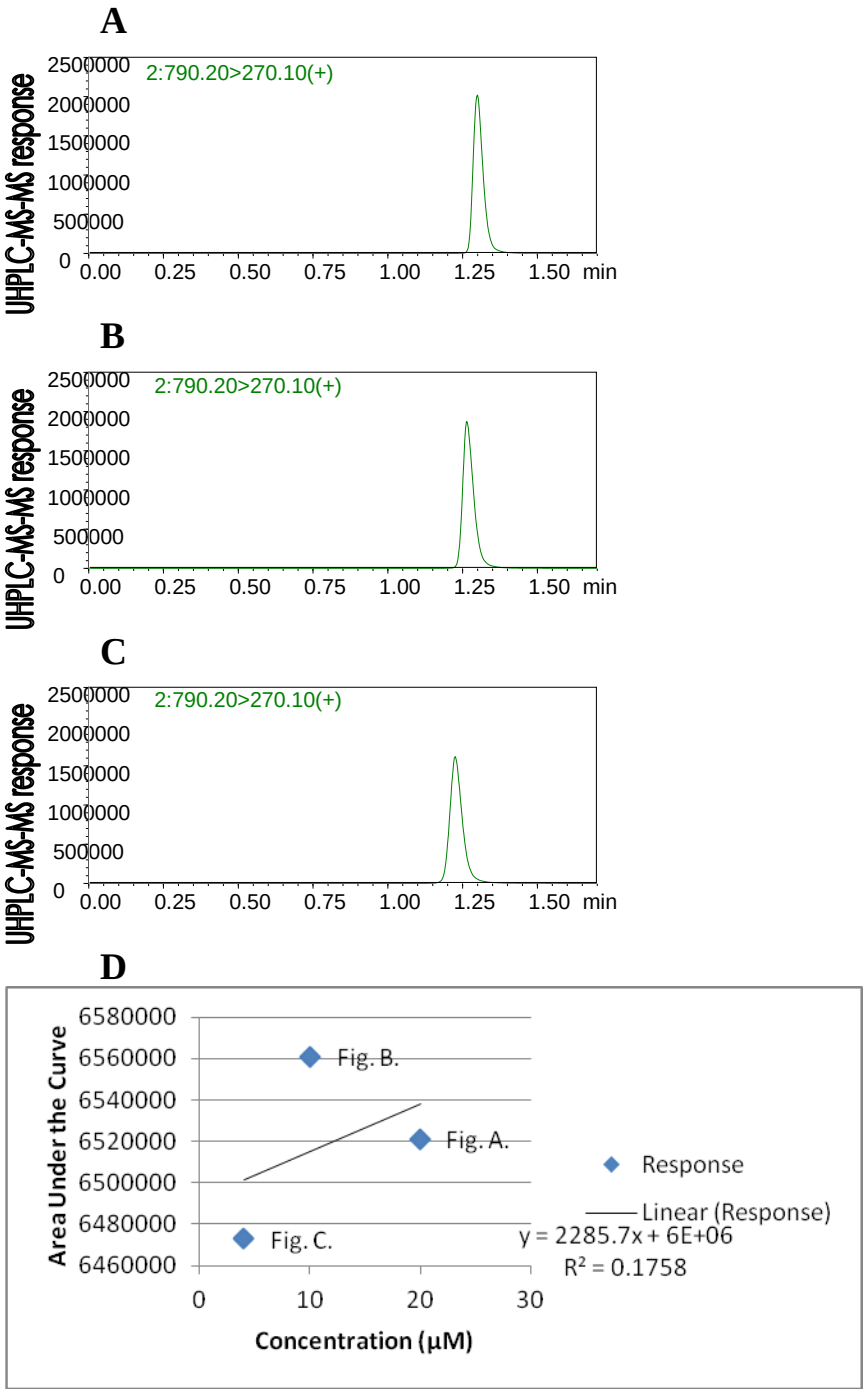

each analysis was roughly equal, indicating that mixing was not occurring throughout the incubation solution. A best fit line was added to the graph to evaluate the linear relationship of concentration to AUC. The coefficient of determination value of the line was 0.1758, showing that the data poorly fit the line and would not be a good indicator of future outcomes.

Due to the poor automated mixing results, it was determined that manual vortex mixing would have to be performed for each sample, which was the technique used by previous investigators. Investigation of mixing in other autosampler vial types was not done because use of a non-conical vial would require a larger amount of natural products and constructs. If new autosampler mixing technology becomes available, automation of mixing could be investigated again.

3.3.2 Evaluation of Nowick's Macrocycle Inhibitor 1a

The inhibitor 1a at a concentration of 40 μM and a control were compared using the previously described assay to determine whether it could be used as a positive control in the high-throughput screen. When treated with the known inhibitor 1a, 38% ± 3.8% of the monomer remained in solution, whereas the control had 22.2% ± 2.8% monomer remaining after 30 min. The graphed results are displayed in Fig. 3.3.

Fig. 3.3. The remaining ratio of AcPHF6 monomer to internal standard relative to the ratio at t=0 was graphed over time for an untreated sample and one treated with inhibitor 1a (n=4). The analysis was extended to 90 min to ensure that the endpoint of aggregation was reached in pane B.

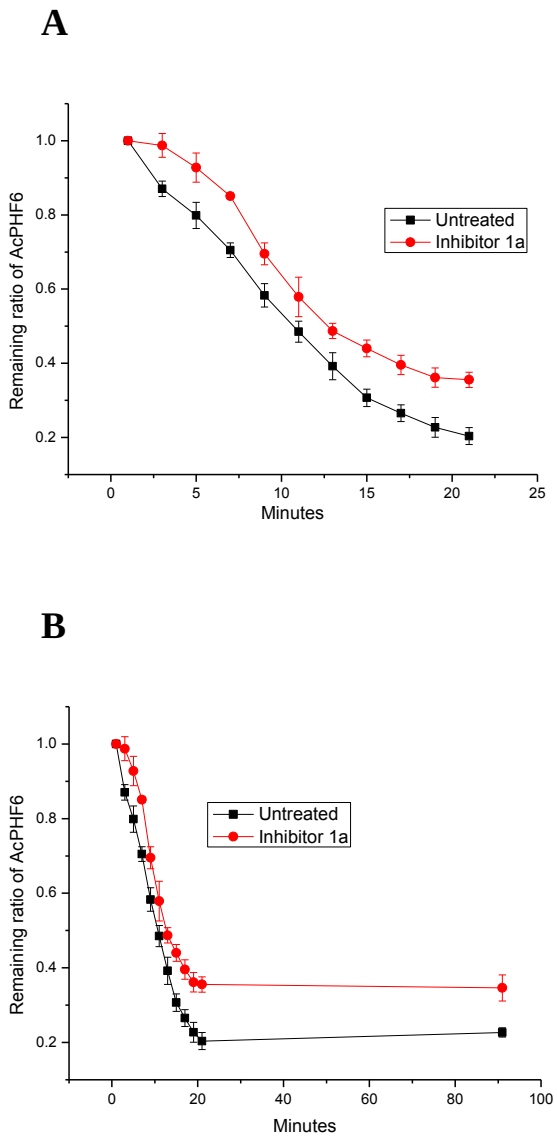

One observation of both the Nowick lab group and the van Breemen lab is that the maximum reading for aggregation varies across analyses. In the fluorescence and mass spectrometry assays, the curves of rationally designed compounds follow a seeded nucleation mechanism and proceed to a static value where further aggregation does not occur. The static value varies from analysis to analysis, so data from each inhibitor should be normalized to the value of the untreated control. Inhibitor 1a was chosen as the positive control for the high throughput assay because it inhibited aggregation at the lowest concentration of inhibitors designed and tested by the Nowick lab. The inhibitor has reasonable storage conditions, stability and solubility in water, making it an effective tool to evaluate an orthogonal assay.

3.3.3 Screening of Marine Actinomycetes Results

Natural product fractions from marine actinomycetes were tested singly in the mass spectrometry based AcPHF6 aggregation assay. Five 96 well plates were tested, though not all wells were filled with a natural product fraction. These empty wells were omitted. The maximum number of wells tested in one work day by one researcher was 96, along with 8 untreated control experiments. The ratio of the AUC of analyte to internal standard at 27 min was divided by the same ratio at the zero time point. This value was divided by the average ratio of the untreated control samples taken each day (Fig. 3.4). The best two inhibitors of aggregation from each day's experiments were chosen for retesting in triplicate.

Fig. 3.4. The results of the high throughput screens of Trays 1, 2, FP1, FP2, and FP3 in panes A, B, C, D and E respectively. The best 2 inhibitors of aggregation were chosen for further investigation from each graph. The hits selected for confirmation testing are circled in green.

A

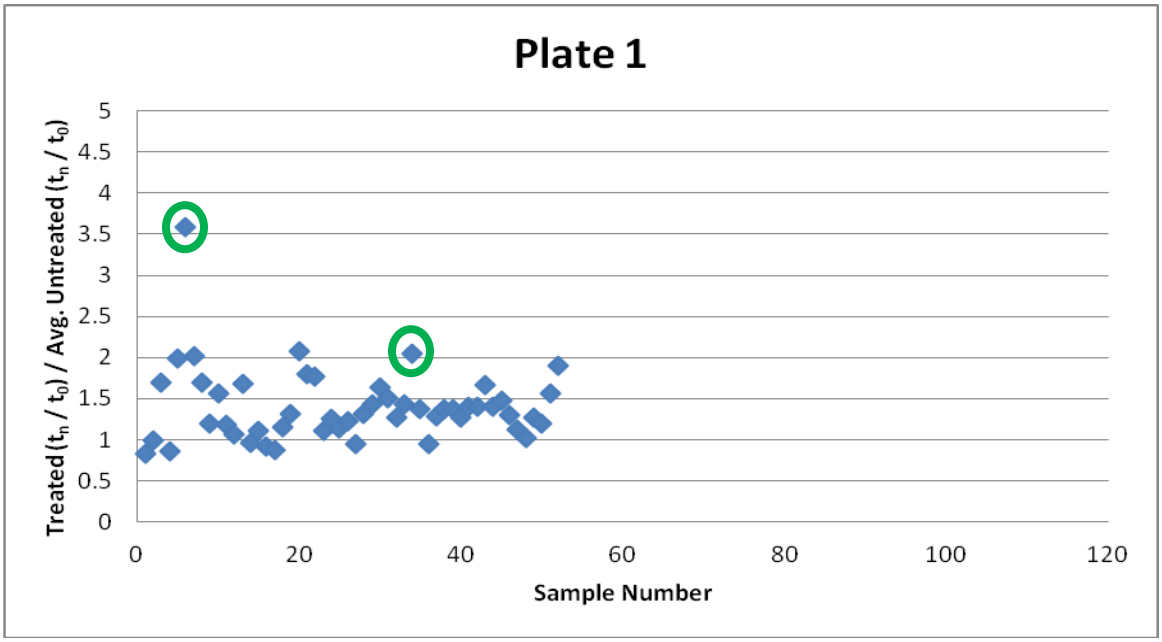

B

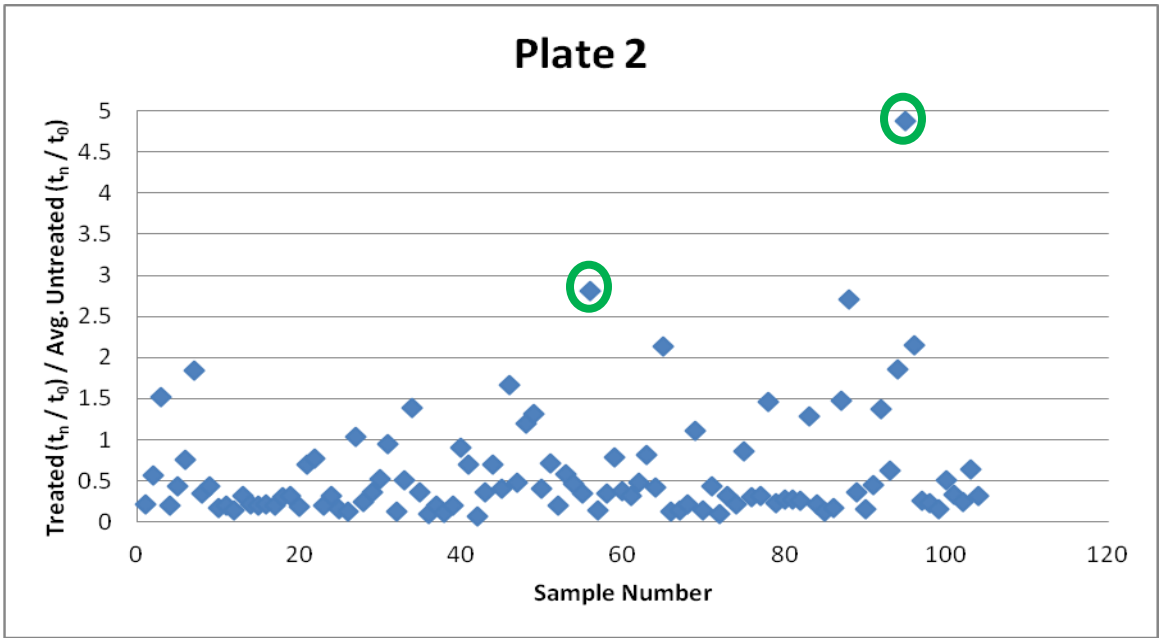

C

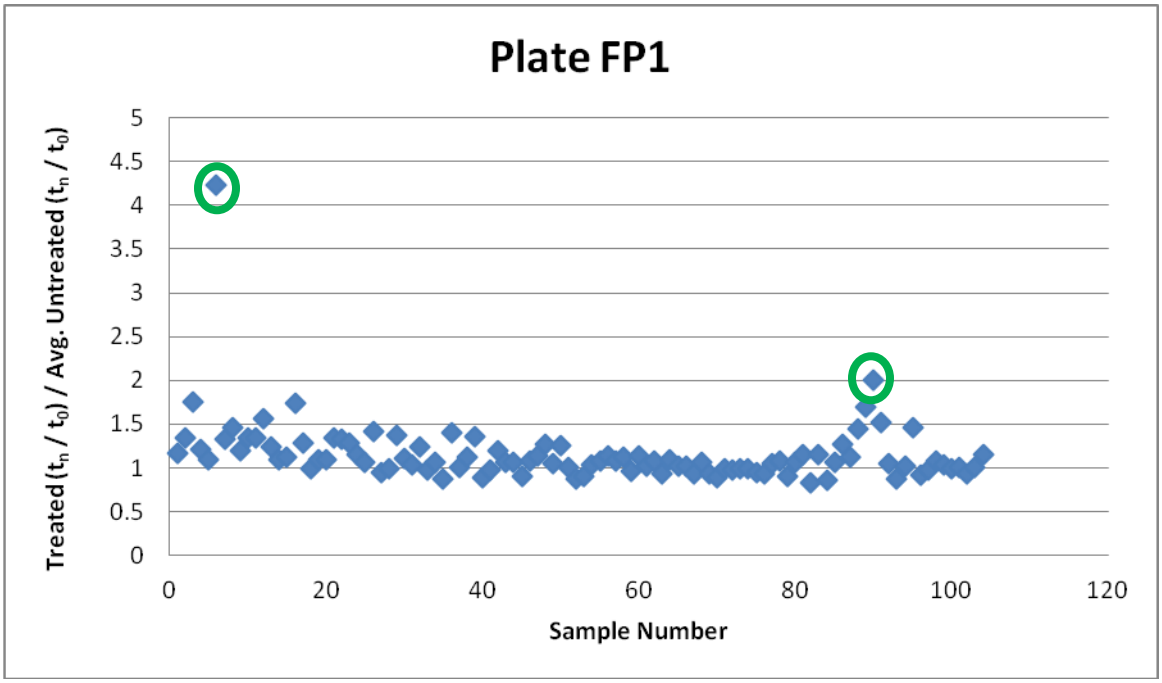
Plate FP1
Treated (t_n / t_0) / Avg. Untreated (t_n / t_0)
5
4.5
4
3.5
3
2.5
2
1.5
1
0.5
0
0
20
40
60
80
100
120
Sample Number

D

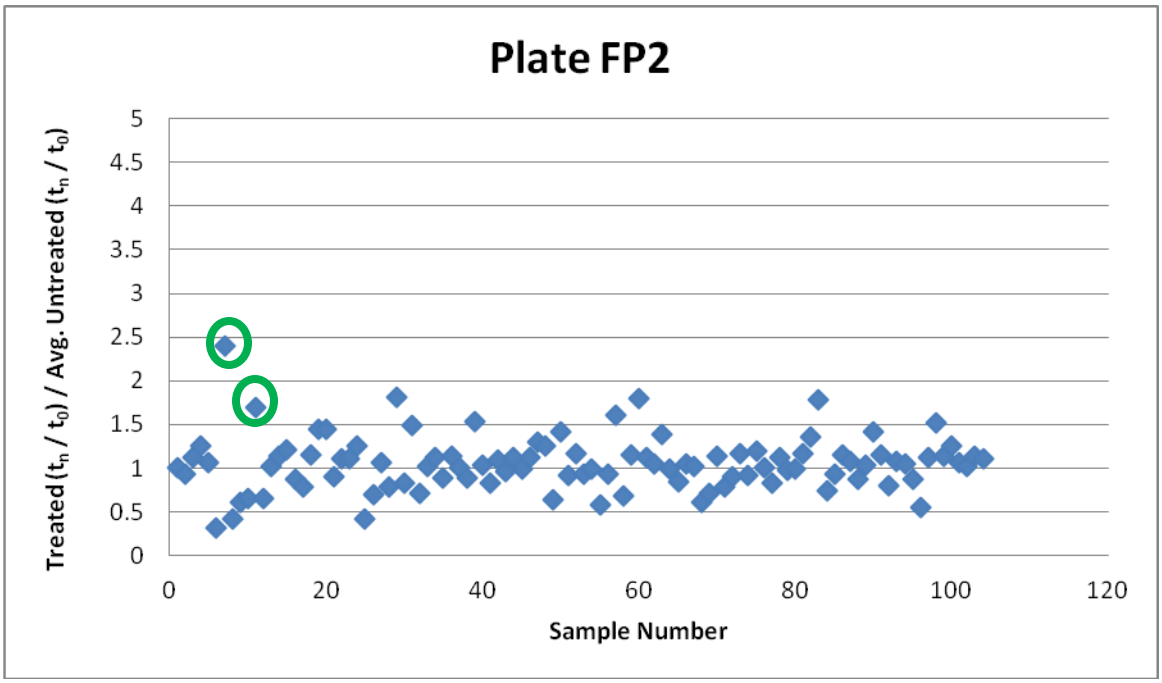
Plate FP2
Treated (t_n / t_0) / Avg. Untreated (t_n / t_0)
5
4.5
4
3.5
3
2.5
2
1.5
1
0.5
0
0
20
40
60
80
100
120
Sample Number

E

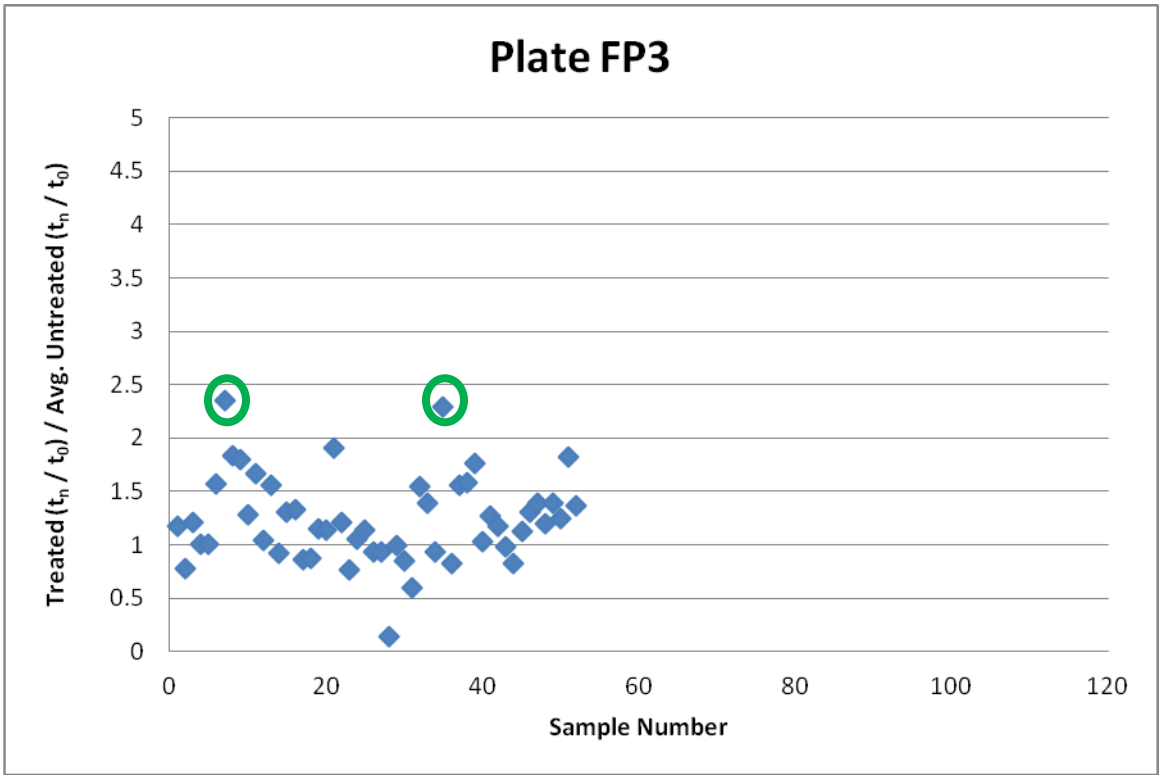
Plate FP3
Treated (t_n / t_0) / Avg. Untreated (t_n / t_0)
5
4.5
4
3.5
3
2.5
2
1.5
1
0.5
0
0
20
40
60
80
100
120
Sample Number

The Z'-factor was calculated for each of the 5 plates' control data using Zhang and colleagues' equation [49]. Each of the 5 plates had a Z'-factor less than 0, indicating the negative and positive control signal variation bands overlap. The signal variation bands are defined as 3 standard deviations of the mean assay signal for the positive and negative controls. This underscores the need for an inhibitor able to prevent AcPHF6 from aggregating better than inhibitor 1a. This screening assay was developed to find the best inhibiting fraction from a library of marine natural products without a positive control.

Fractions with the best inhibition of AcPHF6 aggregation found during the HTS were evaluated again with 3 replicates. The fractions chosen for further testing were B8 and E2 in Plate 1, A3 and E11 in Plate 2, G8 in Plate FP1, H3 and G12 in Plate FP2, and A3 and C5 in Plate FP3. These wells were tested along with inhibitor 1a and an untreated control for comparison purposes and graphed over 280 min in Fig. 3.5.

Three tested wells had statistically significant decreased aggregation when compared with the control. Inhibitor 1a also displayed significant reduction in aggregation as expected. The results for all retested preliminary hits are shown in Table IV. The wells which failed to significantly inhibit AcPHF6 aggregation at 140 minutes were excluded from further evaluation.

Fig. 3.5. The identified hits, FP1 G8, FP2 H3 and FP3 C5 were analyzed 5 times each over 280 minutes to ensure complete aggregation had occurred, not just the delay of aggregation.

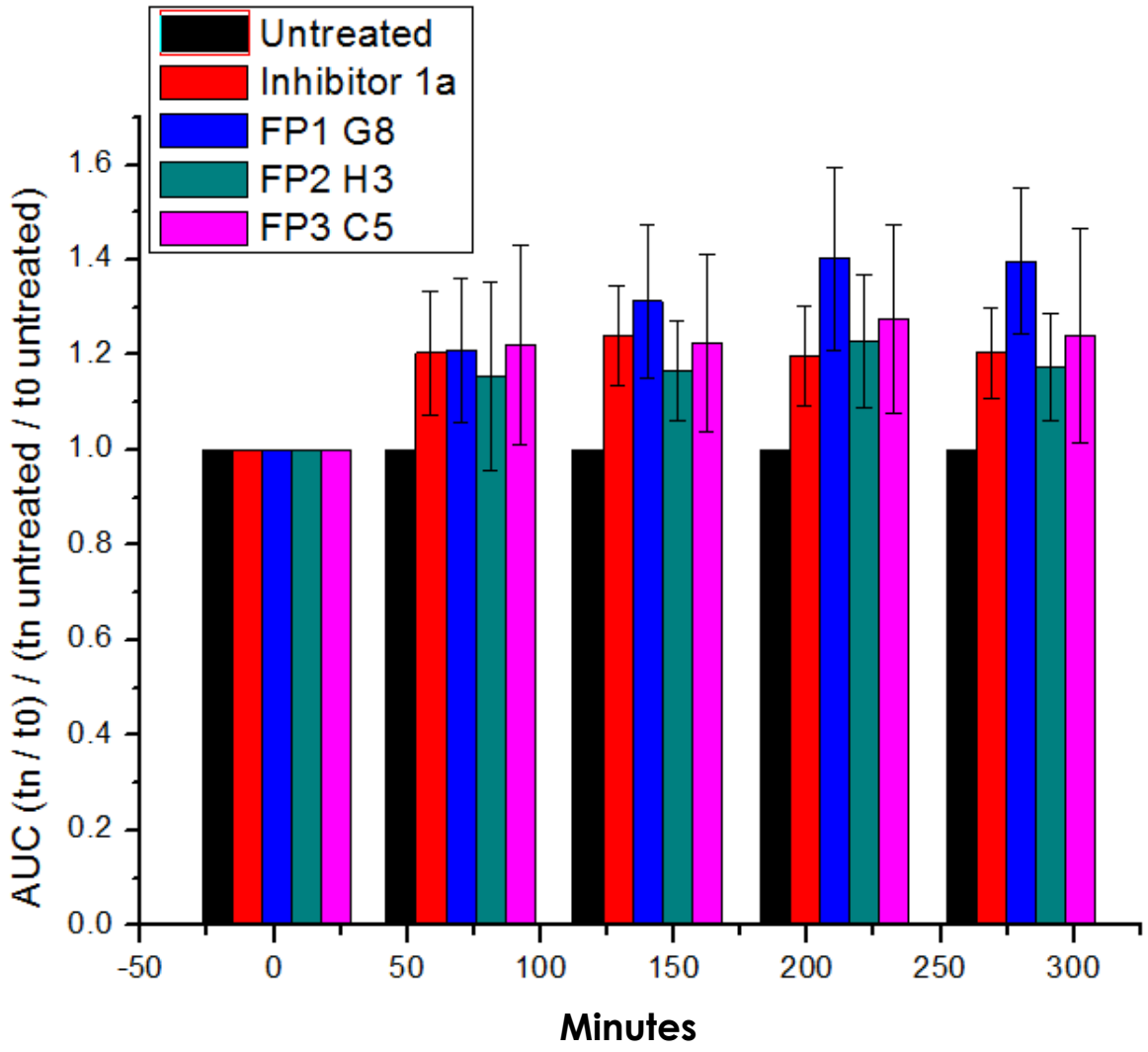

TABLE IV. THE MEAN AND STANDARD DEVIATION OF THE INHIBITION OF ACPHF6 AGGREGATION OF EACH PRELIMINARY HIT ARE SUMMARIZED BELOW AT 140 MINUTES, WITH 3 REPLICATES OF EACH. THE HITS THAT FAILED TO SHOW SIGNIFICANT INHIBITION WERE EXCLUDED FROM FURTHER STUDY.

Inhibitor	**Mean**	**Standard Deviation**
Inhibitor 1a	1.24	0.11
Plate 1 B8	1.03	0.10
Plate 1 E2	1.06	0.15
Plate 2 A3	0.964	0.22
FP1 G8	1.31	0.16
FP1 A4	1.07	0.12
FP2 H3	1.17	0.10
FP2 G12	0.988	0.08
FP3 A3	1.09	0.15
FP3 C5	1.22	0.19

3.4 Conclusion

The mass spectrometry based assay for measuring AcPHF6 aggregation inhibition was able to identify three active fractions from marine actinomycetes. The hits must be further purified and each metabolite tested individually as a pure compound to identify a lead compound for further testing. Identified compounds should next go through testing using a full-length tau aggregation assay.

The newly developed assay was found to be robust, precise and operates with low intrinsic error, making it a good candidate to be performed by other researchers with varied natural product libraries in need of testing. All of the requirements of the assay are easily obtainable and no specialized techniques employed. A basic understanding of LC-MS is all that is required to continue the research. The assay's results showed statistically significant activity of inhibitor 1a, which agrees with the fluorescence assay.

Using the autosampler as a robot to automate sample preparation and decrease hands-on time was not successful. However, this approach should remain an area of interest to enhance the efficiency of the method. Many different robotic preparation conditions should be tested until successful mixing of reagents can be achieved.

Mass spectrometry has rarely been used as a detection technique for *in vitro* assays due to the relatively slow chromatography of conventional HPLC systems and the high cost of instrumentation. With the greater availability of UHPLC systems, per sample analysis times can be decreased by about 5-fold compared with conventional HPLC, allowing for much greater throughput than was previously

possible. While instrumentation costs are still relatively high, the value of difficult to obtain natural product fractions is also very high. The fractions painstakingly gathered and processed would not have been able to be tested by the conventional fluorescence assay, so would have gone unused. So while not able to match the high throughput of other assays, the mass spectrometry assay is able to evaluate high value natural products that would otherwise go untested.

CHAPTER 4

PROFILING OF ACTIVE FRACTIONS BY METABOLOMICS-GUIDED ACCURATE MASS HIGH PERFORMANCE LIQUID CHROMATOGRAPHY TANDEM MASS SPECTROMETRY

4.1 Introduction

Metabolomics is the study of low molecular weight organic biological components and their complex interactions in biological systems. The small molecules can form larger components, such as proteins, RNA, DNA, and cell walls, through metabolic processes, and are important for regulation and signaling [76]. While the metabolomes of plants and animals are also commonly studied, this dissertation focused on microbial metabolomics since fractions of marine actinomycetes were tested in the peptide aggregation assay.

High resolution mass spectrometers, such as quadrupole-time-of-flight (QTOF), ion trap-TOF (IT-TOF), Fourier transform ion cyclotron resonance, or Orbitrap instruments, are commonly used for their ability to predict the molecular formula of the metabolite due to their high mass accuracy and resolution [72,76]. The Shimadzu IT-TOF mass spectrometer (the first production instrument of its kind) is capable of measuring the accurate masses of both precursor and product ions to provide useful structural information [76].

LC-MS/MS can provide a metabolomic "fingerprint" of the positively testing wells from the actinomycetes fractions. These bacteria require a long period of growth, and by matching the fingerprints, one can make certain that the same metabolites responsible for inhibition of aggregation are present. While no single

analytical method can detect 100% of the metabolites present, the vast majority of commercially available standards from three bacterial species could be measured [72]. Identification of the metabolites has proven difficult, since most large metabolomic identification projects like HUSERMET focus on the human metabolome [77]. Fig. 4.1 gives an outline of the quantities of natural products required for each stage of the therapeutic agent development process. A successful compound passing through each step requires much more material and only the most active fractions can be realistically scaled up due to growth time of the bacteria.

4.1.1 Metabolomics Software

Many software packages are available to process metabolomic type data, but only the software used in this dissertation will be discussed in detail. Many of the algorithms used to process the data in commercially available metabolomics software are hidden from the user and not published, so as to maintain a competitive advantage. Open source software showing all of the processing algorithms is available, but requires a large investment of time to learn due to limited graphical interfaces. The closed source commercial products attempt to simplify and streamline the process. The overall purpose of the software used in this study, Profiling Solutions (Shimadzu Scientific Instruments, Columbia, MD), was to filter raw data, detect, align and normalize features.

Fig. 4.1. The amount of natural product required increases exponentially as the compound is advanced through the drug development scheme shown here [55]. The actinomycetes fractions provided for high throughput screening contained only µg amounts of active compounds, thereby limiting the progression. The focus of this study was to identify bioactive fractions.

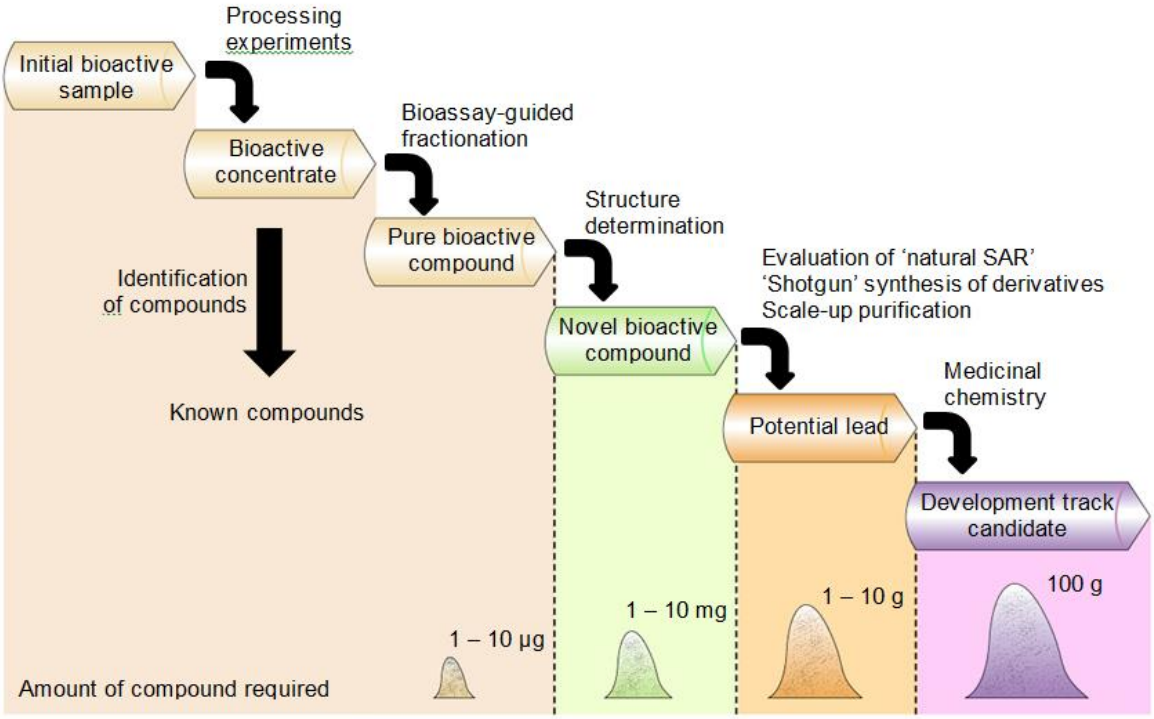

Profiling Solutions is based on the open source XCMS platform, whose acronym comes from "X" forms of Chromatography Mass Spectrometry [78]. LC-MS features, consisting of an accurate mass and a retention time, have their retention times aligned, then their intensities are compared. In samples without internal standards, XCMS is capable of dynamically identifying common metabolites across samples to calculate a nonlinear retention time correction profile for each sample. If internal standards are used, they can be identified by the researcher and used to align peaks, which is what was done in this study since there may not be common metabolites in all analyses. After either of the retention time alignment options, the intensity of each feature is normalized to that of the internal standard and then compared across samples from various fractions. Additional Shimadzu software can then be used to predict formulas for important unknown compounds, and their accurate masses, product ion tandem mass spectra and predicted formula can then be used to search any available database singly or in combination.

4.2 Materials and Methods

4.2.1 Reagents

LC-MS grade acetonitrile was purchased from Thermo Fisher Scientific (Hanover Park, IL). Deionized water was produced fresh each day using a Siemens (Warrendale, PA) PURELAB Ultra system. Pyrimethamine, FA and reserpine were purchased from Sigma Aldrich (St. Louis, MO).

4.2.2 Hit Fraction Preparation

Each of the three hit fractions identified in the AcPHF6 high throughput screen were diluted 50-fold into a solvent consisting of 70% acetonitrile and 30% deionized water. Reserpine and pyrimethamine were added to make 500 nM final concentrations. These two compounds were added to function as internal standards and also to aid in aligning retention times from analysis to analysis. A pooled sample from 10 inactive fractions was prepared and used to test for commonly occurring metabolites. Each fraction was analyzed one time in each of the ionization modes described below. The analytical blank was analyzed once before and once after each ionization mode group.

4.2.3 Liquid Chromatography and Mass Spectrometer Conditions

A Shimadzu IT-TOF hybrid mass spectrometer coupled with a Shimadzu LC20-XR HPLC system was used for data acquisition. Reverse phase UHPLC was used to separate metabolites by polarity. A 5 µL injection was made onto a Shimadzu Shimpack III XR-ODS 2.0 x 50 mm UHPLC column containing 1.6 µm packing. Mobile phase A consisted of 0.1% FA in deionized water and mobile phase B was acetonitrile. The flow rate was 0.35 mL/min, and the gradient is described in Table V.

TABLE V. THE GRADIENT SETTINGS USED FOR REVERSE PHASE SEPARATION OF HIT FRACTION METABOLITES.

%Mobile Phase B Setting	**Time (minutes)**
5% B	0 to 2
70% B	12
95% B	20
95% B	24
5% B	24.1 to 30

The mass spectrometer was operated in scan mode from *m*/z 100-1500 with Automatic Sensitivity Control activated and set to a total ion current of 1,000,000 ions. Automatic, dynamic product ion scanning was utilized to obtain MS-MS data, and the product ion scan range of the most abundant ion was set from *m*/z 50 to 1000. After three product ion scans of the same precursor were completed, that mass was excluded from further MS-MS analysis. Ions from *m*/z 157.03 to 157.04 were put on the excluded ion list, due to the high abundance of the $[2\ DMSO + H]^+$ ion resulting from the DMSO used to store the natural product fractions. Each fraction was subjected to four separate LC-MS-MS analyses as follows: electrospray positive, electrospray negative, atmospheric pressure chemical ionization (APCI) positive, and APCI negative. The different ionization sources were used to give a well-rounded picture of the metabolites present in the fractions. Although the instrument was capable of polarity switching, separate positive and negative mode analyses were performed because the duty cycle exceeded 2 s to perform the scan and product ion scan in each mode. Some analytes might only elute for 5 to 10 s and would be missed if all modes of analysis were carried out sequentially during a single analysis. Fortunately, the low number of fractions to test allowed for the separate analyses using each ionization mode.

4.2.4 Profiling Solutions Software

Shimadzu Profiling Solutions software was utilized to process features in the LC-MS-MS analysis following a metabolomics guided workflow. A feature consists of an accurate mass measurement, its retention time and the intensity of the peak. The software is used to determine whether a feature is found in the blank, one or

multiple fractions. Metabolites that should be analyzed further should occur in one or more of the hit fractions and be considerably more abundant than in the fractions collected immediately before and after. Each feature is calculated from many user-defined parameters, requiring adjustment by the mass spectrometrist to adequately describe the peak. For most of the features, the following integration settings were used: minimum peak width at half-height of 5 seconds, peak start and end requiring a slope of 500 counts per minute, minimum AUC of 10,000 counts. This area count threshold was chosen because random noise with only one consecutive data point tends to fall below 10,000 on the Shimadzu IT-TOF. The feature alignment *m/z* tolerance was set to 10 mDa, and the retention time tolerance was set to 0.5 min. Savitzky-Golay smoothing with 25 point width was applied to remove random noise without undue degradation of the underlying data [77].

4.2.5 Rationale for Identification of Active Compounds

The approach used in this study is to perform the time consuming compound identification tasks last, after the likely feature responsible for activity is identified. The features selected for purification and retesting as single components or simplified mixtures should be present in a relatively high abundance. The abundance is estimated from LC-MS response from ESI and APCI ionization in both positive and negative modes. The inhibition of tau and AcPHF6 aggregation has previously been shown to be concentration dependent[70,79,80].

The likely active features are further narrowed by removing features which appear in the bookending fractions collected from the same specimen. The features which are present in other samples, but did not result in activity are

deemed unimportant for further study. These two steps greatly reduce the number of retesting experiments required.

4.3 Results and Discussion

The accurate mass LC-MS-MS analysis in four different ionization configurations was performed to profile the active fractions and to characterize metabolites that were potentially responsible for anti-aggregation activity. The HTS, retesting in triplicate and profiling experiments depleted all of the active natural product fractions available. The process of incubating a larger batch of the actinomycetes and hopefully collecting the same fractions will take several months, and it is important to know exactly which fractions tested positive in the assay. The second batch of metabolite fractions can be analyzed following the same method and compared to the metabolomics guided profile.

The positive-testing fractions, named after the fraction plate (FP) and well position code, FP1 G8, FP2 H3, and FP3 C5, and blank samples were analyzed using the procedure described in Chapter 4.2.3. Each sample was analyzed using positive ion and negative electrospray as well as positive ion and negative ion APCI to get a broad picture of the metabolites present in the samples. The total ion chromatograms (TICs) from each are displayed in Figs. 4.2 - 4.7. The blank analysis is used to identify contaminants and background noise inherent to the system and the analytes that were identified can be subtracted from the hit fractions using Profiling Solution software. The metabolites found in the pooled sample of inactive fractions can be ruled out as active compounds since they were not responsible for aggregation inhibition.

By using an untargeted metabolomics approach, one can compare the features of one fraction to another without requiring full identification of the metabolites. Determining the chemical formula and ultimately, identifying the chemical structure of a lead compound is challenging and time consuming, so this approach allows that step to be taken last. Using this approach, it is possible to characterize compounds and compare their relative concentrations while removing interfering molecules and noise. Profiling Solutions (Shimadzu, Kyoto, Japan) software was used to integrate, align and filter the features acquired in the chromatograms shown in Figs 4.2 to 4.7. The internal standards reserpine and pyrimethamine were used to align peaks from different analysis (Fig. 4.8). The retention time of analytes can vary slightly from analysis to analysis, so the processing software uses these standards to correct for retention time variation. Where only one internal standard was detected, it was used solely to correct retention time. Features can be "binned" together based on their accurate mass measurement within a given error margin and their corrected retention time within a given error margin. The AUCs from the binned features can be compared to give a relative concentration, whether the feature is present or not. The large number of features identified makes it difficult to present the data, but the processing of one feature can be illustrative of the workflow involved

Fig. 4.2. The total ion chromatograms of fraction FP1 G8 obtained using positive ion and negative ion electrospray (ESI) and APCI positive and negative modes. Reserpine eluted at 13.5 min, and pyrimethamine eluted at 5.5 min.

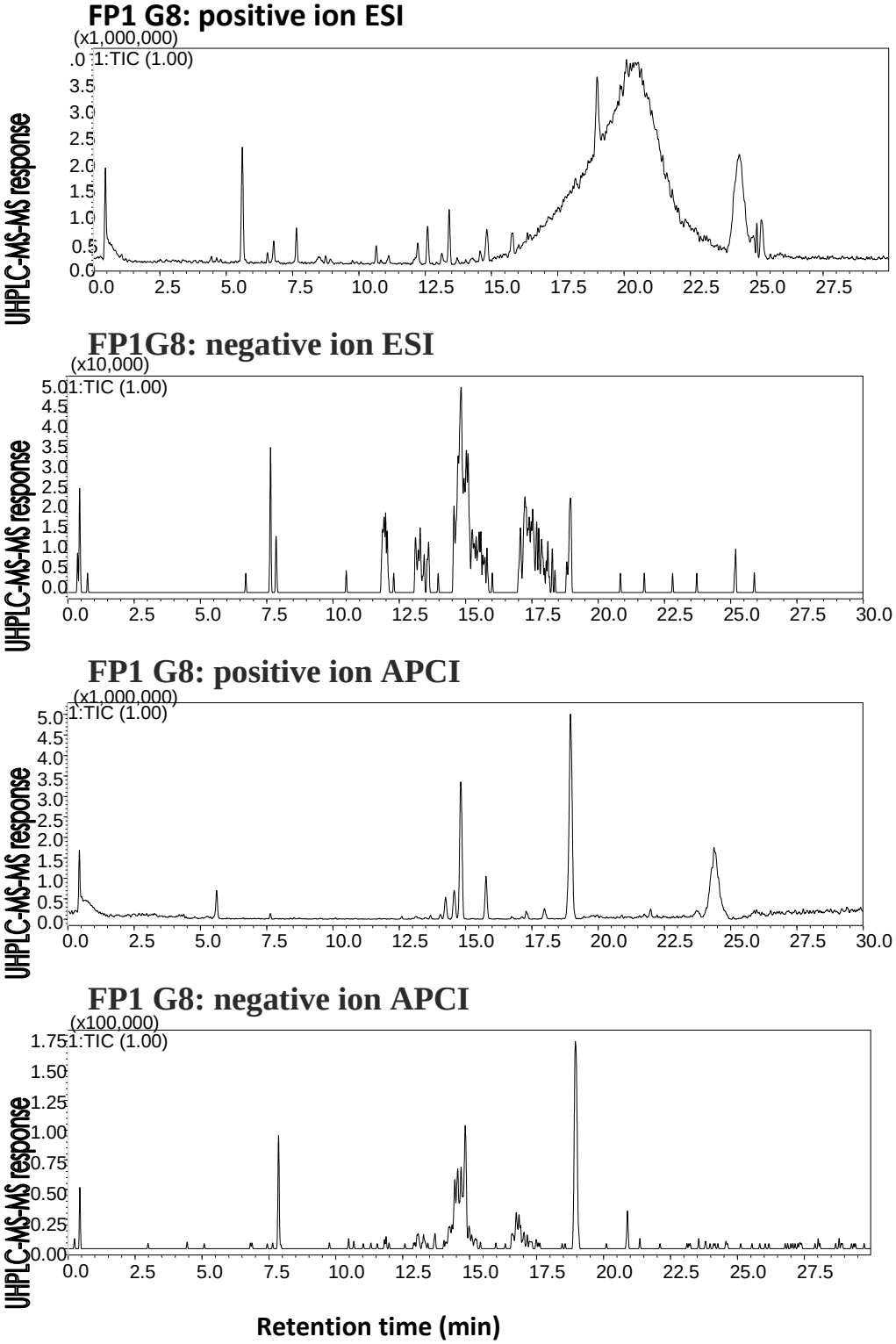

Fig. 4.3. The total ion chromatograms fraction FP2 H3 in ESI positive and negative and APCI positive and negative modes. Reserpine and pyrimethamine were included as internal standards.

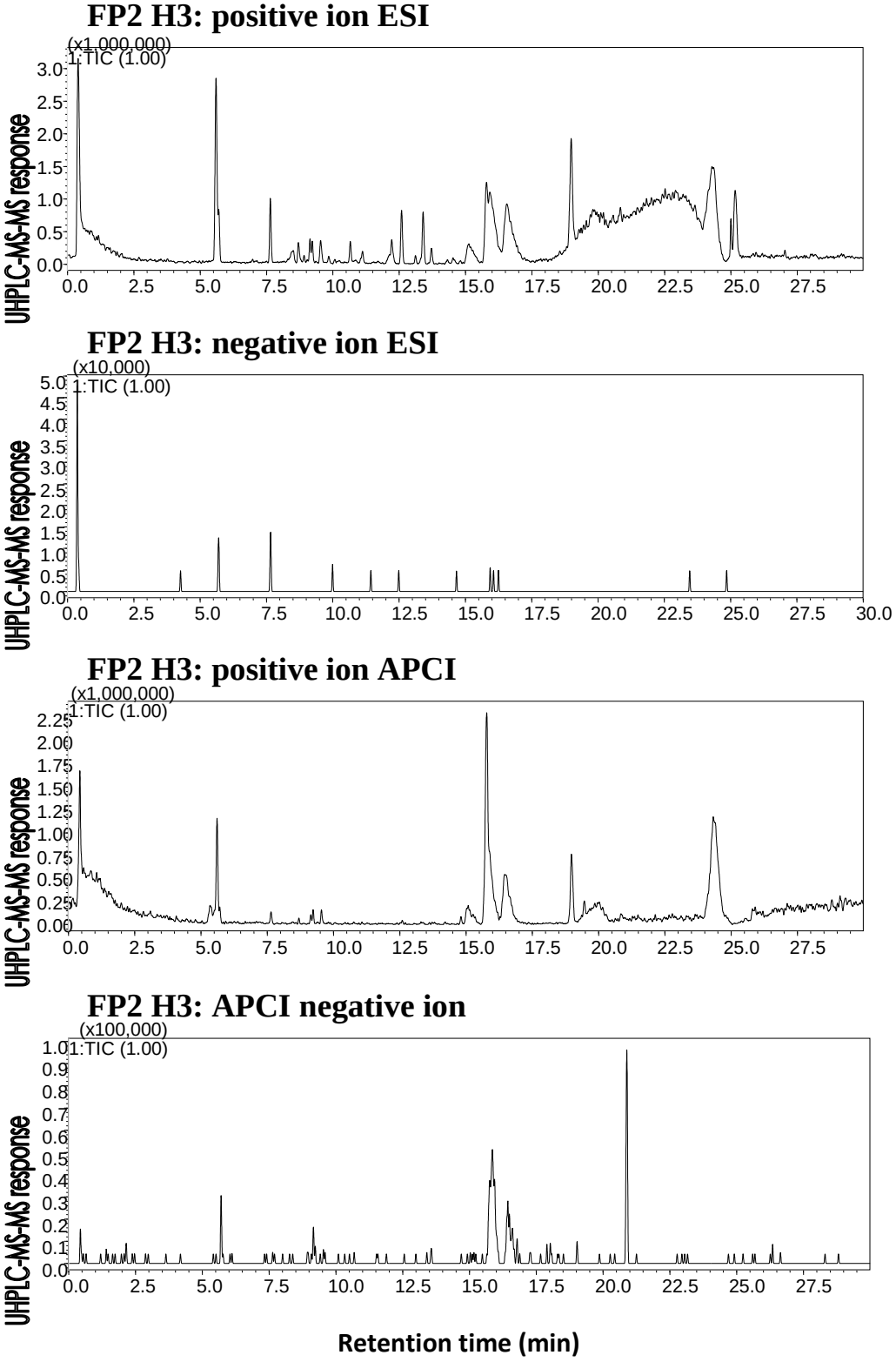

Fig. 4.4. The total ion chromatograms fraction FP3 C5 in ESI positive and negative and APCI positive and negative modes. Reserpine and pyrimethamine were used as internal standards.

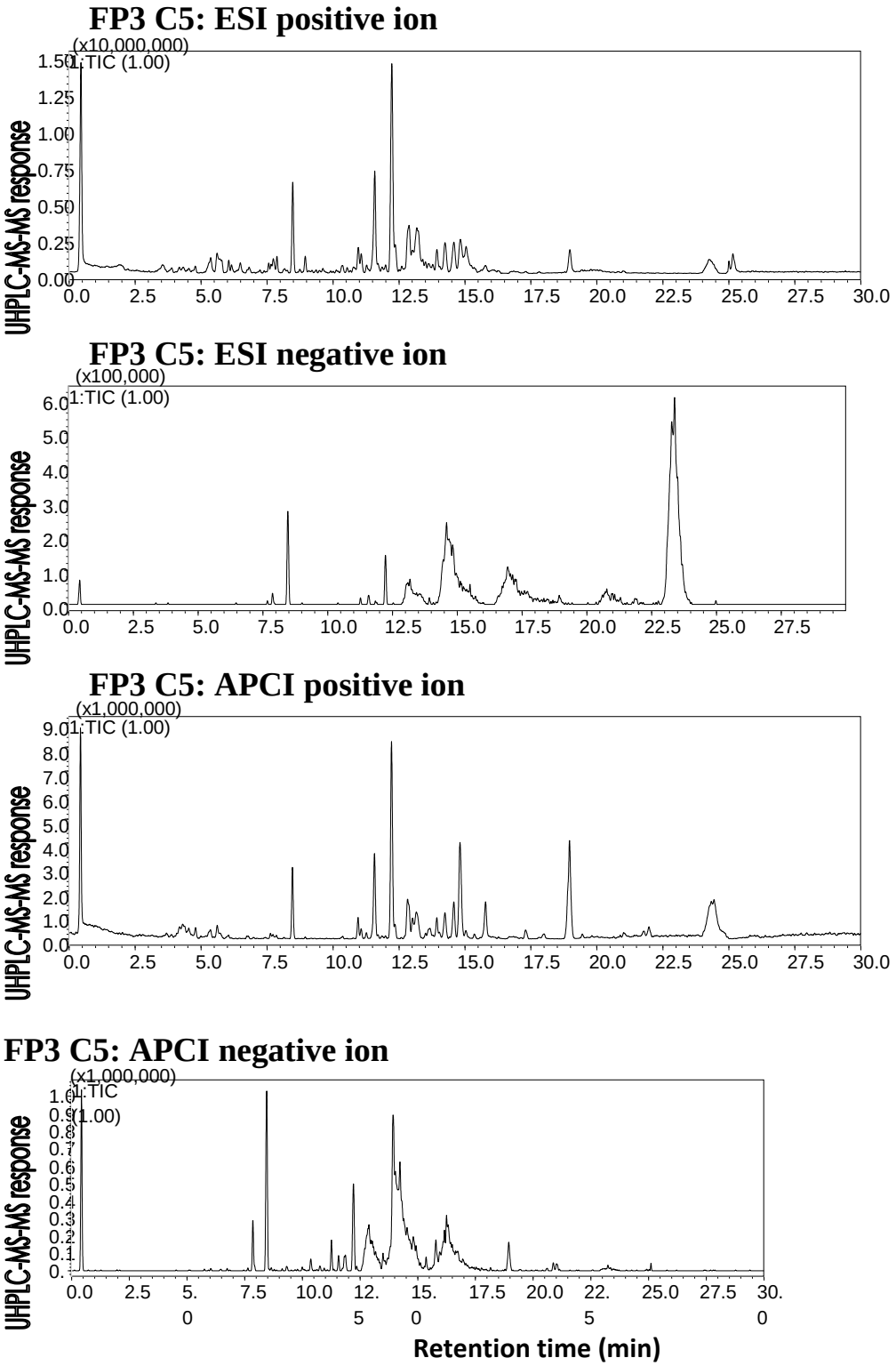

Fig. 4.5. The total ion chromatograms of the pooled sample in ESI positive and negative and APCI positive and negative modes. Reserpine and pyrimethamine eluted at 13.5 at 5.5 min, respectively.

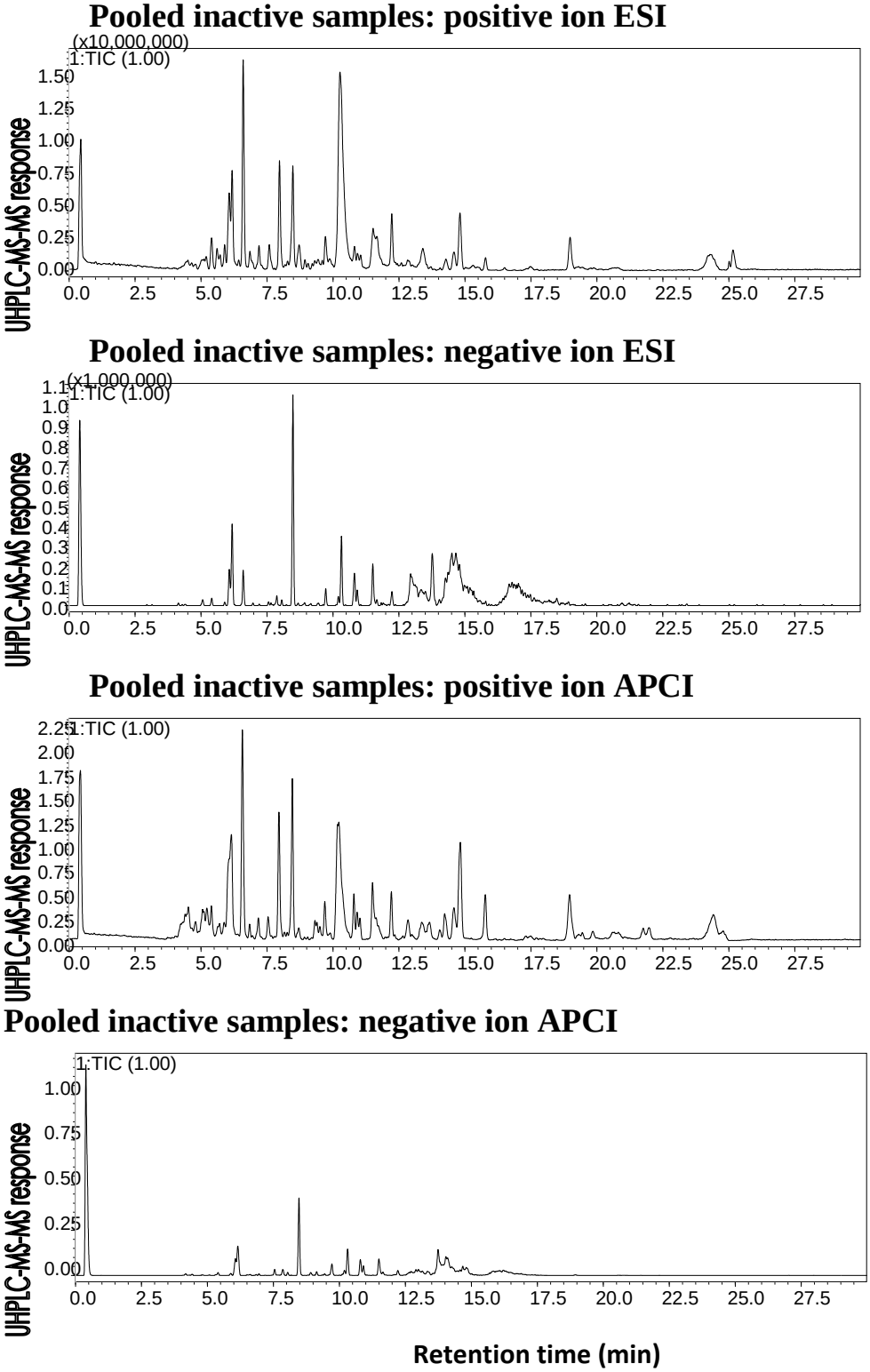

Fig. 4.6. The total ion chromatograms of the blank sample in ESI positive and negative and APCI positive and negative modes. Reserpine and can be seen at 13.5 and pyrimethamine at 5.5 min.

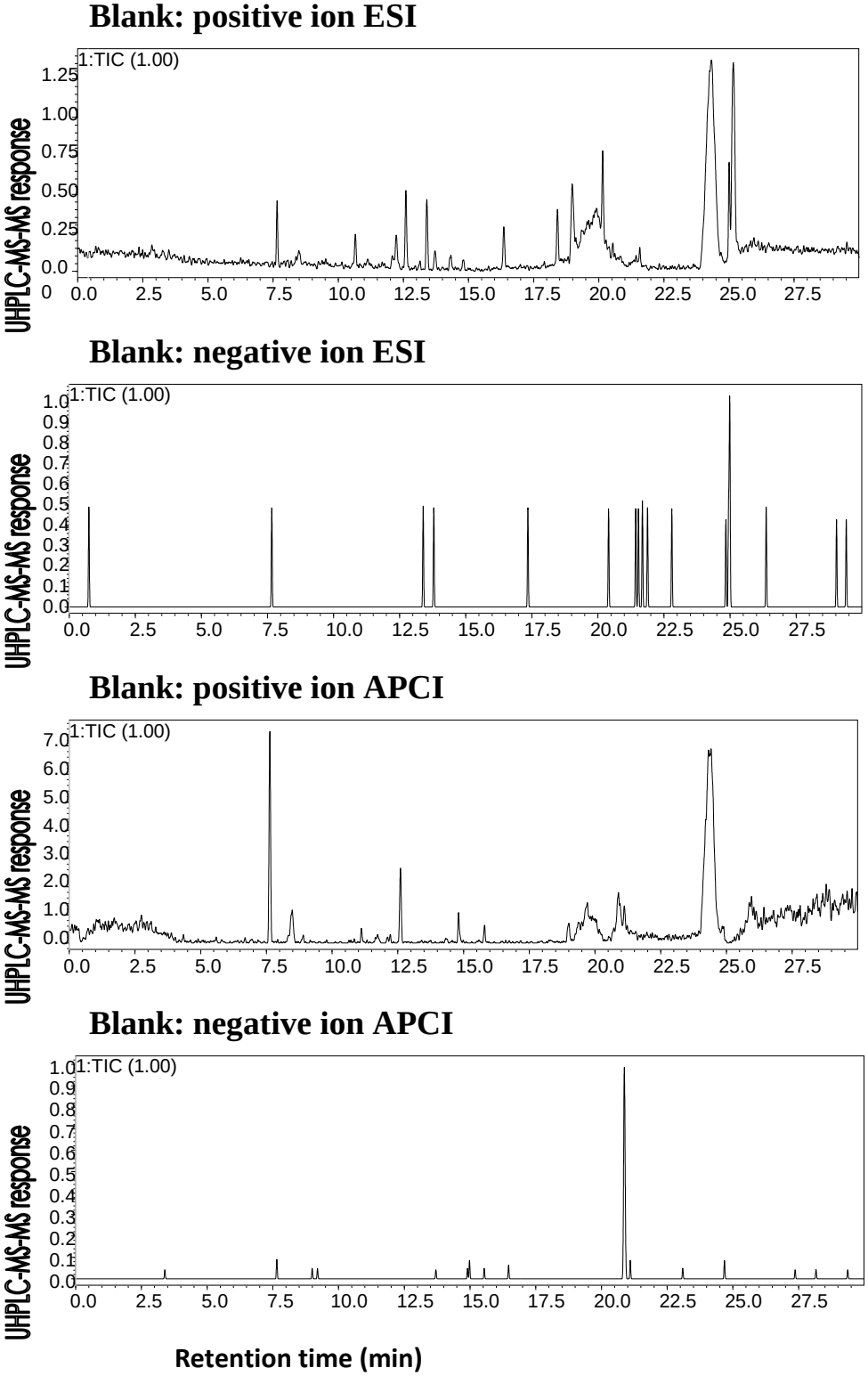

Fig. 4.7. Computer-reconstructed mass chromatograms for the internal standards show the slight variation in retention time from analysis to analysis in the analysis of FP1 G8 (A), FP2 H3 (B), FP3 C5 (C), Pooled (D) and Blank (E). The mass chromatograms have been overlaid onto the TIC and enlarged 5-fold and 15-fold for pyrimethamine and reserpine, respectively.

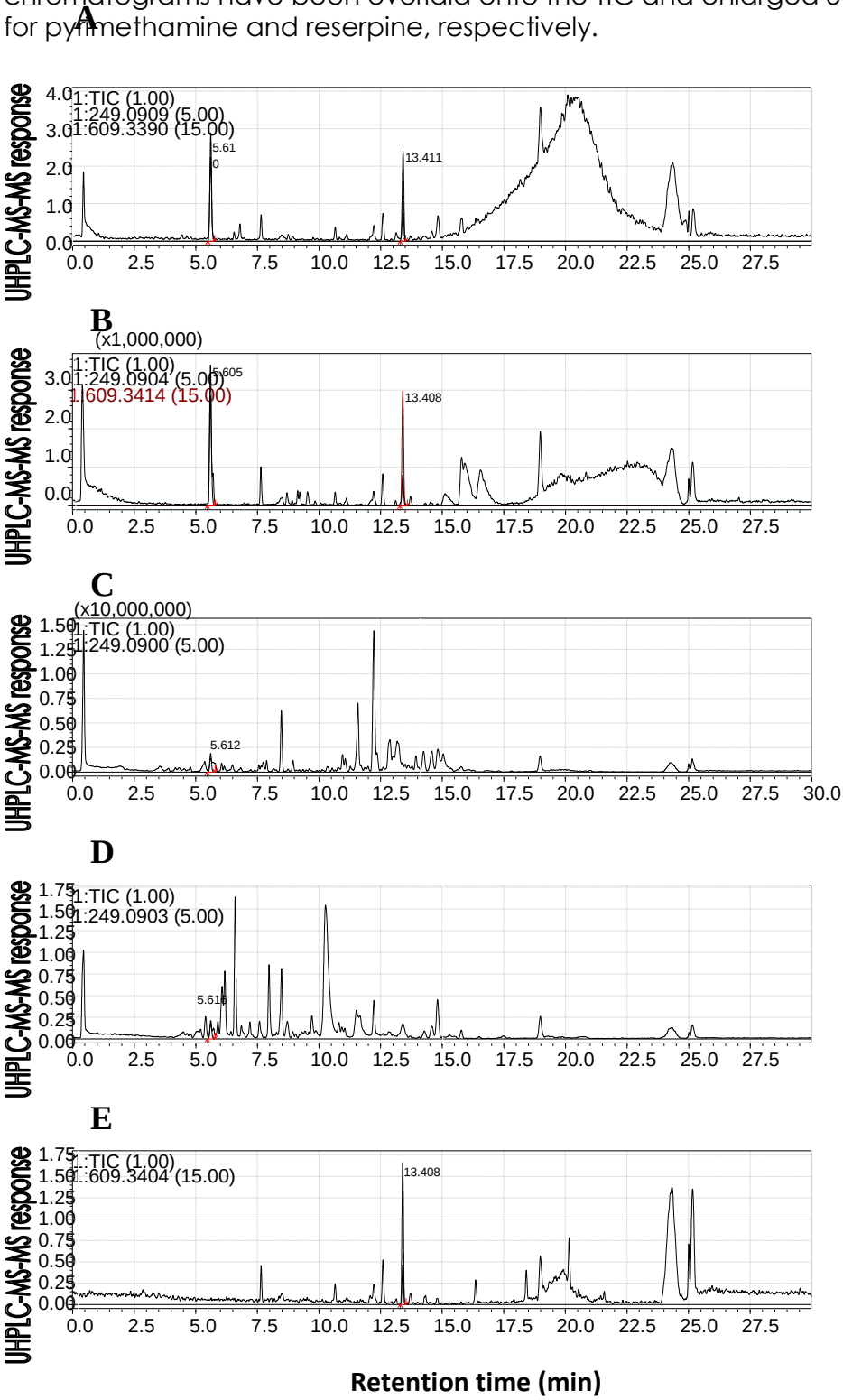

Profiling Solution identified a feature of *m*/z 611.5387 found using positive ion ESI in hit well FP2 H3, but not in the other hits, the pooled sample or the blank. The integration settings used for this and all data processing were described in section 4.2.4.

To further evaluate the peak picking and binning parameters, manual inspection of the data helped to rule out low abundance or noise peaks and was used to look more closely for the same feature in other fractions. This was done to be sure a commonly occurring metabolite did not slip through the requirements and report as a false positive. The extracted ion chromatogram of *m*/z 611.5387 is displayed in Fig. 4.8. This feature was not detected above threshold levels in the other hit fractions, pooled or blank sample, showing that this feature is not a commonly occurring metabolite, or noise. The extracted ion chromatogram of the pooled sample is shown in Fig. 4.9.

The high resolution capability of the IT-TOF facilitated the resolution of the isotope peaks for this feature. The isotope peaks are important for determining the number of charges found on the ion, making mass determination possible based on the measured *m*/z values, even when the ions are multiply charged [81]. The isotope peaks shown in Fig. 4.10 are spaced 1.0056 units apart, which is very close to the theoretical mass of a proton of 1.0073 units [82].

Fig. 4.8. The computer-reconstructed mass chromatogram of the mass range *m/z* 611.53 to 611.55 displayed for the positive ion electrospray analysis of fraction FP2 H3. The Shimadzu LabSolutions software calculated a retention time of 15.925 min for the feature.

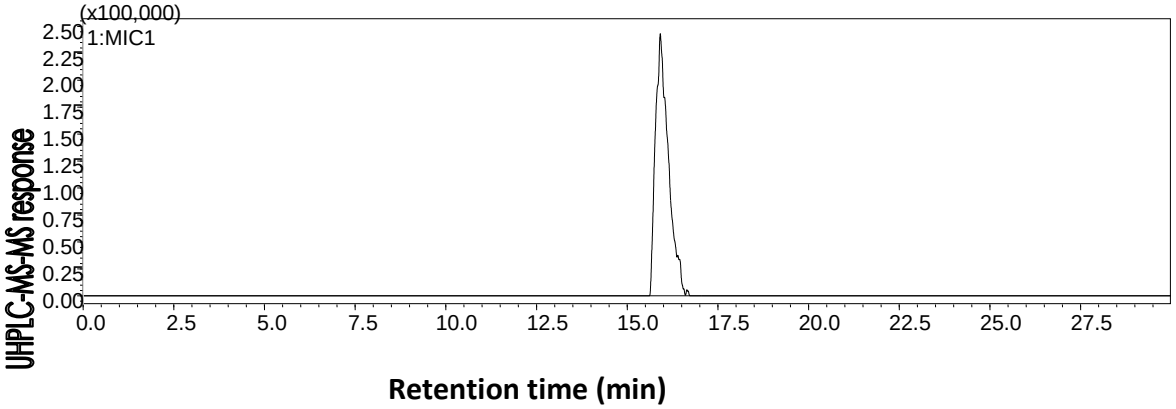

Fig. 4.9. The extracted ion chromatogram of the mass range *m/z* 611.53 to 611.55 displayed for the positive ion electrospray analysis for the pooled sample. While a small peak is visible, it falls below the threshold area of 10,000.

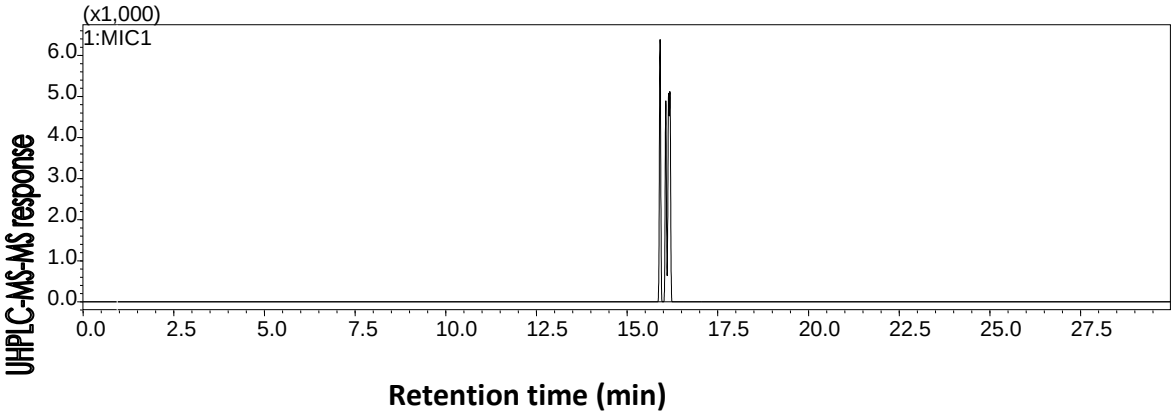

Fig. 4.10. Expanded view of the isotope peaks of the feature of *m/z* 611.5. Because the isotope spacing is approximately 1 unit, the feature represents a singly charged protonated molecule, $[M+H]^+$.

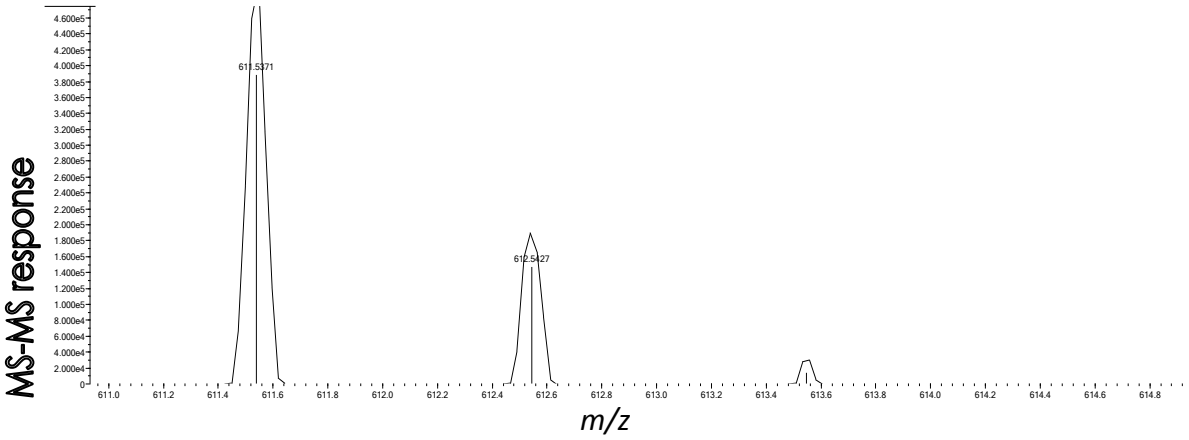

Knowing the denominator in the *m*/z ratio is 1, the mass of the compound can be determined by subtracting the mass of a proton from the measured *m*/z value. The calculated monoisotopic mass of the compound shown here is approximately 610.5314. The monoisotopic mass shown in these examples varies slightly due to peaks being averaged in slightly different widths. The profile acquired during each scan is centroided by LabSolutions software and then averaged over the selected number of scans.

Formula Predictor software from Shimadzu is capable of using the accurate mass measurements and the spacing and abundance of isotope peaks to propose chemical formulas for this ion, which can be useful for searching databases, such as ChemSpider [83]. The potential chemical formulas are scored by a proprietary algorithm and can be sorted based on probability as shown in Table VI.

In addition to the accurate mass measurements, dynamic, automatic product ion scanning was used to record the fragment ions of the most abundant ion in each cycle. The dynamic term means that once a precursor was subjected to product ion scanning a maximum of three times, it would be skipped and the next most abundant precursor used. This is important for wide peaks or polymer smears, so that more, lower abundance precursors can be recorded as well. The wealth of data provided in each LCMS analysis is difficult to reduce to paper. As an example, the MS and MS-MS analyses of the feature of *m*/z 611.53 are shown in Fig. 4.11.

TABLE VI. RANKING OF PREDICTED CHEMICAL FORMULAS FROM THE FORMULA PREDICTOR SOFTWARE FOR THE FEATURE OF *M/Z* 611.5.

Rank	Score DBE	Formula (M)	Ion	Meas. m/z	Pred. m/z	Diff (mDa)	Diff (ppm)	Iso Score
1	78.10 3.0	C36 H70 N2 O5	[M+H]+	611.5371	611.5358	1.3	2.13	80.37
2	77.71 8.0	C37 H66 N6 O	[M+H]+	611.5371	611.5371	0.0	0.00	77.71
3	69.94 -2.0	C33 H74 N2 O5 S	[M+H]+	611.5371	611.5391	-2.0	-3.27	74.15
4	66.54 -1.0	C29 H70 N8 O3 S	[M+H]+	611.5371	611.5364	0.7	1.14	66.78
5	62.04 -6.0	C29 H74 N2 O10	[M+H]+	611.5371	611.5416	-4.5	-7.36	93.43

Fig. 4.11. Positive ion electrospray mass spectrum of the feature eluting at 15.9 min during the analysis of FP2, well H3. (A). The number in parentheses describes the charge state of the ions as determined from the isotope pattern. The data-dependent product ion tandem mass spectrum were acquired for the most abundant precursor ion (*m*/*z* 611) resulting in the dynamic acquisition shown (B). The region *m*/*z* 300 to 400 of the product ion scan is shown enlarged (C).

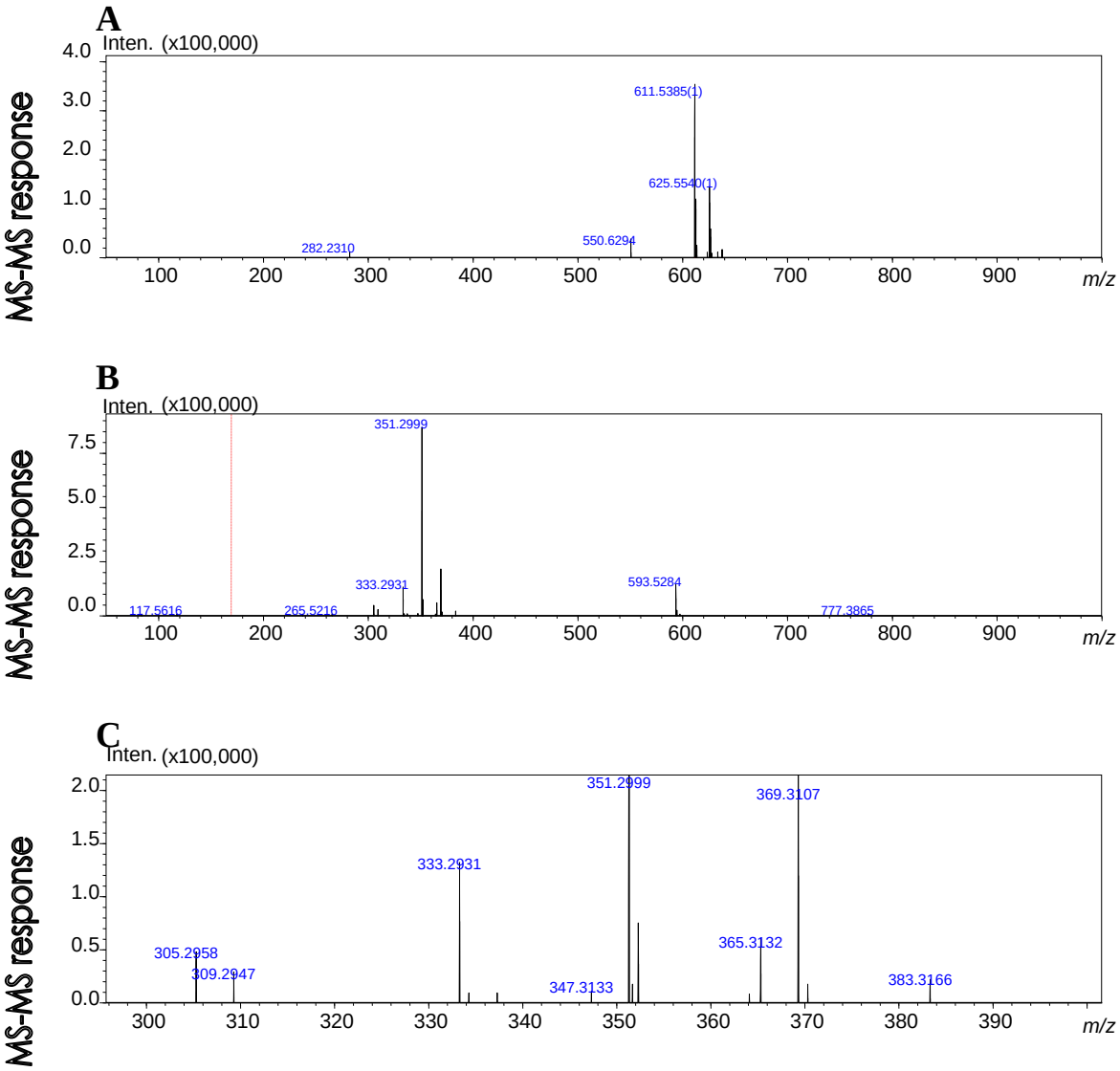

The preceding example displays the amount of information that may be obtained for a single analyte during metabolomics type testing. Features were binned together, and the AUCs for each sample, blanks and pooled sample were sorted to identify the major metabolites that are likely responsible for the inhibition of AcPHF6 aggregation described in Chapter 3. The fractions prepared immediately before and after the hit fraction were analyzed in the metabolomics guided profiling assay following the same protocol as described previously. Features with less than 1,000,000 AUC were disregarded to limit the data to high abundance molecules. The raw area found in the blank was subtracted from the feature's area which was then divided by the neighboring fraction's area. A minimum ratio of 10 was used to determine promising hits because the much higher concentration of those compounds would be responsible for the inhibition of aggregation. The features identified using positive ion electrospray mass spectrometry and subjected to this data processing are displayed in Tables VII, VIII and IX.

The absolute identification of marine actinomycetes secondary metabolites is a challenge. The amount of each metabolite is in the nanogram to microgram range, whereas milligrams are necessary for further purification and NMR spectroscopy. Another, less certain method is the comparison and scoring of the accurate mass MS-MS data to a thorough database containing likely matches. However, the easily accessible databases for an academic researcher currently have the following limitations. Analytes originating from the CAS Registry populate the Scifinder database [84]. Chemspider is only capable of searching by monoisotopic mass, which does not take advantage of the isotope pattern and MS-

TABLE VII. POSITIVE ION ELECTROSPRAY MASS SPECTROMETRY WAS USED TO IDENTIFY FEATURES IN WELL FP1 G8 WHICH ARE TENFOLD MORE ABUNDANT THAN THE PRECEDING (FP1F8) AND SUBSEQUENT (FP1 H8) FRACTIONS.

m/z	**RT**	**FP1 G8**	**Blank**	**FP1 F8**	**FP1 H8**	**Ratio to F8**	**Ratio to H8**
610.1888	20.089	15376322	0	0	0		
612.1859	20.541	3078349	0	0	0		
611.1846	20.399	2820229	0	0	0		
613.1894	20.114	2640606	0	0	0		
663.4566	21.302	1824750	415189	0	0		
591.4303	14.83	1529823	0	0	0		
604.3867	13.412	1501854	603232	0	0		
684.207	24.834	1324038	0	0	0		
611.189	17.509	1314633	0	0	0		
637.3035	15.782	1211004	0	0	0		
550.6316	19.493	1079832	436788	0	0		
685.2184	24.853	1063849	0	0	0		

TABLE VIII. POSITIVE ION ELECTROSPRAY MASS SPECTROMETRY WAS USED TO IDENTIFY FEATURES IN WELL FP2 H3 WHICH ARE TENFOLD MORE ABUNDANT THAN THE PRECEDING (FP2 G3) FRACTION.

m/z	**RT**	**FP2 H3**	**Blank**	**FP2 G3**	**Ratio to G3**
611.5401	15.5	15302112	0	248808	61.5
625.5503	16.245	9154697	0	113149	80.9
515.4254	23.673	8298582	0	352125	23.6
612.5422	15.908	6048604	0	0	
597.524	15.132	4055420	0	0	
626.5565	16.552	3584378	0	0	
257.1489	0.387	3172345	0	0	
684.2071	22.646	3054847	0	0	
159.0795	0.475	2423373	0	80248	30.2
550.6343	19.274	2176268	325514	0	
684.21	19.997	2036377	0	0	
686.2058	20.853	1992630	0	0	
685.2065	22.936	1979528	0	0	
663.4652	19.005	1797905	1521633	0	
685.2052	23.954	1769955	0	0	
637.3115	15.789	1757019	0	0	
387.3197	9.226	1509946	0	0	
686.2051	22.912	1409842	0	0	
604.3848	13.413	1340838	805098	0	
664.4599	19.827	1236862	260743	0	
685.2145	19.934	1235275	0	0	
550.6283	19.683	1170242	826960	0	
550.6411	18.815	1105226	325514	0	
244.1919	7.605	1079474	531790	51949	10.5
687.2097	22.2	1021619	0	0	

TABLE IX. POSITIVE ION ELECTROSPRAY MASS SPECTROMETRY WAS USED TO IDENTIFY FEATURES IN WELL FP3 C5 WHICH ARE TENFOLD MORE ABUNDANT THAN THE PRECEDING (FP3 B5) AND SUBSEQUENT (FP3 D5) FRACTIONS.

m/z	RT	FP3 C5	Blank	FP3 B5	FP3 D5	Ratio to B5	Ratio to D5
395.3652	17.05	8270271	0	553668	0	14.9	
268.1069	0.479	5074845	0	0	283826		17.9
591.4303	14.828	4674925	0	0	0		
411.3636	14.82	3458627	0	0	0		
732.5479	13.102	3342584	0	55333	0	60.4	

MS data acquired by the IT-TOF mass spectrometer [75]. METLIN is capable of searching MS-MS data, but currently contains only about 64,000 metabolites, most of which are mammalian [85].

A hybrid approach to characterization and possibly identification is required to take advantage of any information that can be obtained from these low abundance metabolites. One workflow described by Dr. George Chlipala proceeds in the following manner: collect sediment, isolate bacteria, ferment a batch, homogenize and fractionate the natural products. The fractions can then be tested in various biological assays and the active fraction selected for repurification by liquid chromatography with an ultraviolet detector if necessary. The pure compound can then be characterized by NMR spectroscopy and MS-MS then tested to check whether activity is retained. Obtaining enough pure compound can be quite tedious and requires multiple fermentation and purification steps. The overall outcome is to obtain as much structural data about the analyte as possible, and structure elucidation can be performed manually, or could be determined by matching in a proprietary database.

Daunorubicin was originally isolated from terrestrial actinobacteria, and many structural analogs have been studied over the past 50 years[69]. The features from Tables VII, VIII and IX were investigated for the possibility of being an anthracycline. Each feature was converted to a molecular weight resulting from [M+H]+ and [M+Na]+ and searched in the Massbank database. No structurally related compounds were found. Daunorubicin and doxorubicin form several common product ions when subjected to CID. The *m/z* ratios of 321.07, 306.05,

130.08, and 86.06 were searched in automatic, dynamic product ion scan data from the metabolomics guided profiling experiments. This was done to see if structural analogs to daunorubicin and doxorubicin were present in the important features of the hit fractions. A mass width of 0.2 was used and investigated manually. No evidence of structurally related features were found.

4.4 Conclusions

The hit fractions identified by the high throughput screen were profiled using accurate mass spectrometry and dynamic product ion scanning to further understand the analytes present in each. It will be useful to match the same fractions after the long culturing time required for obtaining more biomass from marine actinomycetes. The new fractions could then be analyzed using the same approach to guarantee that the same metabolites are present. Some structural information can be gathered from the product ion scans. A particularly interesting compound can be manually investigated, and potential structures can be proposed and evaluated.

Potentially active compounds for the inhibition of AcPHF6 aggregation can be pulled out of the large feature list by subtracting commonly occurring metabolites and noise peaks found in the blank. This untargeted metabolomics based approach moves the difficult structure elucidation step to the end of the lead identification process, reducing the work on compounds that will not progress.

CHAPTER 5

QUANTITATIVE ANALYSIS OF PRX-07034 IN RAT TISSUE

5.1 Introduction

5-HT6 receptors may serve as a target to improve cognitive function in a wide variety of neurological disorders. The receptors are localized in the frontal cortex, striatum, and hippocampus; regions affected by tau related neuronal death, and are involved in cognition, memory and learning [83]. Though no compounds are yet approved, research is ongoing to discover and develop compounds that will restore cognition to AD patients through the 5-HT6 receptor [86]. Cognitive decline follows along with the progression of neurodegeneration, and the current course of treatment calls for the administration of cholinesterase inhibitors, which mask symptoms short term, but do not change the progression of the disease. The inhibition of the metabolism of acetylcholine extends the half-life and potentiates the effects of the neurotransmitter, making up for the decreased number of neurons. Serotonin modulators given in concert with neuroprotective compounds, such as tau aggregation inhibitors, would provide synergistic benefit [81].

In addition to cognitive benefits, the 5-HT6 receptor antagonist P7C3 (an analog of latrepirdine, see Fig. 5.1) has been shown to cause neurogenesis and might restore neurons lost during the pre-diagnostic period of the disease [87]. Latrepirdine (Dimebon) is a prototypical 5-HT6 antagonist and was originally developed as an antihistamine. It showed positive effects in AD animal models [18], a phase 2 trial, and a double-blinded phase 3 trial with AD patients [38]. Further clinical

trials were aborted by the investigating drug companies because no improvement was seen in mild to moderate AD patients [38]. However, latrepiridine has been shown to act as a neuroprotective agent through multiple mechanisms, including inhibiting Aβ toxicity [18].

PRX-07034 (Fig. 5.1) is another selective 5-HT6 receptor antagonist, and may prove to be valuable in increasing working memory in patients with a deficit, as well as acting as a neuroprotective and neurogeneration agent like its related compounds [50]. The inhibition of serotonin receptor subtype increases retention of memory in rat models, but does not increase the formation of new memories [49]. Structural analogs SB-271046-A and SB357134-A significantly increased memory retention in rats using a water maze task, whereas the acetyl cholinesterase inhibitor donepezil showed no effect [88]. The structures of these compounds are shown in Fig. 5.1.

PRX-07034 has a high affinity for the 5-HT6 receptor, with a K_i of 4 to 8 nM, as determined by a radioligand binding assay described by McCreary and colleagues [89]. The tested compound also has good selectivity for the GPCR receptor subtype. The binding affinity of PRX-07034 was determined for other 5-HT receptors as well as 59 other proteins, including GPCRs, ion channels, and transporters to test target specificity. It was found to bind the 5HT6 receptor with a much greater affinity than any other tested protein. These results are summarized in Table X.

Fig. 5.1. The structures of PRX-07034 (A), SB-271046-A (B) , SB357134-A (C), latrepirdine (D), P7C3 (E), and donepezil (F).

A

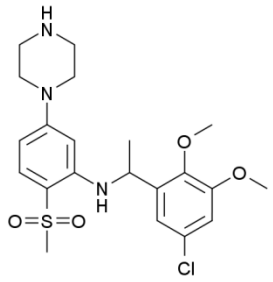

B

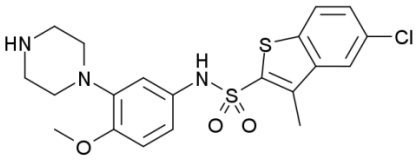

C

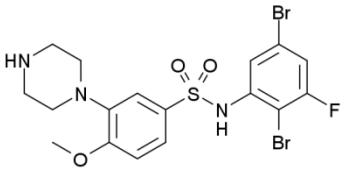

D

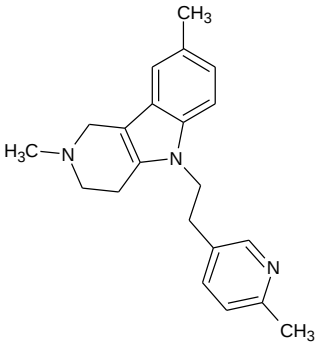

E

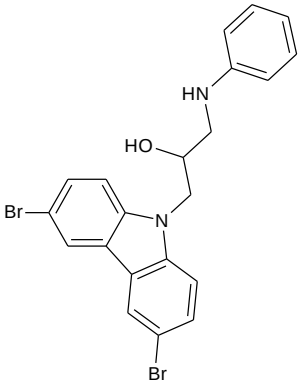

F

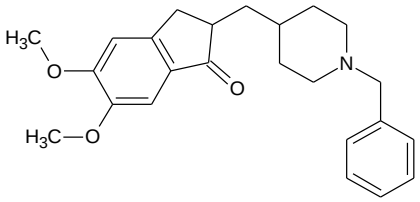

TABLE X. THE RECEPTOR BINDING PROFILE OF PRX-07034 WITH RELATED 5HT RECEPTORS, GPCRS, DOPAMINE AND OPIOID RECEPTORS. THE BINDING AFFINITIES WERE DETERMINED BASED ON THE PERCENT DISPLACEMENT OF PRX-07034 BY KNOWN LIGANDS.

Receptor	**Ligand**	**Tissue/receptor source**	**PRX-07034 Ki/IC_{50}**
5-HT_6	Serotonin/LSD	Human cDNA	4-8 nM
5-HT_{1A}	8-OH-DPAT	Human cDNA	420 nM
5-HT_{1B}	Serotonin/cyanopindolol	Rat cerebral cortex	260 nM
5-HT_{1D}	Serotonin/antag not tested	Bovine caudate	2.8 µM
5-HT_{2A}	Ketanserin	Human cDNA	2.5 µM
5-HT_{2B}	Agonist not tested/LSD	Human cDNA	2.5 µM
5-HT_{2C}	Mesulergine	Human cDNA	3.7 µM
5-HT_3	MDL 72222/BRL 43694	Human cDNA	>5 µM
5-HT_4	Agonist not tested/GR113808	Human cDNA	>5 µM
5-HT_{5A}	Serotonin/LSD	Human cDNA	>5 µM
5-HT_7	Serotonin/LSD	Human cDNA	>5 µM
Other GPCRs			
Dopamine D_3	(+)Butaclamol	Human cDNA	71 nM
Histamine H_2	Cimetidine	Guinea pig cerebellum	0.64 µM
Opioid µ	DAMGO	Human cDNA	0.45 µM

Though dietary, memory and behavioral effects of PRX-07034 have been documented in rats since 2006 [44,86,90], no experimental evidence has been reported that the compound passes the blood-brain barrier (BBB) and enters the brain. By measuring the concentration in the brain, further work can be justified in animal disease models, which are more expensive to perform.

5.2 Materials and Methods

5.2.1 Reagents

PRX-07034 was obtained from Epix Pharmaceuticals (Lexington, MA). Optima grade acetonitrile was purchased from Thermo Fisher (Fair Lawn, NJ). FA and erythromycin were purchased from Sigma Aldrich (St. Louis, MO).

5.2.2 Animals

The study followed protocols established by the Guide for the Care and Use of Laboratory Animals [91]. All animal handling, care and sample collection was performed by Phillip Baker in the UIC Department of Psychology. Male Long-Evans (Charles River Laboratories, Indianapolis, IN) rats weighing approximately 350 g were used for the BBB penetration study. They were given an intraperitoneal injection of either vehicle or 3 mg/kg PRX-07034, with 3 replicates for each condition. The rats were sacrificed by decapitation 30 min post-injection and their brains removed. One mL of blood was collected at the time of sacrifice from which serum was prepared and frozen until analysis.

5.2.3 Sample Preparation

Whole rat brains were rinsed 3 times with deionized water, weighed and homogenized (Polytron Kinematica, Bohemia, NY) on ice with ice-cold 0.1% FA in deionized water, using 1 mL of buffer spiked with 50 nM erythromycin to 100 mg of tissue. Aliquots (100 µL) of brain homogenate were portioned out to 0.6 mL microcentrifuge tubes. Standard curve and recovery samples were spiked into control rat brain homogenate with the listed amount of PRX-07034, and the samples were vortex-mixed. The "crash and shoot" method of sample preparation was used by doing the following steps [86]. Ice-cold acetonitrile (400 µL) was added to each vial to precipitate the protein, and then vortexed for 10 s and sonicated (Branson 2210R-MTH) for 5 min. The samples were centrifuged (Eppendorf 5804R) for 10 min at 8,000 x *g* and the supernatant was removed from the pellet and dried under a stream of nitrogen in separate microcentrifuge tubes.

Internal standard erythromycin (50 nM) was added to each 100 µL aliquot of serum in 0.6 mL microcentrifuge tubes. Standard curve and recovery samples were spiked with the listed amount of PRX-07034, and the samples were vortex-mixed. Ice-cold acetonitrile (400 µL) was added to each vial to precipitate the protein, and the vials were vortexed for 10 s and sonicated for 5 min. The samples were centrifuged for 10 min at 8,000 x *g*, and the supernatant was removed from the pellet and evaporated to dryness under a stream of nitrogen in separate microcentrifuge tubes. At the time of analysis, samples were reconstituted in 50 µL of initial mobile phase, vortexed and centrifuged at 3000 x *g* to remove particulates.

Aliquots (40 µL) of each sample were loaded into autosampler vials for analysis using LC-MS-MS.

Blank brain and serum samples were used to evaluate recovery of the analyte and internal standard. PRX-07034 (611 pg) and erythromycin (50 pg) were spiked into the blank samples either before or after extraction and processed as described above. The raw LC-MS-MS peak areas of the analytes in each set of samples were compared to estimate the recovery of each after reconstitution in starting mobile phase.

5.2.4 Quantitative Analysis Using Liquid Chromatography-Mass Spectrometry

A Shimadzu UHPLC (Nexera LC-30AD) system equipped with an autosampler was used to inject 1 µL of each sample onto a Shimadzu Shimpack XR-ODS III reverse phase column (2 x 50 mm, 1.6 µm packing). The column was maintained at 40° C in a column oven. Mobile phase A consisted of 0.2% formic acid in deionized water, and mobile phase B consisted of 0.2% formic acid in acetonitrile. A linear gradient from 28% B to 50% B over 2 min at 0.3 mL/min, and the column was reequilibrated at 28% B for 1.5 min.

A Shimadzu (LCMS-8030) triple quadrupole mass spectrometer equipped with an electrospray source and controlled by Lab Solutions software, was used to record the SRM transitions *m*/z 454 to 199 and *m*/z 734 to 158 for the protonated molecules of PRX-07034 and the internal standard, respectively. The AUC ratio was calculated by the LabSolutions Browser software using the following settings. Automatic integration by area was performed for one peak per transition with a minimum width of 5 seconds to be considered a peak. The chromatograms were

smoothed using the standard method using 2 counts. This smoothing function replaces the measured intensity of each point with the average of the two adjacent points [87]. The peaks were identified using the window method by absolute retention time, choosing the closest peak within a 10% target window and 20% reference ion ratio window. A reference transition of *m*/z 454 to 184 was used to further confirm the identity of the PRX-07034 transition of *m*/z 454 to 199. The set spectrum intensity of the qualifier ion was set to 50% of the quantifier with a default ion allowance of 20%. Quantitation was performed using the internal standard method with a constant concentration of erythromycin. A best fit curve was fit to the data points linearly and was weighted, using 1/C. 1/C weighting increases the accuracy of lower concentration unknown and quality control samples. The data at the high end of the calibration curve can dominate the linear regression because the absolute error of the instrument is larger at those points, but the relative error is constant over the curve [18]. The curve was not forced through zero. The lower limit of detection (LLOD) was defined as S/N of at least 3, and the lower limit of quantitation (LLOQ) was defined as a S/N greater than 10. Noise was calculated by the method recommended by the American Society for Testing and Materials for the whole range, which incorporates short-term noise, long-term noise, and drift.

The stock of PRX-07034 was analyzed by high resolutions mass spectrometry (HRMS) to confirm the presence of PRX-07034 and check for degradation or contamination of the standard. A Shimadzu HPLC (Prominence LC-20AD-XR) system equipped with an autosampler was used to inject 1 µL of each sample using flow injection analysis. Mobile phase A consisted of 0.1% formic acid in deionized water, and mobile phase B consisted of 0.1% formic acid in acetonitrile. An isocratic flow

of 50% B over 1 min at 0.2 mL/min was use to acquire data. A Shimadzu (LCMS-IT-TOF) ion trap-time of flight hybrid mass spectrometer equipped with an electrospray source operated in positive mode and controlled by Lab Solutions software, was used to scan the *m*/z range of 100 to 1000. The accurate mass determination is capable of predicting the molecular formula of the analyte, and can be used to confirm the identity of PRX-07034.

5.3 Method Validation

The recoveries of both PRX-07034 and erythromycin were tested for both matrices by spiking 2.45 ng/ 100 µL serum or brain homogenate into samples before sample preparation and after. Three replicates of each condition were performed. The raw LC-MS-MS peak areas were determined by using LabSolutions software, and the ratio of averages was used to determine recovery.

The accuracy of the assay was evaluated by spiking known amounts of PRX-07034 into blank serum and brain samples using the same protocol as the standard curve samples. Two quality controls were used for each matrix, one in the lower third of the standard curve, and one in the upper third, but not the same concentration as any standard curve.

The linearity of response of the LC-MS-MS analysis of PRX-07034 in biological matrices was evaluated by preparing a 9-point standard curve in both rat brain homogenate and rat serum. While a 3-order of magnitude standard curve is usually sufficient, the range of linearity was determined to greater than 4 orders of magnitude since the actual concentration of analyte was unknown prior to sample

preparation. A best fit line, weighted 1/C, was applied, and the equation of the line was determined by Lab Solutions software.

5.4 Results and Discussion

Validation of the analytical method described above requires analysis of the recovery of the analyte during sample cleanup. An ideal sample preparation removes most small molecules, proteins and particulate matter from the analyte of interest, while being as cost and time effective as possible. Small molecules found in biological matrices can suppress the ionization of PRX-07034 and the internal standard, causing diminished response and sensitivity by the LC-MS-MS instrument. However, not all small molecules can be discarded, as the analyte and internal standard must be retrieved from the matrix for analysis. By comparing the raw area of each peak when extracted against the raw area of samples which were post-extraction spiked with 2.45 ng / 100 µL sample, the recovery was determined and the results are shown in Table XI.

PRX-07034 and erythromycin were recovered in the range of 54 to 123% from the two matrices. 100% extraction efficiency, while ideal, is not necessary for accurate quantitation. The standard curve samples were spiked into the biological matrices and extracted, so the differences in extraction efficiency are taken into account during quantitation. The recovery percentages exceed 100% due to instrument variation in raw AUC for each analysis. The internal standard was structurally different so raw AUCs had to be compared, instead of normalization to the IS.

TABLE XI. THE RESULTS OF THE RECOVERY EXPERIMENT FOR PRX-07034 AND ERYTHROMYCIN (INTERNAL STANDARD) IN RAT BRAIN HOMOGENATE AND SERUM. THREE REPLICATES WERE AVERAGED AND THE AVERAGE AUC OF THE PRESPIKED SAMPLE WAS COMPARED TO THE POSTSPIKED AVERAGE. THIS METHOD WAS USED SINCE THE INTERNAL STANDARD IS NOT STRUCTURALLY SIMILAR AND HAS DIFFERENT RECOVERY CHARACTERISTICS.

Analyte (2.45 ng / 100 µL)and Matrix	**Mean Recovery %**	**% Relative Standard Deviation**
PRX-07034 in rat brain homogenate	114	12
PRX-07034 in rat serum	110	3.1
Erythromycin in rat brain homogenate	54	2.4
Erythromycin in rat serum	123	21

The accuracy of the analytical method was assessed by spiking known amounts of PRX-07034 into blank matrices, processing and analyzing the samples, then calculating the error of the result. A low concentration of 2.46 ng / 100 µL and a high concentration of 198 ng / 100 µL were used. The accuracy results are shown in Table XII.

The lower limits of detection and quantitation were determined using the S/N ratios of 3 and 10 respectively, by preparing a serial 3-fold dilution of standards and spiking into pre-extracted serum and brain homogenate. For the brain homogenate matrix, the chromatogram for the LLOD (91 pg / 100 µL) and LLOQ (272 pg / 100 µL) are shown in Figs. 5.2 and 5.3 respectively.

The same concentration levels were found for the LLOD and LLOQ in serum. The chromatograms are shown in Figs. 5.4 and 5.5. S/N was calculated by LabSolutions software, with noise calculated by the ASTM method over the entire analysis. This study was used to determine the lowest range the analytical assay could measure reliable.

The linearity of the analytical method described for the quantitation of PRX-07034 was evaluated for both matrices. Matrix matched standard curve samples were prepared as described in the methods section and analyzed by UHPLC-MS-MS. The analysis was linear over more than 4 orders of magnitude for both matrices. Mass spectrometers tend to have sigmoidal response curve to increasing concentrations, so the range of linearity needs to be determined for each analysis. The R^2 value was found to be 0.999 and 0.994 for the brain and serum samples.

TABLE XII. QUALITY CONTROL DATA WAS ACQUIRED TO TEST THE ACCURACY OF THE ASSAY AT LOW AND HIGH CONCENTRATIONS FOR BOTH BRAIN AND SERUM.

Type	**Spiked Concentration**	**Calculated Concentration**	**Relative Accuracy (%)**
Serum - low	2.46 ng/100 µL serum	2.03 ng/100 µL serum	17.5%
Serum - high	198 ng/100 µL serum	213 ng/100 µL serum	7.6%
Brain – low	2.46 ng/10 mg brain	1.75 ng/10 mg brain	28.8%
Brain – high	198 ng/10 mg brain	262 ng/10 mg brain	32.3%

Fig. 5.2. Positive ion UHPLC-MS-MS (Shimadzu 8030) analysis of homogenized rat brain spiked with 91 pg / 100 µL PRX-07034 (top) and internal standard erythromycin (bottom) using CID and SRM.

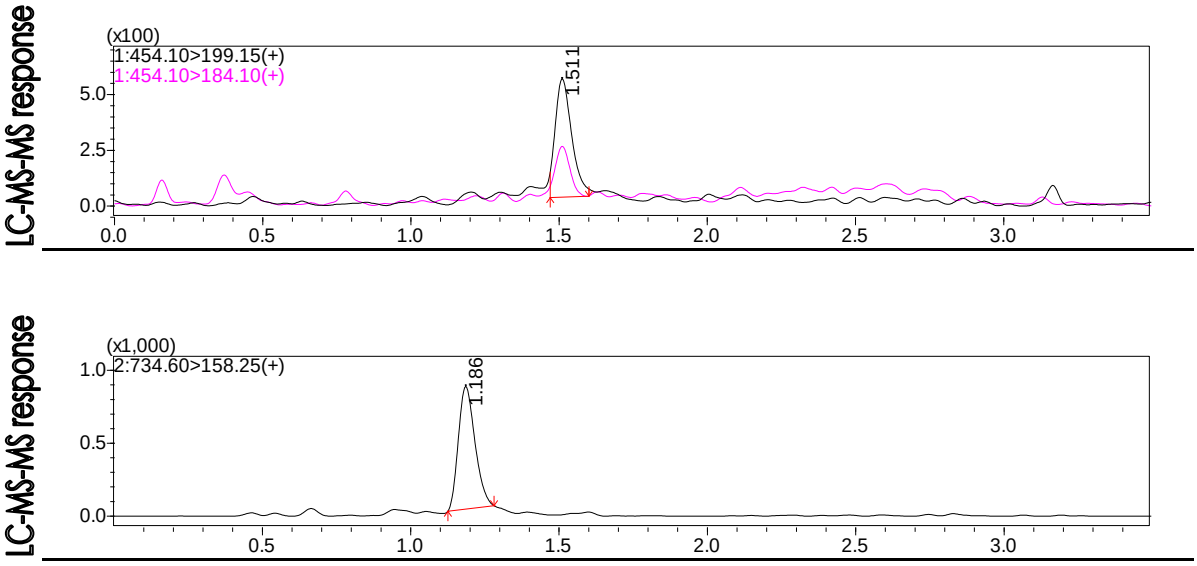

Fig. 5.3. Positive ion UHPLC-MS-MS (Shimadzu 8030) analysis of homogenized rat brain spiked with 272 pg/100 µL PRX-07034 (*m*/*z* 454 → 199 and 184) and internal standard erythromycin (*m*/*z* 734 → 158) using CID and SRM.

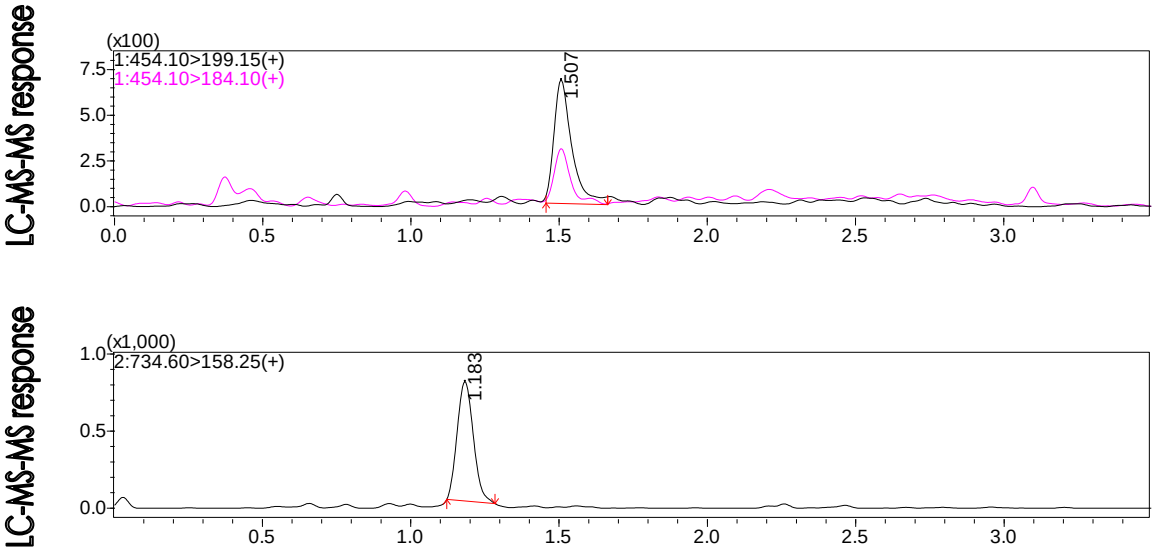

Fig. 5.4. Positive ion LC-MS-MS (Shimadzu 8030) analysis of rat serum spiked with 91 pg / 100 µL PRX-07034 (top) and internal standard erythromycin (bottom) using CID and SRM.

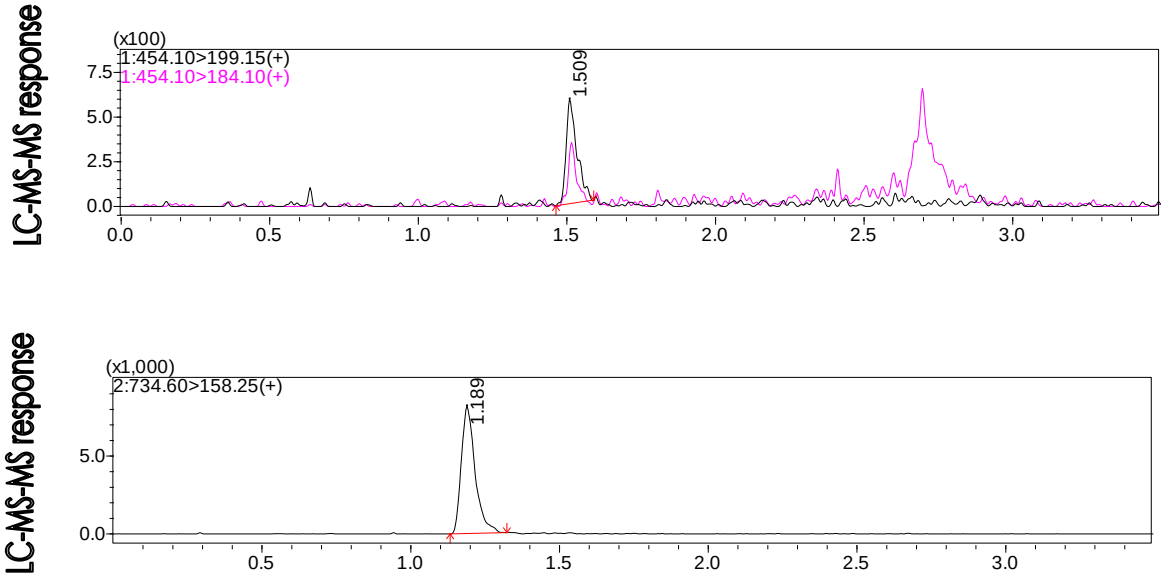

Fig. 5.5. Positive ion LC-MS-MS (Shimadzu 8030) analysis of rat serum spiked with 272 pg/100 µL PRX-07034 (top) and the internal standard erythromycin (bottom) using CID and SRM

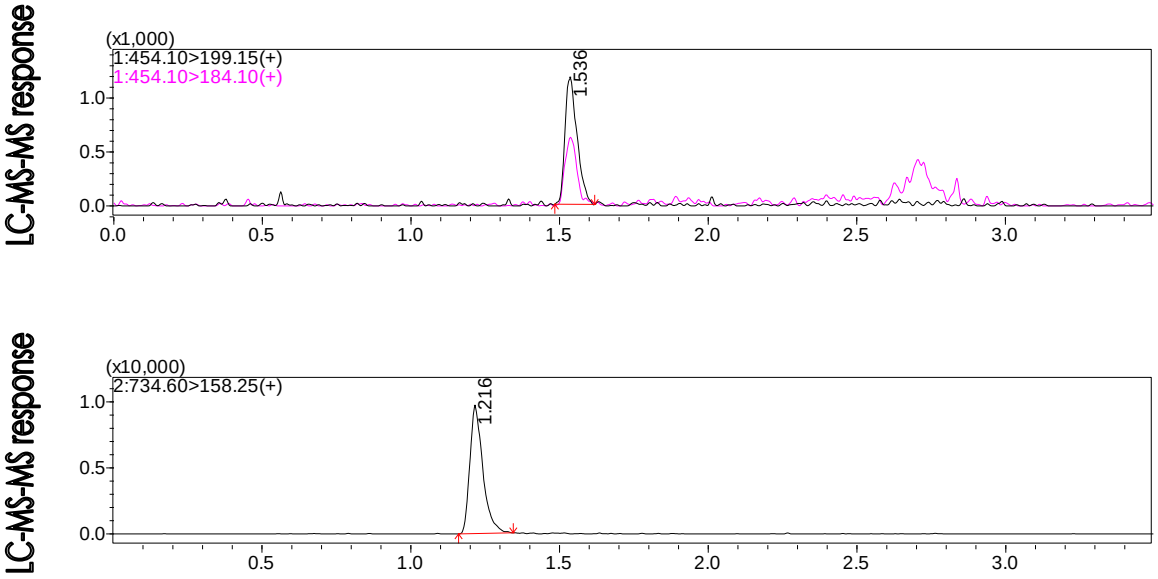

The standard curve and best fit line equation are shown in Fig. 5.6 for rat brain samples and 5.7 for rat serum. While no standard value makes a method acceptable, the R^2 values exceed even the most rigorous linearity requirement, which is 0.990 or better.

The standard of PRX-07034 was confirmed by HRMS, which was performed by flow injection on a Shimadzu IT-TOF hybrid mass spectrometer. The results confirmed the elemental composition of PRX-07034 and did not detect any significant impurities or degradation products. The isotopic envelope of the base peak corresponding to $[M+H]^+$ is shown in Fig. 5.8. Formula Predictor software was used to compare the experimentally determined envelope to theoretical envelopes, and to determine the chemical formulas that would produce such an isotopic ratio. An overall score was given to the experimental data taking into account the mass accuracy of the monoisotopic and isotopic peaks, as well as their relative abundance. The closest theoretical match gave a chemical formula of $C_{21}H_{29}ClN_3O_4S$, which confirmed the expected formula of PRX-07034.

Three analytical replicates of serum and brain from 3 different treated rats were prepared and analyzed by using the UHPLC-MS-MS method described previously. Three untreated rats were used for the collection and pooling of matrix matched standard curve samples, and these samples were interspersed among the unknowns during UHPLC-MS-MS analysis. The mean and standard deviation were calculated for the analytical replicates for each of the 3 rats in serum (Fig. 5.9) and brain (Fig. 5.10). PRX-07034 was detected and quantitated in all serum and brain

Fig. 5.6. The 9-point standard curve of PRX-07034 in rat brain in 3-fold steps from 0.09 to 1782 ng/10 µg brain tissue. The best fit line was weighted using 1/C and not forced through zero, having the equation Y = 106.67X + 0.355 and an R^2 value of 0.999.

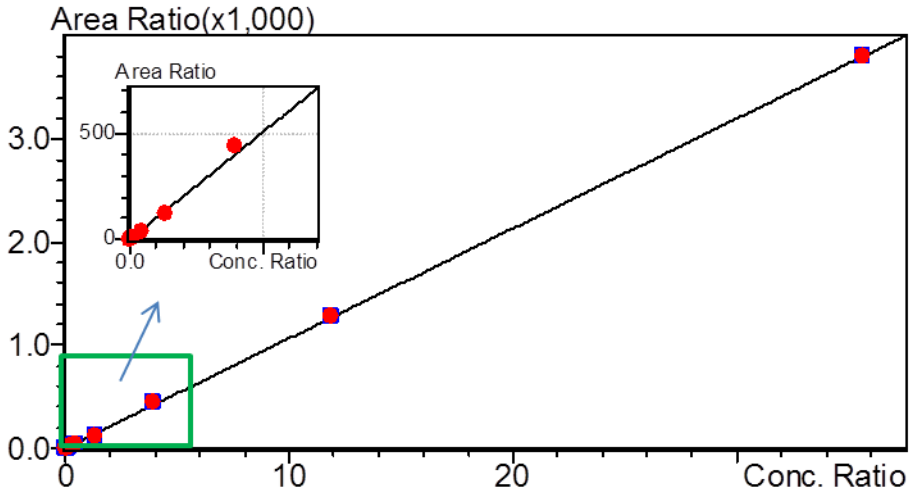

Fig. 5.7. The 9-point standard curve of PRX-07034 in rat serum in 3-fold steps from 0.09 to 1782 ng/100 µL serum. The best fit line was weighted using 1/C and not forced through zero, having the equation Y = 39.770X – 0.100 and an R^2 value of 0.994.

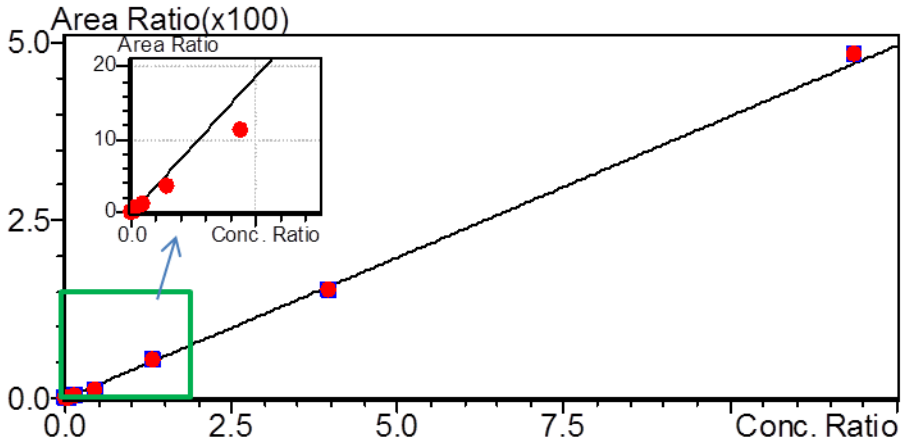

Fig. 5.8. PRX-07034 was analyzed by flow injection – high resolution mass spectrometry to confirm its elemental composition. The isotope ratios of the compound (A) were compared with the theoretically derived values (B). The compound received an isotope score of 62, a mass error of 4.84 ppm and was determined to contain 9.0 double bond equivalents, which was consistent with the expected elemental composition of $C_{21}H_{29}ClN_3O_4S$.

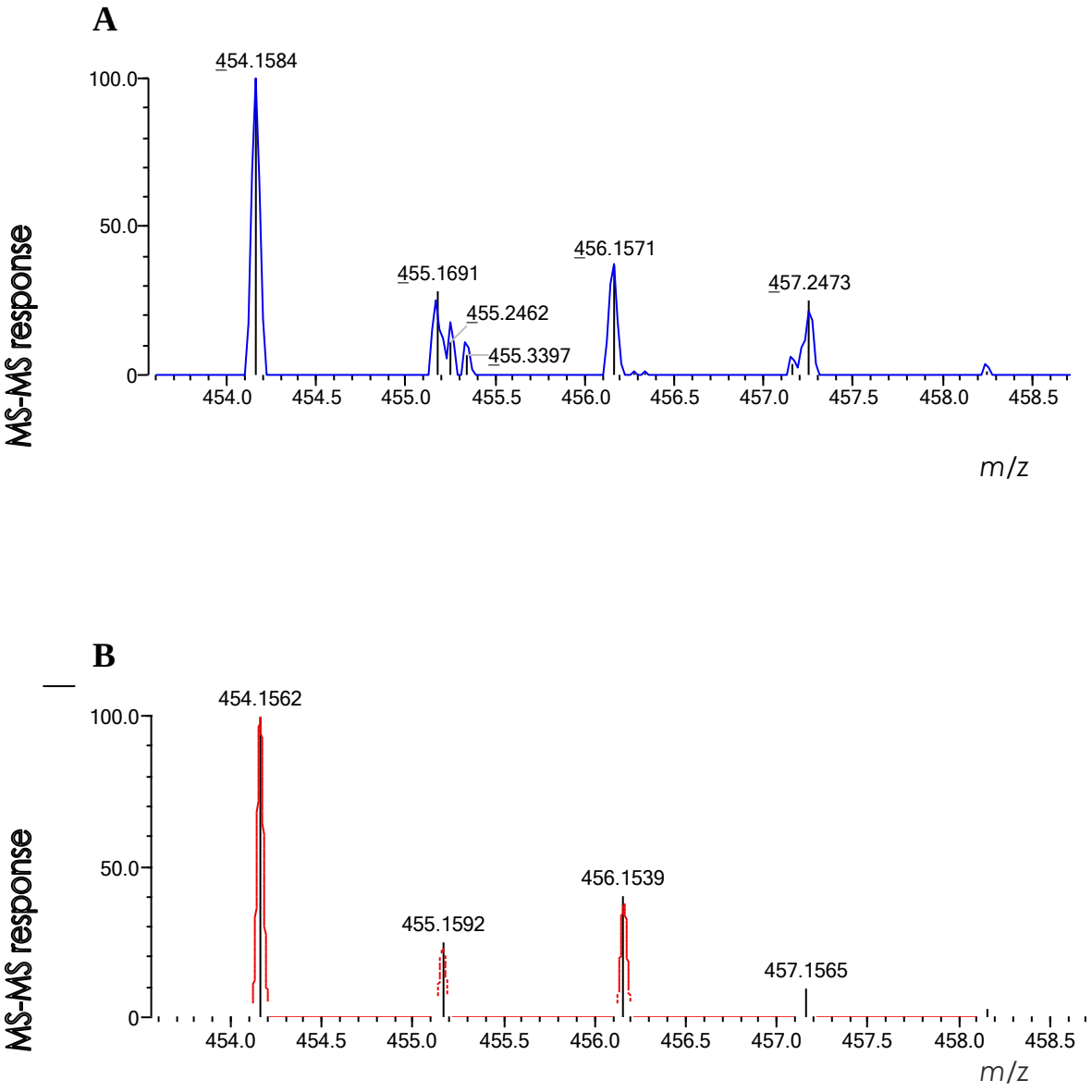

Fig. 5.9. The concentration of PRX-07034 (ng/100 µL) in serum for the 3 rats tested with 3 analytical replicates each.

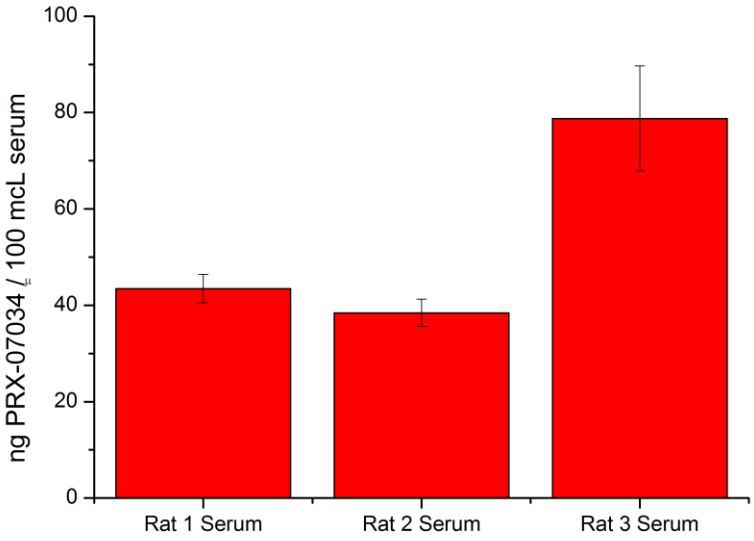

Fig. 5.10. The concentration of PRX-07034 (ng/100 µg tissue) in brain homogenate of the 3 rats tested with 3 analytical replicates each.

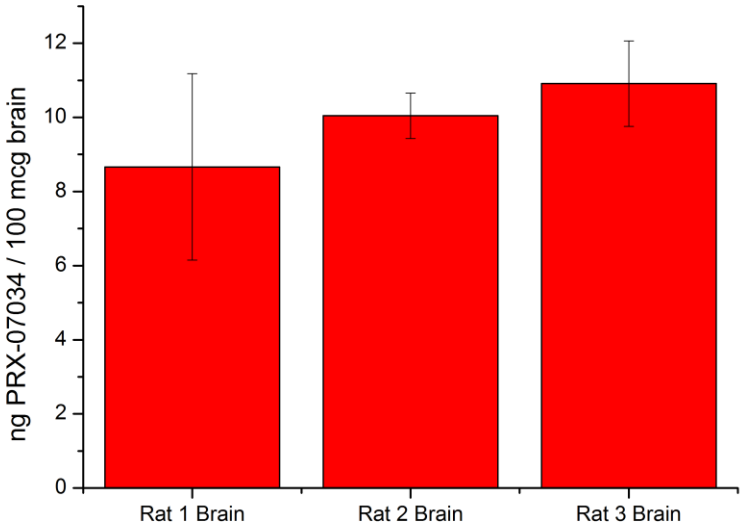

samples, showing that an appreciable proportion of the drug reached the brain and was still present for at least one half hour post-intraperitoneal injection. This is first analytical method for the direct measurement of PRX-07034 in vivo and the first confirmation that this compound crosses the BBB. Previously, PRX-07034 was presumed to cross the BBB based on indirect observation of behavioral changes post administration.

The brain samples were not perfused and voided of residual arterial blood, which contributes a small amount of PRX-07034 to the calculated brain concentration that did not actually cross the BBB. The apparent plasma water space of Sprague-Dawley rats was determined to be 10.3±0.54 µL per gram of brain tissue[92]. This volume of blood contributes up to 4.7% of the PRX-07034 measured in the brain tissue of rat 1, 3.8% in rat 2, and 7.2% of rat 3. While this is a significant amount, the study still proves that a significant amount of PRX-07034 crosses the BBB.

5.5 Conclusion

One of the limitations to treatment of AD and other frontotemporal dementias with therapeutic agent is the ability of the tested compound to cross the BBB and remain in the tissue to elicit a biological change. PRX-07034 was conclusively shown to reach the brain following intraperitoneal injection, agreeing with the dietary, behavioral and memory effects previously described related to presumed selective inhibition of 5HT6 receptors.

Once the marine microbes that were identified as active in the AcPHF6 anti-aggregation assay in Chapter 3 can be recultured, additional active fractions can be prepared. Then, the active compounds can be isolated and identified.

Thereafter, the active compounds can be administered to rats following the same protocol described in this chapter. If the compound can penetrate the BBB in normal rats, it would become a good candidate for testing in biological models of the tauopathies. If the compound cannot be measured in the brain, then structural modification of the lead compound may be possible that could enhance its BBB permeability and other factors such as bioavailability.

A thorough investigation of the absorption, distribution, metabolism, excretion, and toxicology of PRX-07034 would be the next step in this study. This single time point study was able to positively confirm that the PRX-07034 is somewhat stable in serum in rats. Furthermore, the compound is capable of crossing the BBB and reaching the brain, but at a lower concentration than the serum at 30 min post intraperitoneal injection. While serum can be collected from one rat at several time points necessary for nonlinear kinetics studies, brain samples require sacrifice. This increases the number of animals required and decreases the number of analytical replicates possible.

Oral bioavailability of PRX-07034 also needs to be evaluated because capsules and pills provide a convenient route of administration. Dosing schedules for human trials are based on the half-life of the compound in serum. Distribution studies into more organs can be investigated to see where PRX-07034 partitions for potential organ toxicities. The metabolic fate of the compound requires investigation and can be studied in vitro by incubation with rat liver microsomes and accurate mass LC-MS-MS analysis for common metabolic transformations. Live animals are required to study the excretion profile of the compound, and UHPLC-

MS-MS may be used as described above, but the metabolites must also be identified and measured. Analytical standards for metabolites are difficult to obtain and require synthesis or large scale in vitro metabolism and purification, adding a large amount of work to the study. Toxicology should be evaluated at high doses of the compound in otherwise healthy animals. Overall, the ADMET studies require a large expenditure of time and funds, so the efficacy of the compound must justify such investment.

CHAPTER 6

CONCLUSIONS AND FUTURE DIRECTIONS

A novel LC-MS-MS tau aggregation assay was developed to test natural product fractions which would not be possible with the commonly utilized fluorescence assay. The previous assay was limited to testing pure, single compounds. Mass spectrometry allowed for the use of smaller volumes and lower concentrations of the natural product fraction and peptide construct. The assay described in this dissertation also fixes the high rate of false positives and negatives caused by absorption of excitation or emission wavelengths that plague the fluorescence assay. The mass spectrometry based assay did not suffer from the quenching of fluorescence by iron or copper ions, as happens in the previous method.

The novel assay can be used to study the aggregation of full length tau proteins. While more expensive than the peptide construct, hit fractions or purified compounds could be tested in the same manner with the protein. The mass spectrometry based assay would still be superior to the fluorescence assay because it uses lower concentrations of the aggregating species.

Throughput of the natural product fraction screening could be increased by using the autosampler as a liquid handling robot. This would remove most of the hands on time required for screening and extend the workday from 8 to 24 hours. The Nexera SIL-30 autosampler is capable of handling 96 well plates and could make the mixture of incubation solution, natural product fraction and peptide

construct just prior to analysis. This was attempted during assay development, but it appeared that mixing was insufficient. A small advance in mixing ability for the autosampler would be required, either by increasing the dispensing speed or sample loop volume.

Rationally designed Inhibitor 1a was found to inhibit AcPHF6 aggregation in the mass spectrometry based assay, as it did in the fluorescence assay, which agreed with previously published literature. While likely limited by multiple violations of Lipinski's rules from reaching the marketplace, Inhibitor 1a can act as a positive control for tau aggregation assays. Additional natural product fractions from any source could be tested for activity in the aggregation assay, especially with the automation of liquid handling.

Three fractions from marine actinomycetes cultures were found to have significant activity in the novel assay. Once a greater volume of actinomycetes can be grown up, each of the hit fractions should be further purified to isolate single compounds, which would then be retested in the aggregation assay. Once the single small molecule responsible for inhibition is isolated, the structure could be determined using NMR, IR, and mass spectroscopy. Very few databases are available for searching, as is typically done with human metabolites, which are much more commonly studied.

The three fractions were profiled following a metabolomics approach, which will guarantee the active fractions of the next, higher volume reculture can be tested again. Features from the hit fractions were identified and sorted that had the highest abundance and didn't also appear in a pooled sample or the blank

analysis. This removes commonly occurring metabolites and system noise. Chemical formulas were proposed that most closely match the accurate mass measurement and MS-MS data when available. This process helps to move the identification step to the end of the study, because it is the most difficult and time consuming step of natural product screening assays.

The 5-HT6 receptor antagonist PRX-07034 was quantified in both rat serum and brain, showing the small molecule reached the brain *in vivo*, which had never been proven previously. The UHPLC-MS-MS method was validated within common guidelines and was accurate and specific for PRX-07034. A single time point study was used to decrease the number of animals required, but a full DMPK study should be undertaken. The oral bioavailability of the antagonist remains unknown because intraperitoneal injections were used for delivery. The same analytical method validated in this study can be followed for the samples collected at multiple time points. The metabolic products and method of excretion would be the next areas study to bring this compound closer to clinical use.

CITED LITERATURE

1. Murphy DB, Borisy GG. Association of high-molecular-weight proteins with microtubules and their role in microtubule assembly in vitro. *Proceedings of the National Academy of Sciences.* 1975;72(7):2696-2700.

2. Himmler A, Drechsel D, Kirschner MW, Martin DW, Jr. Tau consists of a set of proteins with repeated C-terminal microtubule-binding domains and variable N-terminal domains. *Molecular and cellular biology.* 1989;9(4):1381-1388.

3. Lee G, Cowan N, Kirschner M. The primary structure and heterogeneity of tau protein from mouse brain. *Science.* 1988;239(4837):285-288.

4. Alonso AD, Zaidi T, Novak M, Barra HS, Grundke-Iqbal I, Iqbal K. Interaction of tau isoforms with Alzheimer's disease abnormally hyperphosphorylated tau and in vitro phosphorylation into the disease-like protein. *J Biol Chem.* 2001;276(41):37967-37973.

5. Ballatore C, Lee VM, Trojanowski JQ. Tau-mediated neurodegeneration in Alzheimer's disease and related disorders. *Nat Rev Neurosci.* 2007;8(9):663-672.

6. Weingarten MD, Lockwood AH, Hwo SY, Kirschner MW. A protein factor essential for microtubule assembly. *Proceedings of the National Academy of Sciences of the United States of America.* 1975;72(5):1858-1862.

7. Kopke E, Tung YC, Shaikh S, Alonso AC, Iqbal K, Grundke-Iqbal I. Microtubule-associated protein tau. Abnormal phosphorylation of a non-paired helical filament pool in Alzheimer disease. *J Biol Chem.* 1993;268(32):24374-24384.

8. Kountouras J, Tsolaki M, Gavalas E, et al. Relationship between Helicobacter pylori infection and Alzheimer disease. *Neurology.* 2006;66(6):938-940.

9. Crapper DR, Krishnan SS, Quittkat S. Aluminum, neurofibrillary degeneration and Alzheimer's disease. *Brain.* 1976;99(1):67-80.

10. Coyle JT, Price DL, DeLong MR. Alzheimer's disease: a disorder of cortical cholinergic innervation. *Science.* 1983;219(4589):1184-1190.

11. Hynd MR, Scott HL, Dodd PR. Glutamate-mediated excitotoxicity and neurodegeneration in Alzheimer's disease. *Neurochem Int.* 2004;45(5):583-595.

12. Sommer B. Alzheimer's disease and the amyloid cascade hypothesis: ten years on. *Curr Opin Pharmacol.* 2002;2(1):87-92.

13. Voet D, Voet J. *Biochemistry.* John Wiley and Sons, Inc.; 2004.

14. Hardy J, Selkoe DJ. The amyloid hypothesis of Alzheimer's disease: progress and problems on the road to therapeutics. *Science.* 2002;297(5580):353-356.

15. Mudher A, Lovestone S. Alzheimer's disease – do tauists and baptists finally shake hands? *Trends in Neurosciences.* 2002;25(1):22-26.

16. Wang R, Meschia JF, Cotter RJ, Sisodia SS. Secretion of the beta/A4 amyloid precursor protein. Identification of a cleavage site in cultured mammalian cells. *Journal of Biological Chemistry.* 1991;266(25):16960-16964.

17. Lamb BT, Sisodia SS, Lawler AM, et al. Introduction and expression of the 400 kilobase precursor amyloid protein gene in transgenic mice. *Nature genetics.* 1993;5(1):22-30.

18. Dolan J. Calibration Curves, Part V: Curve Weighting. 2009; http://www.chromatographyonline.com/lcgc/Column%3A+LC+Troubleshooting/Calibration-Curves-Part-V-Curve-Weighting/ArticleStandard/Article/detail/613591. Accessed 12/23/2013, 2013.

19. Duff K, Holcomb L, Gordon MN, et al. Accelerated Alzheimer-type phenotype in transgenic mice carrying both mutant amyloid precursor protein and presenilin 1 transgenes. *Nature Medicine.* 1998;4(1):97-100.

20. Dickson DW, Crystal HA, Mattiace LA, et al. Identification of Normal and Pathological Aging in Prospectively Studied Nondemented Elderly Humans. *Neurobiology of Aging.* 1992;13(1):179-189.

21. Iqbal K, Liu F, Gong CX, Alonso Adel C, Grundke-Iqbal I. Mechanisms of tau-induced neurodegeneration. *Acta Neuropathol.* 2009;118(1):53-69.

22. Baki L, Shioi J, Wen P. PS1 activates PI3K thus inhibiting GSK-3 activity and tau overphosphorylation: effects of FAD mutations. *EMBO J.* 2004(23):2586-2596.

23. Alonso Adel C, Mederlyova A, Novak M, Grundke-Iqbal I, Iqbal K. Promotion of hyperphosphorylation by frontotemporal dementia tau mutations. *J Biol Chem.* 2004;279(33):34873-34881.

24. Khatoon S, Grundke-Iqbal I, Iqbal K. Brain Levels of Microtubule-Associated Protein ? Are Elevated in Alzheimer's Disease: A Radioimmuno-Slot-Blot Assay for Nanograms of the Protein. *Journal of Neurochemistry.* 1992;59(2):750-753.

25. Mah VH, Eskin TA, Kazee AM, Lapham L, Higgins GA. In situ hybridization of calcium/calmodulin dependent protein kinase II and tau mRNAs; species differences and relative preservation in Alzheimer's disease. *Brain Res Mol Brain Res.* 1992;12(1-3):85-94.

26. Inouye H, Sharma D, Goux WJ, Kirschner DA. Structure of Core Domain of Fibril-Forming PHF/Tau Fragments. *Biophysical Journal.* 2006;90(5):1774-1789.

27. Guo JL, Lee VM. Seeding of normal Tau by pathological Tau conformers drives pathogenesis of Alzheimer-like tangles. *J Biol Chem.* 2011;286(17):15317-15331.

28. Alonso AC, Grundke-Iqbal I, Iqbal K. Alzheimer's disease hyperphosphorylated tau sequesters normal tau into tangles of filaments and disassembles microtubules. *Nature Medicine.* 1996;2(7):783-787.

29. Alonso AD, Grundke-Iqbal I, Barra HS, Iqbal K. Abnormal phosphorylation of tau and the mechanism of Alzheimer neurofibrillary degeneration: sequestration of microtubule-associated proteins 1 and 2 and the disassembly of microtubules by the abnormal tau. *Proceedings of the National Academy of Sciences of the United States of America.* 1997;94(1):298-303.

30. Maeda S, Sahara N, Saito Y, Murayama S, Ikai A, Takashima A. Increased levels of granular tau oligomers: an early sign of brain aging and Alzheimer's disease. *Neurosci Res.* 2006;54(3):197-201.

31. Kim I, Xu W, Reed JC. Cell death and endoplasmic reticulum stress: disease relevance and therapeutic opportunities. *Nat Rev Drug Discov.* 2008;7(12):1013-1030.

32. Cheng X, van Breemen RB. Mass spectrometry-based screening for inhibitors of beta-amyloid protein aggregation. *Anal Chem.* 2005;77(21):7012-7015.

33. Wischik CM, Novak M, Thogersen HC, et al. Isolation of a fragment of tau derived from the core of the paired helical filament of Alzheimer disease. *Proceedings of the National Academy of Sciences of the United States of America.* 1988;85(12):4506-4510.

34. Goux W, Kopplin L, Nguyen A, et al. The Formation of Straight and Twisted Filaments from Short Tau Peptides. *The Journal of Biological Chemistry.* 2004;279(26):26868-26875.

35. Pardridge WM. The blood-brain barrier: bottleneck in brain drug development. *NeuroRX.* 2005;2(1):3-14.

36. Lang AE, Gill S, Patel NK, et al. Randomized controlled trial of intraputamenal glial cell line-derived neurotrophic factor infusion in Parkinson disease. *Ann Neurol.* 2006;59(3):459-466.

37. Pardridge WM. Drug and gene delivery to the brain: the vascular route. *Neuron.* 2002;36(4):555-558.

38. Pardridge WM. *Brain drug targeting: the future of brain drug development.* Cambridge University Press; 2001.

39. Davson H, Segal MB. The blood-brain barrier. *Physiology of the CSF and of the Blood-Brain Barrier*. New York: CRC; 1995:49-91.

40. Stewart PA, Wiley MJ. Developing Nervous-Tissue Induces Formation of Blood-Brain-Barrier Characteristics in Invading Endothelial-Cells - a Study Using Quail-Chick Transplantation Chimeras. *Developmental Biology.* 1981;84(1):183-192.

41. Brightman M. Implication of astroglia in the blood-brain barrier. *Ann N Y Acad Sci.* 1991;633(1):343-347.

42. Kroeze WK, Kristiansen K, Roth BL. Molecular Biology of Serotonin Receptors - Structure and Function at the Molecular Level. *Curr. Top. Med. Chem.* 2002;2(6):507-528.

43. Raymond JR, Mukhin YV, Gelasco A, et al. Multiplicity of mechanisms of serotonin receptor signal transduction. *Pharmacology & Therapeutics.* 2001;92(2–3):179-212.

44. Shacham S, Heal D, Cheetham S, et al. PRX-07034, a potent and selective 5-HT 6 receptor antagonist, reduces food intake and body weight in dietary-induced obese (DIO) rats. 2006 Abstract Viewer/Itinerary Planner, Program No. 62.10. *Society for Neuroscience, Washington, DC.* 2006.

45. Kohen R, Metcalf MA, Khan N, et al. Cloning, Characterization, and Chromosomal Localization of a Human 5-HT6 Serotonin Receptor. *Journal of Neurochemistry.* 1996;66(1):47-56.

46. Dunnett SB, Evenden JL, Iversen SD. Delay-dependent short-term memory deficits in aged rats. *Psychopharmacology.* 1988;96(2):174-180.

47. Riemer C, Borroni E, Levet-Trafit B, et al. Influence of the 5-HT6 Receptor on Acetylcholine Release in the Cortex: Pharmacological Characterization of 4-(2-Bromo-6-pyrrolidin-1-ylpyridine-4-sulfonyl)phenylamine, a Potent and Selective 5-HT6 Receptor Antagonist†. *J. Med. Chem.* 2003;46(7):1273-1276.

48. Bentley J, Sleight A, Marsden C, Fone K. 5-HT6 antisense oligonucleotide icv affects rat performance in the water maze and feeding. *J Psychopharmacol.* 1997;11(3 Suppl):A64.

49. Zhang J, Chung TD, Oldenburg KR. Validation of High Throughput Screening Assays. *Journal of Biomolecular Screening.* 1999;4(2).

50. Woolley ML, Marsden CA, Sleight AJ, Fone KCF. Reversal of a cholinergic-induced deficit in a rodent model of recognition memory by the selective 5-HT[sub 6] receptor antagonist, Ro 04-6790. *Psychopharmacology.* 2003;170(4):358-367.

51. Hegner YL, Lee Y, Grodd W, Braun C. Comparing tactile pattern and vibrotactile frequency discrimination: a human fMRI study. *Journal of neurophysiology.* 2010;103(6):3115-3122.

52. Bartus RT, Fleming D, Johnson HR. Aging in the Rhesus Monkey: Debilitating Effects on Short-term Memory. *Journal of Gerontology.* 1978;33(6):858-871.

53. Henkel T, Brunne RM, Müller H, Reichel F. Statistical Investigation into the Structural Complementarity of Natural Products and Synthetic Compounds. *Angewandte Chemie International Edition.* 1999;38(5):643-647.

54. Newman DJ, Cragg GM, Snader KM. Natural Products as Sources of New Drugs over the Period 1981−2002. *Journal of Natural Products.* 2003;66(7):1022-1037.

55. Koehn FE, Carter GT. The evolving role of natural products in drug discovery. *Nat Rev Drug Discov.* 2005;4(3):206-220.

56. Peczuh MW, Hamilton AD. Peptide and protein recognition by designed molecules. *Chem. Rev.* 2000;100(7):2479-2493.

57. Evans BE, Rittle KE, Bock MG, et al. Methods for drug discovery - development of potent, selective, orally effective cholecystokinin antagonists. *J. Med. Chem.* 1988;31(12):2235-2246.

58. Zhang CO, DeLisi C. Estimating the number of protein folds. *J. Mol. Biol.* 1998;284(5):1301-1305.

59. Finkelstein AV, Ptitsyn OB. Why do globular proteins fit the limited set of foldin patterns? *Progress in Biophysics and Molecular Biology.* 1987;50(3):171-190.

60. Anantharaman V, Aravind L, Koonin EV. Emergence of diverse biochemical activities in evolutionarily conserved structural scaffolds of proteins. *Curr. Opin. Chem. Biol.* 2003;7(1):12-20.

61. Zuckerkandl E, Pauling L. Molecules as documents of evolutionary history. *Journal of Theoretical Biology Journal of Theoretical Biology.* 1965;8(2):357-366.

62. Dumont FJ. FK506, an immunosuppressant targeting calcineurin function. *Curr. Med. Chem.* 2000;7(7):731-748.

63. Abraham RT, Wiederrecht GJ. Immunopharmacology of rapamycin. *Annu. Rev. Immunol.* 1996;14:483-510.

64. Chen TS, Li XH, Petuch B, Shafiee A, So L. Structural modification of the immunosuppressants FK-506 and ascomycin using a biological approach. *Chimia.* 1999;53(12):596-600.

65. Rojas Quijano FA, Morrow D, Wise BM, Brancia FL, Goux WJ. Prediction of Nucleating Sequences from Amyloidogenic Propensities of Tau-Related Peptides†. *Biochemistry.* 2006;45(14):4638-4652.

66. McMahon JB, Beutler JA, O'Keefe BR, Goodrum CBB, Myers MA, Boyd MR. Development of a Cyanovirin-N-HIV-1 gpl20 Binding Assay for High Throughput Screening of Natural Product Extracts by Time-Resolved Fluorescence. *Journal of Biomolecular Screening.* 2000;5(3):169-176.

67. Rahimi Y, Goulding A, Shrestha S, Mirpuri S, Deo SK. Mechanism of copper induced fluorescence quenching of red fluorescent protein, DsRed. *Biochemical and Biophysical Research Communications.* 2008;370(1):57-61.

68. Goux WJ, Kopplin L, Nguyen AD, et al. The formation of straight and twisted filaments from short tau peptides. *J Biol Chem.* 2004;279(26):26868-26875.

69. Di Marco A, Gaetani M, Orezzi P, et al. Daunomycin', a new antibiotic of the rhodomycin group. *Nature.* 1964;201:706-707.

70. Zheng J, Liu C, Sawaya MR, et al. Macrocyclic β-Sheet Peptides That Inhibit the Aggregation of a Tau-Protein-Derived Hexapeptide. *Journal of the American Chemical Society.* 2011;133(9):3144-3157.

71. Nowick JS, Chung DM, Maitra K, Maitra S, Stigers KD, Sun Y. An Unnatural Amino Acid that Mimics a Tripeptide β-Strand and Forms β-Sheetlike Hydrogen-Bonded Dimers. *Journal of the American Chemical Society.* 2000;122(32):7654-7661.

72. Kundu A, Kishore N. 1,1,1,3,3,3-hexafluoroisopropanol induced thermal unfolding and molten globule state of bovine a-lactalbumin: Calorimetric and spectroscopic studies. *Biopolymers.* 2004;73(4):405-420.

73. Chaudhary N, Singh S, Nagaraj R. Morphology of self-assembled structures formed by short peptides from the amyloidogenic protein tau depends on the solvent in which the peptides are dissolved. *J Pept Sci.* 2009;15(10):675-684.

74. Nowick JS, Lam KS, Khasanova TV, et al. An Unnatural Amino Acid that Induces β-Sheet Folding and Interaction in Peptides. *Journal of the American Chemical Society.* 2002;124(18):4972-4973.

75. *Nexera SIL-30AC Instruction Manual.* Shimadzu Corporation, Analytical and Measuring Instruments Division;2011.

76. Dunn WB, Broadhurst D, Begley P, et al. Procedures for large-scale metabolic profiling of serum and plasma using gas chromatography and liquid chromatography coupled to mass spectrometry. *Nat. Protocols.* 2011;6(7):1060-1083.

77. Savitzky A, Golay MJE. Smoothing and Differentiation of Data by Simplified Least Squares Procedures. *Analytical Chemistry.* 1964;36(8):1627-1639.

78. Smith CA, Want EJ, O'Maille G, Abagyan R, Siuzdak G. XCMS: Processing Mass Spectrometry Data for Metabolite Profiling Using Nonlinear Peak Alignment, Matching, and Identification. *Analytical Chemistry.* 2006;78(3):779-787.

79. Pickhardt M, Gazova Z, von Bergen M, et al. Anthraquinones Inhibit Tau Aggregation and Dissolve Alzheimer's Paired Helical Filaments in Vitro and in Cells. *Journal of Biological Chemistry.* 2005;280(5):3628-3635.

80. Taniguchi S, Suzuki N, Masuda M, et al. Inhibition of Heparin-induced Tau Filament Formation by Phenothiazines, Polyphenols, and Porphyrins. *Journal of Biological Chemistry.* 2005;280(9):7614-7623.

81. Meyerson S, Haar RWV. Multiply Charged Organic Ions in Mass Spectra. *The Journal of Chemical Physics.* 1962;37(10):2458-2462.

82. Silverstein R, Webster F. *Spectrometric identification of organic compounds.* Wiley. com; 2006.

83. Pence HE, Williams A. ChemSpider: an online chemical information resource. *Journal of Chemical Education.* 2010;87(11):1123-1124.

84. Fone KCF. An update on the role of the 5-hydroxytryptamine6 receptor in cognitive function. *Neuropharmacology.* 2008;55(6):1015-1022.

85. Scripps Center for Metabolomics. METLIN: Metabolite and Tandem MS Database. 2012; http://metlin.scripps.edu/. Accessed 08/01/2012, 2012.

86. Polson C, Sarkar P, Incledon B, Raguvaran V, Grant R. Optimization of protein precipitation based upon effectiveness of protein removal and ionization effect in liquid chromatography–tandem mass spectrometry. *Journal of Chromatography B.* 2003;785(2):263-275.

87. O'Haver T. Smoothing. 2008; http://terpconnect.umd.edu/~toh/spectrum/Smoothing.html. Accessed 12/10/2013, 2013.

88. Rogers C, Hagan J. 5-HT6 receptor antagonists enhance retention of a water maze task in the rat. *Psychopharmacology.* 2001;158(2):114-119.

89. McCreary AC, Glennon JC, Ashby CR, et al. SLV313 (1-(2, 3-Dihydro-Benzo[1, 4] Dioxin-5-yl)-4-[5-(4-Fluoro-Phenyl)-Pyridin-3-ylmethyl]-Piperazine Monohydrochloride): A Novel Dopamine D2 Receptor Antagonist and 5-HT1A Receptor Agonist Potential Antipsychotic Drug. *Neuropsychopharmacology.* 2006;32(1):78-94.

90. Mohler E, Baker P, Gannon K, et al. The effects of PRX-07034, a novel 5-HT6 antagonist, on cognitive flexibility and working memory in rats. *Psychopharmacology.* 2012;220(4):687-696.

91. Care of Animals Council NR. *Guide for the Care and Use of Laboratory Animals: Eighth Edition.* The National Academies Press; 2011.

92. Friden M, Ljungqvist H, Middleton B, Bredberg U, Hammarlund-Udenaes M. Improved measurement of drug exposure in the brain using drug-specific correction for residual blood. *J Cereb Blood Flow Metab.* 2009;30(1):150-161.

APPENDIX

The animal research plan was approved by the Animal Care Committee prior to beginning this study. The approval number is 09-173.

VITA

NAME	Kevin M. Krock
EDUCATION	Ph.D. candidate, Medicinal Chemistry, University of Illinois at Chicago, Chicago, Illinois
	B.S., Pharmaceutical Sciences: Pharmaceutics, University of Toledo, Toledo, Ohio (2007)
RESEARCH EXPERIENCE	Shimadzu Scientific Instruments, Applications Laboratory, Pleasanton, California: LC-MS Application Scientist, 2012-Present
	Department of Medicinal Chemistry and Pharmacognosy, University of Illinois at Chicago, Chicago, Illinois: Research Assistant, 2007-2012
	Research Resource Center (RRC), University of Illinois at Chicago, Chicago, Illinois: Research Assistant 2011-2012
TEACHING EXPERIENCE	Department of Medicinal Chemistry and Pharmacognosy, University of Illinois at Chicago, Chicago, Illinois: Teaching Assistant, 2007-2009
PROFESSIONAL MEMBERSHIP	American Association of Pharmaceutical Scientists, former Chairman of UIC Student Chapter
	American Society for Mass Spectrometry
PUBLICATIONS	van Breemen, R.B.; Liang, W.; Banuvar, S.; Shulman, L.P.; Pang, Y.; Tao, Y.; Nikolic, D.; Krock, K.M.; Fabricant, D.S.; Chen, S-N.; Hedayat, S.; Bolton, J.L.; Pauli, G.F.; Piersen, C.E.; Krause, E.C.; Geller, S.E.; and Farnsworth, N.R., Pharmacokinetics of 23-Epi-26-Deoxyactein in Women After Oral Administration of a Standardized Extract of Black Cohosh. Clinical Pharmacology and Therapeutics 2010, **87**, 219-225